International School for Advanced Studies

Doctoral Thesis

Multicomponent strongly correlated fermions in optical lattices

Author:
Lorenzo Del Re

Supervisor:
Massimo Capone

A thesis submitted for the degree of Doctor of Philosophy

in

Condensed Matter

CONTENTS

Part I

Introduction

The present thesis is devoted to the study of physical phenomena emerging from strong correlations in strongly interacting quantum many-body systems with several components. Hubbard models are widely used as minimal models which take into account the interactions between particles and they have been studied in relation to phenomena such as Mott localization, unconventional superconductivity, quantum magnetism and many others. All of these striking phenomena share their origin from the strong correlations among fermions induced by their mutual interactions.

Furthermore, condensed matter models are usually realized only in an approximate fashion in actual solid-state systems, making the situation all the more puzzling and hard to be treated analytically or numerically.

Therefore, a great effort has been performed to simulate Hubbard models in a system of atoms cooled down to ultra low temperatures and trapped in optical lattices. The most peculiar feature of cold atoms experiments consists in the possibility of tuning relevant physical parameters of the systems, as the density or the interactions among atoms, using laser and/or magnetic fields. This paved the way to the observation of fundamental quantum states of matter as the weakly interacting Bose-Einstein condensate, the superfluid to Mott insulator transition, the superfluid BEC-BCS crossover, the Mott transition in systems of composite fermions and so on. Hence, it is considered of great interest establishing connections between the quantum simulations cold atomic toolbox and systems realized in solid-state physics.

This idea perfectly fits within the central aim of the thesis. Indeed, simulations of $SU(N)$-symmetric Hubbard models achieved experimentally with a cold atomic gas of ytterbium atoms (^{173}Yb) represents the main inspiration of the entire work. The higher spin degeneracy is brought by the nature of the atomic collisions that will be discussed extensively in the progress of this introductory part. Another experimental success that embodies an additional source of inspiration consists in the realization of artificial gauge fields exploiting light-matter interactions in cold atomic systems.

In this work, the interest of studying such symmetric models has not to be found in the possibility of carrying out a large-N expansion, leading to a semiclassical description of the model. Conversely, $N \geq 2$ is rather considered to be a finite integer number, in order to establish a correspondence with solid-state physics, where the interplay among the internal degrees of freedom of electrons (spin, orbital) are believed to play a crucial role in many physical phenomena of interest.

In the progress of this introduction, a prelude about multi-orbital systems is given in

order to provide such a correspondence. Afterwards, the last achievements within cold atomic experiments in optical lattices are reviewed. In particular, it will be shown how the realization of the above mentioned $SU(N)$-symmetric Hubbard models is experimentally achieved using alkaline-earth or alkaline-earth like atoms. Furthermore, the actual experimental scheme for the realization of artificial gauge fields is also explained in detail. Finally, a brief plan of the second part, containing the main results of this work is presented.

CHAPTER 1

PRELUDE: MULTIORBITAL PHYSICS IN SOLID STATE

In the last few years, the field of strongly correlated electron systems and exotic superconductors has shifted the focus on multicomponent systems, in which more than one orbital contributes to the low-energy electronic structure and/or more bands cross the Fermi energy or lie very close to it [27]. This may lead to a variety of phenomena which can not be described merely as a superposition of individual components, but show distinctive phenomena which have just been started to be characterized and understood. Among these systems can be actually counted a variety of transition-metal oxides, like, e.g. rhutenates, iridates, vanadates and nickelates with the notable exemption of the copper-based high-temperature superconductors, where a single band crosses the Fermi level. A special role in this context is played by iron-based superconductors and related compounds, where a distinctive multiband structure is believed to be crucial for the superconducting pairing [19]. Finally, a multiorbital electronic structure is crucial to give rise to strongly correlated electron-phonon driven superconductivity in alkali-metal doped fullerides [14].

The motivation of the present thesis is the beginning of a cross-fertilization between this evolving field and the world on "quantum simulations" with cold atoms in optical lattices. As explained in detail in the next section, also the field of cold-atoms is now

developing in the direction of multicomponent systems, which are here exemplified by Ytterbium (^{173}Yb) atoms, which have two electrons in their outer shell and feature a large nuclear spin as well as the possibility to populate also an excited electronic configuration besides the ground state.

When a solid-state system has a multiorbital character, the interactions become immediately richer. Even in the simplest tight-binding approximation where we also assume that the Coulomb interaction is screened and it becomes effectively local, it happens that the more familiar Hubbard repulsion which controls the charge fluctuations on each atom is supplemented by a Hund's exchange interaction, whose main effect is essentially to make energetically favorable that two electrons on the same atom occupy different orbitals with the same spin. This leads to another energy scale, typically significantly smaller than the Hubbard repulsion, which however can strongly influence the physics. Another crucial parameter is a local hybridization between orbitals (essentially a local "hopping") which also introduces a new energy scale by splitting the degenerate levels.

A second direct consequence of the multiorbital nature of the electronic structure is the possibility that some parameters differentiate the various orbitals. For example one can have an orbital-dependent hopping or Coulomb interaction (if the rotational invariant is broken), or a crystal-field splitting, which favors an uneven occupation of the orbitals. All these effect promote different observables in the different orbitals, a different which can be strongly enhanced by an increase of the overall Coulomb interaction. A notable example is the so-called orbital-selective Mott transition, in which by increasing the Coulomb interaction, one or more of the orbitals become Mott localized for a weaker coupling than the others, leading to a window of parameter in which part of the system is localized, while another part is still metallic.

The identification of the conditions for orbital-selective Mott transitions in diferent simple models [23, 22, 41] has triggered also studies of actual materials which identified an orbital-selective degree of correlation as a key organizing principle to understand the properties of iron-based superconductors [21]. The latter compounds have been indeed the ground where most of the current understanding of the peculiar properties of multiorbital systems has been forged, including the role of the Hund'd coupling [34] and the realization of a potentially new kind of correlated material which goes under the name of a Hund's metal and features anomalous responses [68, 33].

In this work we explore how some of this physics can be realized with multicomponent

cold-atom system. As mentioned before, ultracold gases of ^{173}Yb are the ideal playground to establish this connection. Indeed these systems allow to realize an immense number of opportunities including an orbital degree of freedom, an internal spin degree of freedom which can take up to six values (which may also been seen as a discrete synthetic dimension), and which can feature artificial gauge fields mimicking spin-orbit coupling as well as a tunable exchange term.

This thesis focuses mainly on some specific quantum systems which can be realized with ^{173}Yb atoms and in particular on the possibility of "flavor selective" physics that generalizes somehow the orbital-selective physics discussed in solid state. The minimal system has been addressed is indeed a three-component gas where only three spin flavors are selected. It is discussed the possibility of selective localization of the different flavors when artificial gauge fields are included. For this reason the simple case of real fields is considered, which mimic an hybridization in solid state, rather than the complex fields describing an artificial spin-orbit coupling. In this regard a particular attention has been paid to the possible instabilities towards orbital-selective phase transition and charge instabilities. The competition with magnetism and the possibility of finite-temperature divergence of the response functions is also addressed.

This work indeed only starts to scratch the surface of an incredibly rich world of quantum simulations, leaving an incredible number of interesting physical situations for future works.

CHAPTER 2

QUANTUM SIMULATIONS WITH ULTRACOLD ^{173}YB ATOMS

Quantum gases of atoms cooled down to ultracold temperatures provide a powerful tool to manage quantum information and build quantum simulators of ideal condensed-matter models which are only approximately realized in actual solid state systems. The power of ultracold atom systems relies mainly in the ability to control and tune the most relevant physical parameters, from the strength and the nature of the interactions to the geometry and the statistics of the constituents. Therefore, the cold atoms setup seems to embody the original idea of Feynman [25] for constructing physical quantum emulators of systems or situations whose properties are hardly accessible to numerical simulations. In many-body systems with strong inter-particle interactions such a situation is rather the rule than the exception and one of the main directions in the field of cold atoms is indeed the quantum simulations of strongly correlated many-body systems[8].

In particular, optical lattices allow for the quantum simulations of popular lattice models, such as the Hubbard model (see below) and many others [24][32][31]. The realization of an optical lattice exploits the fact that atoms subject to a laser field experience an effective potential whose absolute value is proportional to the intensity of the laser beam. This is due to the interaction of the induced dipole moment

of the atoms with laser light. If the frequency of the laser is below the atomic resonance frequency, the atoms are attracted toward regions of high intensity[1]. Hence, a periodic potential can be synthesized using standing waves with the appropriate geometry tuned with an appropriate frequency. The case of a three dimensional optical lattice is depicted in Fig.(2.1), where the periodic potential is given by $V(x, y, z) = V_0 \left[\cos^2(k\,x) + \cos^2(k\,y) + \cos^2(k\,z)\right]$, where $k = \frac{2\pi}{\lambda}$, with λ being the wavelength of the laser. However, two and one-dimensional lattices as well as more involved geometries can be easily realized .

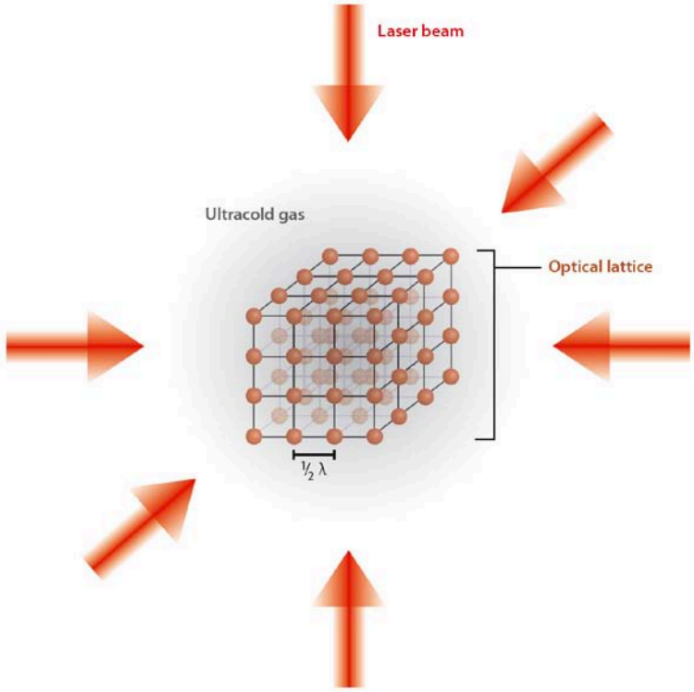

Figure 2.1: Schematic representation of an optical lattice in three dimension [24]. The lattice is created by three mutually perpendicular laser standing waves. Interference terms between two perpendicular beams can be avoided by choosing suitable polarizations and frequency offsets for the standing waves. The atoms experience a periodic attractive potential whose minima correspond to the intensity peaks of the standing waves. The lattice spacing is given by $\lambda/2$, where λ is the wavelength of the laser.

Furthermore, atom-light interaction can be exploited to simulate the effect of a gauge field (the most notable example being the electromagnetic field) onto an electron. Since the atoms are neutral, one has to resort to Artificial Gauge Fields (AGF) [20][29][64][17][50] which have been engineered in order to mimic static electric and

[1] A derivation of the effective potential experienced by an atom subject to a laser field is provided in Appendix(C.1)

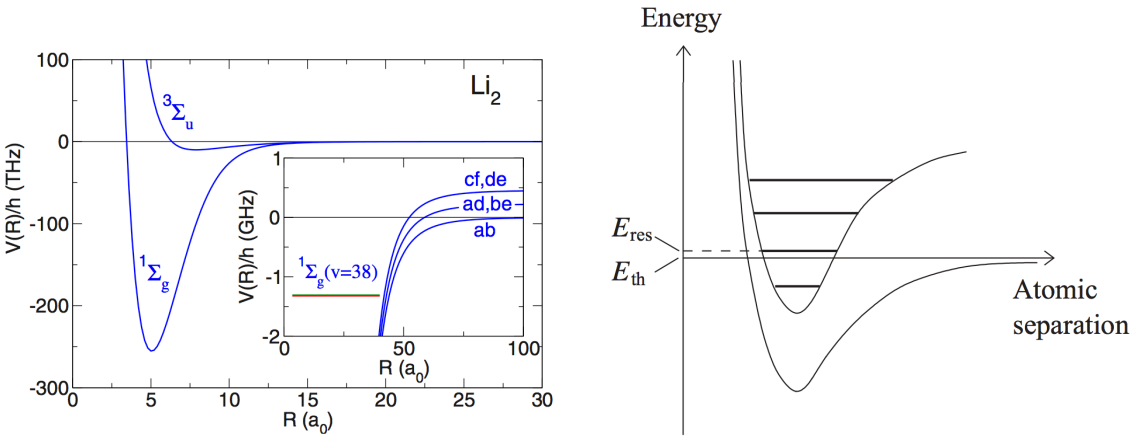

Figure 2.2: (On the left) Molecular potentials as functions of the atomic separation for two ground state ^{6}Li atoms with electrons in singlet and triplet states [18]. (On the right) Sketch of potential energy curves for two different scattering channels. E_{res} refers to the bound state energy in the closed channel closed to E_{th} that indicates the threshold energy of the open channel [59].

magnetic fields, as well as Spin-Orbit Coupling (SOC)[63][37], whose intensities can be tuned with lasers in a controlled manner.

As mentioned above, one of the fundamental features of cold atoms experiments consists in the possibility to tune the interactions between atoms. For dilute gases the interactions between atoms occur via two-body scattering processes governed by interatomic potentials, while three-body scattering is usually neglected because of the low density. Even when the interactions between atoms are strong, they occur only when two atoms are very close to each other, i.e. the range of the interactions is much lower than typical interatomic distances. Therefore, a great simplification in treating cold atomic systems is given by replacing the full inter-atomic potential with an effective one which depends only on the scattering length a, which can be computed using scattering theory [61][59] starting from the full interatomic potential. The effective potential can then be written as $U(\mathbf{r}) = (4\pi\hbar^2 a/m)\,\delta(\mathbf{r})$, where m is the mass of the atoms. Atomic collisions may occur within different *channels* that are determined by the internal degrees of freedom of the atoms, as for instance the spin. Different channels correspond to different interatomic potential curves. To understand this, consider the specific case of alkali atoms that have one electron outside a closed shell. When the two valence electrons relative to the two colliding atoms are in a singlet state they can occupy the same orbital leading to covalent bonding. Conversely, when the electronic spin configuration is symmetric, the spatial wave-function must be

anti-symmetric with respect particle exchange, and therefore the reduction in energy due to two electrons sharing the same orbital is absent. This is illustrated on the left side of Fig.(2.2) that shows the interaction potentials for two ^{6}Li atoms in their ground state when the two valence electrons are in the singlet and triplet spin states. Both the potentials are repulsive for short distances and at greater separations they are attractive. Nevertheless the minimum relative to the singlet state is much lower than the triplet state. Each potential tends toward a constant when evaluated at large distances that is often called *threshold energy.*

In real systems different channels are coupled with each other. This coupling is usually weak, nevertheless becomes relevant if a bound state of one channel is very close to the threshold energy of the other as depicted on the right side of Fig.(2.2). When such a situation occurs, the scattering length relative to the open channel, i.e. the channel with lower threshold energy, is dramatically affected and in particular has the following behavior

$$a \sim \frac{C}{E - E_{res}}, \tag{2.1}$$

where C is a constant, E is the energy of the particles in the open channel and E_{res} is the bound state energy relative to the closed channel, i.e. the channel with higher threshold energy[2]. Therefore the scattering length diverges at the resonance and changes its sign when E crosses E_{res}.

This can be achieved by tuning the relative distance between the threshold energies of the two channels, which in certain cases can accomplished using a magnetic field. Such a phenomenon is called *Feshbach resonance* [18][59][39][54][36] and it is of course of great interest, because it allows to tune the effective interactions among atoms using an external parameter that can be easily controlled.

The use of Feshbach resonances combined with optical lattices allows to simulate tight-binding models with tunable interactions between atoms which hop on the same

[2]It is worth to notice, that at low energies, i.e. when E is close to the threshold energy of the open channel, there cannot be direct transitions from the open channel to the closed one. In fact, in a scattering process at low energies, two particles that interact in the open channel must be at rest at infinite distance. This cannot occur if there is a direct transition to the closed channel, because the particles would be trapped in a finite region forever. Nevertheless second order virtual processes are allowed, and two particles colliding in the open channel can scatter in an intermediate state in the closed channel and after decay back to the open channel.

lattice site, realizing the celebrated Hubbard model [40][66]

$$H = -t \sum_{\langle \mathbf{R}\mathbf{R}' \rangle, \sigma} c^{\dagger}_{\mathbf{R}\sigma} c_{\mathbf{R}'\sigma} + U \sum_{\mathbf{R}} \hat{n}_{\mathbf{R}\uparrow} \hat{n}_{\mathbf{R}\downarrow} - \mu \sum_{\mathbf{R}\sigma} \hat{n}_{\mathbf{R}\sigma}, \tag{2.2}$$

where $c_{\mathbf{R}\sigma}$ is the destruction operator of a fermion with spin σ on the site (minimum of the optical latttice) $\mathbf{R}$, $\hat{n}_{\mathbf{R}\sigma} \equiv c^{\dagger}_{\mathbf{R}\sigma} c_{\mathbf{R}\sigma}$ is the number operator, t is the tunneling amplitude between two neighboring minima and U is the tunable Hubbard on-site repulsion which depends on the scattering amplitude. The model (2.2) assumes that the fermions have spin 1/2 and they exist in a single band. This simple version of the model is very popular in solid state both because it is arguably the simplest model which shows the physics of strong correlations and the Mott-Hubbard transition, which we describe in some details in the next chapter, and because the two-dimensional version of this model is believed to be the basis of the theoretical understanding of high-temperature superconductivity in copper oxides. This work, motivated and inspired by multiorbital materials, focuses on multicomponent Hubbard models and their realization with ultracold atoms.

In the progress of this chapter it will be given a brief overview of the main theoretical and experimental facts concerning the simulation of multi-orbital and $SU(N)$-symmetric Hubbard Models which can also feature artificial gauge fields. In particular it will be discusses the case of atoms with two electrons in the outer shell, sharing the external electronic configuration with alkaline-earth atoms. The most popular example in the field is the quantum degenerate gas of Ytterbium (^{173}Yb) atoms, which has a nuclear spin $I = 5/2$ which is essentially decoupled from the electronic degrees of freedom. As a consequence the scattering length does not depend on the nuclear spin indices, so that the interaction have a full $SU(N)$ symmetry, where $N = 2I + 1$ is the number of possible "flavors" for the fermions, and reaches the value of 6 for Ytterbium [31]. The experimental evidences relative to the exchange interactions between two different atomic species and the possibility of tuning such an interaction through Feshbach resonance will be also summarized [15][62][54][36]. Finally the actual experimental scheme adopted for simulating AGF will be presented [17][50] and the many body hamiltonian will be derived from the atomic one.

2.1 Simulation of two-band and $SU(N)$-symmetric Hubbard models with Ytterbium atoms

Atoms with two electrons in their outer shell, thereby sharing the configuration of alkaline earths have two main features that make them suitable for many-body simulations:

The first one is the presence of a long lived metastable state $^3P_0$ coupled to the ground state $^1S_0$ via a forbidden dipole transition. The second is based on the almost perfect decoupling of the nuclear spin I from the electronic angular momentum J in these two states, because they both have $J = 0$. This implies that scattering lengths involving any of these states are independent of the nuclear spin, aside from the restrictions imposed by fermionic antisymmetry. Therefore, the interaction of the system are $SU(N)$-symmetric with $N = 2\,I + 1$, where I is the nuclear spin.

The second crucial property stems from the long lifetime of the metastable state $^3P_0$, which gives to the possibility to prepare an interacting system with two different species (corresponding to the two different electronic configurations) of atoms in an optical lattice, which is the quantum simulator of a model with two orbitals per site and two bands.

The two orbital are labeled as $\alpha = e, g$, where $|e\rangle = |^3P_0\rangle$ ($|g\rangle = |^1S_0\rangle$) corresponding to one atom in the excited (ground) state. Hence, the collisions among atoms can occur within four different channels that are labeled respectively ee, gg, eg^+, eg^-. This last correspond to collisions between two atoms that are in triplet orbital states ($|ee\rangle$, $|gg\rangle$, $|eg^+\rangle$) or in the two particle anti-symmetric orbital state $|eg^-\rangle$. These are the only possible configurations, since the interactions are local and therefore the spatial wave function is always symmetric (s-wave). These considerations together with the facts that different channels are weakly coupled and the scattering length does not depend on the spin indices lead to the following hamiltonian for the two

species of alkaline-earth atoms trapped in an optical potential:

$$\begin{aligned}\hat{H} &= \sum_{\alpha m}\int d\mathbf{x}\,\Psi^{\dagger}_{\alpha m}(\mathbf{x})\left(-\frac{\hbar^2}{2m}\nabla^2+V_{\alpha}(\mathbf{x})\right)\Psi_{\alpha m}(\mathbf{x})\\ &+ \hbar\,\omega_0\int d\mathbf{x}\,\left(\rho_e(\mathbf{x})-\rho_g(\mathbf{x})\right)+\frac{g_{eg^+}+g_{eg^-}}{2}\int d\mathbf{x}\,\rho_e(\mathbf{x})\rho_g(\mathbf{x})\\ &+ \sum_{\alpha}\sum_{m<m'} g_{\alpha\alpha}\int d\mathbf{x}\,\rho_{\alpha m}(\mathbf{x})\rho_{\alpha m'}(\mathbf{x})\\ &+ \frac{g_{eg^-}-g_{eg^+}}{2}\sum_{mm'}\int d\mathbf{x}\,\Psi^{\dagger}_{gm}(\mathbf{x})\Psi_{gm'}(\mathbf{x})\Psi^{\dagger}_{em'}(\mathbf{x})\Psi_{em}(\mathbf{x}),\end{aligned} \tag{2.3}$$

where $\Psi^{\dagger}_{\alpha m}(\mathbf{x})$ is the Fermi field that creates one atom in $\mathbf{x}$ with orbital and spin quantum numbers α and m satisfying the anticommutation relations:

$$\begin{aligned}\left\{\Psi^{\dagger}_{\alpha m}(\mathbf{x}),\Psi_{\beta m'}(\mathbf{y})\right\} &= \delta(\mathbf{x}-\mathbf{y})\,\delta_{mm'}\,\delta_{\alpha\beta}\,,\\ \left\{\Psi_{\alpha m}(\mathbf{x}),\Psi_{\beta m'}(\mathbf{y})\right\} &= \left\{\Psi^{\dagger}_{\alpha m}(\mathbf{x}),\Psi^{\dagger}_{\beta m'}(\mathbf{y})\right\}=0\,.\end{aligned} \tag{2.4}$$

$\rho_{\alpha}(\mathbf{x}) = \sum_m \rho_{\alpha m}(\mathbf{x})$, with $\rho_{\alpha m}(\mathbf{x}) \equiv \Psi^{\dagger}_{\alpha m}(\mathbf{x})\Psi_{\alpha m}(\mathbf{x})$ being the density operator relative to the fermionic species labeled by the m and α indices, $V_{\alpha}(\mathbf{x})$ is the optical periodic potential felt by atoms in the α-th orbital, $\hbar\,\omega_0$ is the energy difference between the ground and excited states of the atom. The spin quantum number $m = -I, .., I$ denotes one of the $2\,I+1$ Zeeman level of the nucleus. The values $g_{\alpha\alpha}$, $g_{eg^{\pm}}$ are the strength of the interactions relative to the four different collision channels that are related to the scattering lengths through the relation $g_X = (4\pi\hbar^2/m)\,a_X$, where $X = ee,\ gg,\ eg^+,\ eg^-$. For a more detailed derivation of the interacting terms appearing in the hamiltonian in eq.(2.3) see Appendix(A).

The Fermi field $\Psi^{\dagger}_{\alpha m}(\mathbf{x})$ can be represented in both Bloch and Wannier basis:

$$\begin{aligned}\Psi_{\alpha m}(\mathbf{x}) &\equiv \sum_{\mathbf{k}}\sum_{\lambda}\sum_{m}\psi_{\mathbf{k}\lambda\alpha}(\mathbf{x})\,c_{\mathbf{k}\,\alpha\,\lambda\,m} \qquad \text{(Bloch)}\\ \Psi_{\alpha m}(\mathbf{x}) &\equiv \sum_{\mathbf{R}}\sum_{\lambda}\sum_{m}w_{\mathbf{R}\lambda\alpha}(\mathbf{x})\,c_{\mathbf{R}\,\alpha\,\lambda\,m} \qquad \text{(Wannier)},\end{aligned} \tag{2.5}$$

where $c^{\dagger}_{\mathbf{R}\,\alpha\,\lambda m}$ is the creation operator of a fermion on the lattice site $\mathbf{R}$, with α, m and λ being the orbital, spin and lattice band indices respectively. This operator is related to $c^{\dagger}_{\mathbf{k}\alpha m}$ via Fourier transformation on the lattice, i.e. $c^{\dagger}_{\mathbf{k}\,\alpha\,\lambda\,m} = \frac{1}{N}\sum_{\mathbf{R}} e^{i\mathbf{R}\cdot\mathbf{k}}c_{\mathbf{k}\,\alpha\,\lambda\,m}$. $\{\psi_{\mathbf{k}\lambda\alpha}(\mathbf{x})\}$ and $\{w_{\mathbf{R}\lambda}(\mathbf{x})\}$ are respectively the set of the Bloch and Wannier functions, that are related to each other through the following relation

$w_{\mathbf{R}\lambda\alpha}(\mathbf{x}) = \frac{1}{N}\sum_{\mathbf{k}} e^{-i\mathbf{k}\cdot\mathbf{R}}\,\psi_{\mathbf{k}\lambda\alpha}(\mathbf{x})$. In many cold atoms experiments, it is assumed that only the lowest lattice band is populated, hence the subscript λ will be dropped from now on. Representing the Fermi fields in the Wannier basis, the second quantization expression of the alkaline-earth atoms hamiltonian in eq.(2.3) reads:

$$\begin{aligned}\hat{H} &= \sum_{\mathbf{R}\mathbf{R}'}\sum_{\alpha m} t^{\alpha}_{\mathbf{R}\mathbf{R}'}\, c^{\dagger}_{\mathbf{R}\alpha m} c_{\mathbf{R}'\alpha m} + \sum_{\alpha}\frac{U_{\alpha\alpha}}{2} n_{\mathbf{R}\alpha}(n_{\mathbf{R}\alpha}-1) + V\sum_{\mathbf{R}} n_{\mathbf{R}e} n_{\mathbf{R}g} \\ &+ V_{ex}\sum_{\mathbf{R}} c^{\dagger}_{\mathbf{R}\,gm} c^{\dagger}_{\mathbf{R}\,em'} c_{\mathbf{R}\,gm'} c_{\mathbf{R}\,em} \end{aligned} \tag{2.6}$$

where $t^{\alpha}_{\mathbf{R}\mathbf{R}'} = \int d\mathbf{x}\, w^{*}_{\mathbf{R}\alpha}(\mathbf{x})\left[-\frac{\hbar^2\nabla^2}{2m} + V_{\alpha}(\mathbf{x})\right] w_{\mathbf{R}'\alpha}(\mathbf{x})$ is the hopping integral, $U_{\alpha\alpha} = g_{\alpha\alpha}\int d\mathbf{x}\, w^{4}_{\mathbf{R}\alpha}(\mathbf{x})$ represent the onsite interactions relative to two electrons in the same orbital. $V_{ex} = (U_{eg^+} - U_{eg^-})/2$ and $V = (U_{eg^+} + U_{eg^-})/2$ correspond to the exchange and direct orbital interactions strengths that are given by the relations $U_{eg^\pm} = g_{eg^\pm}\int d\mathbf{x}\, w^2_e(\mathbf{x}) w^2_g(\mathbf{x})$. $c^{\dagger}_{\mathbf{R}\alpha m}$ is the creation operator relative to a fermion on a lattice site $\mathbf{R}$ with orbital and spin quantum numbers α and m respectively, $n_{\mathbf{R}\alpha} = \sum_m n_{\mathbf{R}\alpha m}$, where $n_{\mathbf{R}\alpha m} \equiv c^{\dagger}_{\mathbf{R}\alpha m} c_{\mathbf{R}\alpha m}$.

The hamiltonian in eq.(2.6) is symmetric under $SU(N)$ unitary transformation of the fields, that act on the spin indices, that is a direct consequence of the fact that the scattering lengths relative to the four different channels do not depend on the spin indices. Formally, the hamiltonian commutes with the Lie algebra generators $S^m_{m'}$, that are defined by the commutation relations $[S^m_n, S^p_q] = \delta_{mq} S^p_n - \delta_{pn} S^m_q$, and that can be represented using the second quantization operators as $S^m_{m'} = \sum_{\mathbf{R}\alpha} c^{\dagger}_{\mathbf{R}\alpha m'} c_{\mathbf{R}\alpha m}$. The alkaline earth atoms hamiltonian has an additional symmetry that derives from the elasticity of the electronic collisions. To understand this one can define the $SU(2)$ pseudo-spin algebra as $T^{\mu} = \frac{1}{2}\sum_{\mathbf{R}m}\sum_{\alpha\beta} c^{\dagger}_{\mathbf{R}\alpha m}\left(\sigma^{\mu}\right)_{\alpha\beta} c_{\mathbf{R}\beta m}$, where $\sigma^{\mu=x,y,z}$ are the Pauli matrices and verify that $[H, T^z] = 0$.

2.2 Experimental evidences

An important consequence of the $SU(N)$ symmetry is the conservation of $S^m_m = \sum_{\mathbf{R}m} n_{\mathbf{R}m}$, i.e. the density relative to the the m-th spin index. Therefore atoms with large nuclear momentum as ^{173}Yb ($I = 5/2$) or ^{87}Sr ($I = 9/2$) can be used to reproduce the dynamics of atoms with lower total momentum, choosing an initial state with $\langle S^m_m \rangle = 0$ for some spin indices m. This paves the way for the possibility

of simulating $SU(N)$ symmetric models with $N \leq 2\,I + 1$ using the same atoms [55] [70].

Another distinctive feature of the hamiltonian in eq.(2.6) is the presence of the exchange interaction proportional to V_{ex}. This term is also present in multiorbital models in solid state, where the exchange interactions are responsible of the first two Hund's rules. As we discussed in the first paragraph of this chapter, the Hund's coupling has been recently identified as the source of a variety of remarkable phenomea, ranging from an Orbital Selective Mott Transition [41][67][23][22], where a Mott transition occurs for electrons in certain orbitals and coherent excitations survive only for other orbitals to anomalous metallic states. Furthermore, when this coupling is taken to be negative, as it is effectively realized in superconducting alkali-doped fullerides, it gives rise to unconventional superconductivity as shown for the case of the multi-band Hubbard model [13][14].

Hence, a great effort has been performed experimentally and theoretically, in order to confirm the $SU(N)$-symmetry of alkaline earth atoms collisions, to detect the exchange interaction and to engineer a Feshbach resonance in the eg^- channel allowing for the possibility of tuning the interaction strength V_{ex} [15][62][69][54][36].

In this introductory section it will be given a brief review of the main goals achieved in the experiments reported in Refs.[15][54] taken as illustrative cases.

In particular in the experiment reported in Ref.[15] the exchange interaction has been probed through a direct observation of inter-orbital spin oscillations. More in detail, the experiment has been performed on quantum degenerate Fermi gases of ^{173}Yb in a balanced mixture of two different states out of the $I = 5/2$ nuclear spin manifold $|m\rangle = |+5/2\rangle \equiv |\uparrow\rangle$ and $|m\rangle = |-5/2\rangle \equiv |\downarrow\rangle$ trapped in a deep 3D optical lattice. The longlived $|e\rangle$ state was populated by exciting the ${}^1S_0 \rightarrow {}^3P_0$ clock transition. Given the large lattice depth, tunneling of atoms between different lattice sites is negligible. This amounts to set $t^\alpha = 0$ for every α in the hamiltonian in eq.(2.6), that within this limit becomes a summation of local atomic hamiltonians. Assuming homogeneity in the center of the trap and the experimental condition reported, the subspace of interest is that one with $n = 1$ for each spin and orbital state. Therefore, the hamiltonian within this subspace can be expressed as a 2×2 matrix whose eigenvectors are the singlet and triplet states:

$$\left|eg^{\pm}\right\rangle = \frac{1}{\sqrt{2}}\left(|g\uparrow e\downarrow\rangle \mp |g\downarrow e\uparrow\rangle\right), \tag{2.7}$$

with eigenvalues $V \pm V_{ex}$. Therefore if an initial state is prepared in the state $|\psi(t=0)\rangle = |g\uparrow e\downarrow\rangle$, at time t the probability of finding a ground state atom in the $|g\uparrow\rangle$ state would is given by

$$P(|g\uparrow\rangle)(t) = \frac{1}{2}\left[1 + \cos\left(\frac{2V_{ex}}{\hbar}t\right)\right]. \tag{2.8}$$

Such an initial state could be obtained exploiting the action of a magnetic field that couples the states $|eg^{\pm}\rangle$. This is possible because of the orbital dependence of the Landé factor, amounting in a different splitting between $\uparrow$ and $\downarrow$ in different orbitals [9] as shown schematically in Fig.(2.3). Hence, in presence of a magnetic field B, the

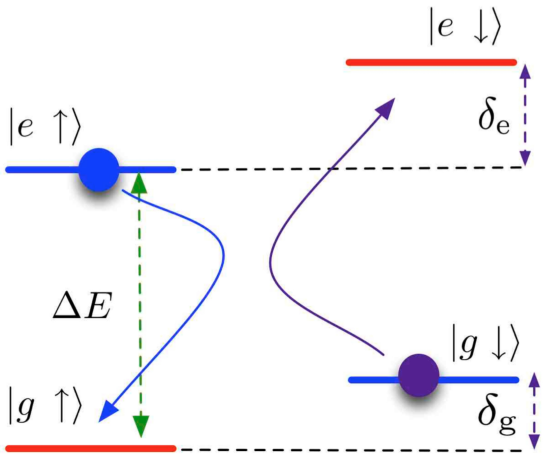

Figure 2.3: Schematic representation of the different splitting between $\uparrow$ and $\downarrow$ states in different orbital due to a non zero differential Landé factor $\delta = \delta_e - \delta_g$.

$|eg^{\pm}\rangle$ states are coupled and the hamiltonian in the $\{|eg^{+}\rangle, |eg^{-}\rangle\}$ basis reads:

$$H = \begin{pmatrix} V + V_{ex} & \Delta\mu\, B \\ \Delta\mu\, B & V - V_{ex} \end{pmatrix}. \tag{2.9}$$

$\Delta\mu\, B = \delta\mu_N \Delta m B$ is called *differential Zeeman shift* , where μ_N is the nuclear magneton, B is the magnetic field intensity, $\delta = \delta_e - \delta_g$ is the differential Landé factor and Δm is the difference between the two quantum numbers $m_\uparrow$, $m_\downarrow$. The eigenvalues of the matrix are $V \pm \sqrt{V_{ex}^2 + \Delta^2}$ and the eigenvectors labeled as $|eg^L\rangle$, $|eg^H\rangle$ are given by superpositions of the $|eg^{\pm}\rangle$ states. These states correspond to $|g\uparrow e\downarrow\rangle$, $|g\downarrow e\uparrow\rangle$ when $\Delta\mu\, B \gg V$. Therefore, the initial state $|\psi_0\rangle = |g\uparrow e\downarrow\rangle$ can be obtained, letting the system relax in its ground state using an intense magnetic field. Hence, after quenching the magnetic field to zero, if $V_{ex} \neq 0$ the system evolves

displaying the spin oscillations in Fig.(2.4).

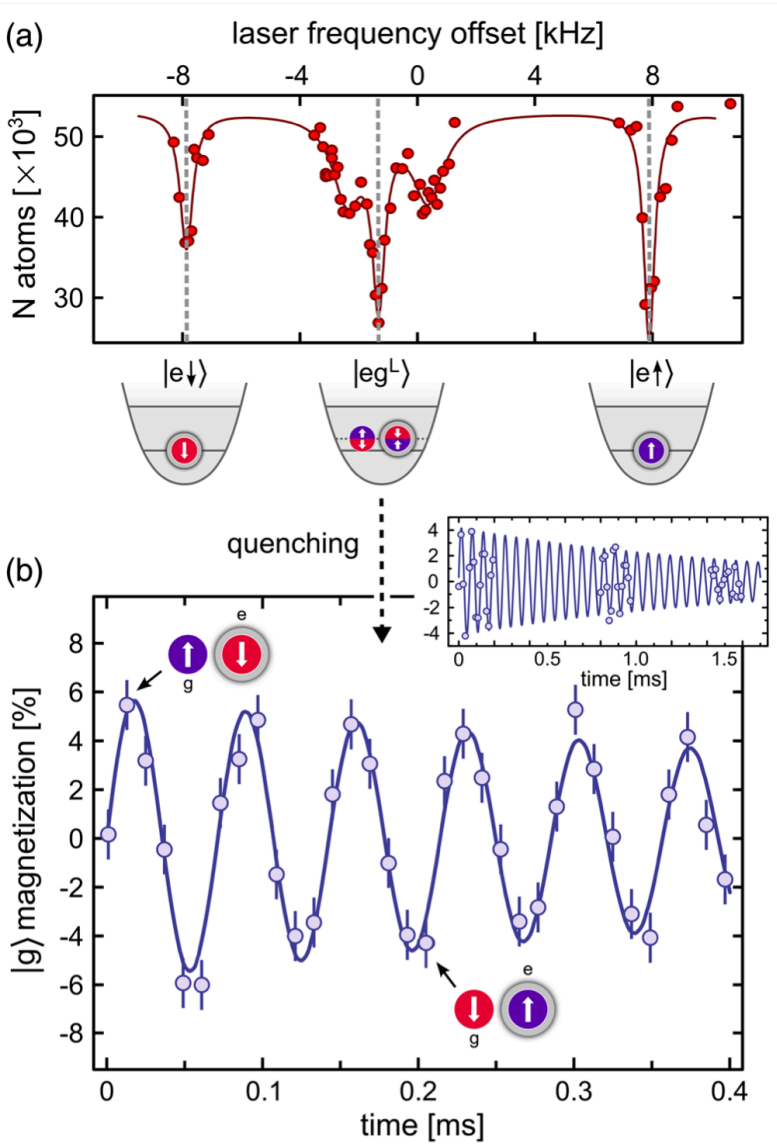

Figure 2.4: (On the top) Data relative to the spectral function of the atomic gas obtained via laser spectroscopy, showing the population of the state $|eg^L\rangle$. (On the bottom) Spin oscillations of the $|g\rangle$ atoms as a function of time after quenching the magnetic field to zero.

Ref.[54] shows the experimental evidences of a Feshbach resonance occurring in the scattering of two ^{173}Yb atoms in different nuclear and electronic states. First of all, it is worth to notice that ^{173}Yb as well as the alkaline earth atoms cannot display a magnetic Feshbach resonance, in its ground state since $J = 0$ and there is no splitting of the Zeeman levels. Nevertheless, a resonance may occur within the eg^- channel, exploiting the above mentioned property of alkaline atoms of having a non zero

differential Landé factor. The scheme for obtaining such a *orbital Feshbach resonance* was provided in Ref.[69]. Consider two ^{173}Yb atoms in two different electronic (orbital) states $|e\rangle$ and $|g\rangle$,and different nuclear spin states $|\uparrow\rangle$ and $|\downarrow\rangle$. When the atoms are separated, interactions between them are negligible and the relevant two-body eigenstates are $|o\rangle = |g\uparrow e\downarrow\rangle$ and $|c\rangle = |g\downarrow e\uparrow\rangle$ which are named open and closed collisional channels, respectively as shown in Fig.(2.5). The energy separation between the two channels is given by the differential Zeeman shift $\Delta\mu B$. As the interatomic distance decreases, the appropriate basis for the description of the scattering is given by the orbital symmetric and antisymmetric states $|eg^{\pm}\rangle$, which are associated with two distinct molecular potentials, giving rise to two very different scattering lengths, a_{eg^+} and a_{eg^-}, respectively. The relative distance between the threshold energy relative to these two different channel can be controlled using the magnetic field, allowing for the Feshbach resonance mechanism described in the previous sections.

Experimentally a cloud of ^{173}Yb atoms was confined in a cigar-shape optical trap. The atomic gas was intially prepared in a balanced spin mixture of ground states atoms in nuclear spin states $m_\uparrow$, $m_\downarrow$, whose difference is $\Delta m = m_\uparrow - m_\downarrow$. The population of the excited metastable state was achieved through the clock transition $^1S_0 \rightarrow {}^3P_0$. The excitation was performed at high magnetic field intensity, in the way to clearly resolve the Zeeman structure and excite only one spin state. In this way it was possible to selectively access the open or the closed channel. Just before the trap was released, the magnetic field was suddenly change to the desired value for probing the resonance. Fig.(2.5) shows the evolution of the atomic cloud and the aspect ratio of the Fermi gas after the trap was released as a function of the time of flight. The aspect ratio is defined as the ratio R_y/R_x of the expanded atomic cloud size along y to the size along x. In the case of a non-interacting Fermi gas, the expansion is ballistic and the cloud tends to assume a spherical shape as a function of time. Therefore, the aspect ratio of non-interacting Fermi gas would tend asymptotically to the unity. Instead, atoms interacting in the eg^- channel displayed an inversion of the aspect ratio, that is an hallmark of hydrodynamic expansion of a Fermi gas, which occurs in regime of strong interactions. Fig.(2.6) shows the experimental data reporting the aspect ratio measured at a large value of the time of flight ($\tau = 28$ ms) as a function of the rescaled magnetic field. The different marks refer to different combination of nuclear spin states, showing that the Feshbach resonance does not depend on the particular spin combination, another confirm of the $SU(N)$ symmetric feature relative to the interactions among alkaline earth atoms.

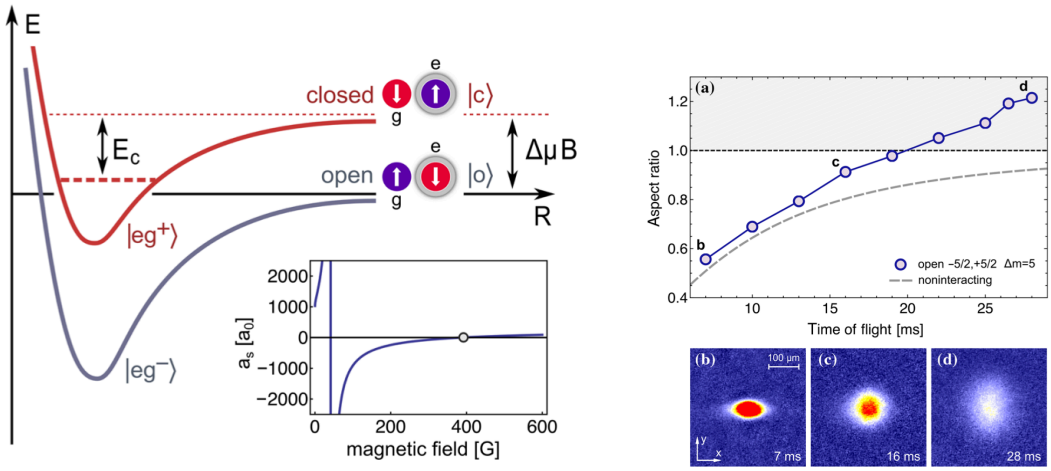

Figure 2.5: (On the left) Schematic representation of different molecular potentials relative to the open and closed channel, and the splitting between the threshold energies as a function of the differential Zeeman shift $\Delta\mu B$. (On the right) Shape of the atomic cloud from for several values of the time of flight τ.

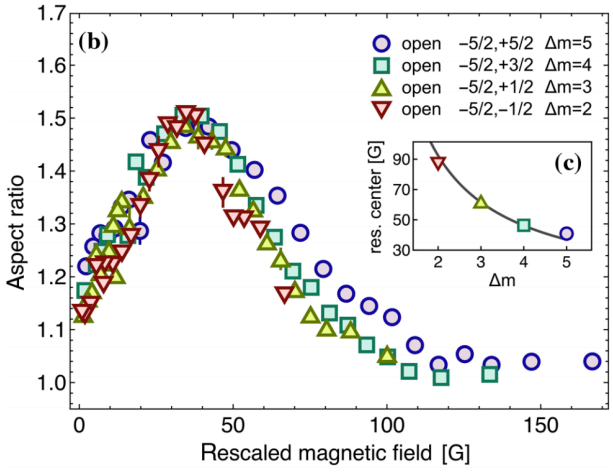

Figure 2.6: Aspect ratio of the atomic cloud prepared in the open channel at $\tau = 28$ ms as a function of the rescaled magnetic field $\tilde{B} \equiv B\Delta m/5$, for different combination of nuclear spin states. The resonance occurs almost at the same values of $\tilde{B}$ for all the combinations, confirming the $SU(N)$ symmetry of the atomic collisions.

2.3 An experimental scheme for simulating AGF in cold atoms systems.

Exploiting light-matter interaction within the cold atoms context allows also for the possibility of simulating artificial gauge fields (AGF). In this introduction will be described a particular scheme, already realized in cold atoms experiment, for simulating a three component fermionic gas pierced by a uniform magnetic field.

The realization of a synthetic uniform magnetic field can be obtained exploiting the combination of a static uniform "real" magnetic field along the z-axis $\mathbf{B} = B_0\mathbf{e}_z$ together with an electromagnetic field composed of two laser beams $\mathbf{E}(t) = \mathbf{E}_{\omega_+}(t) + \mathbf{E}_{\omega_-}(t)$. A practical scheme often used in experiments on AGF is that one of two lasers, Raman beams, counter propagating along the x-axis of equal intensities and crossed linear polarization, i.e. $\mathbf{E}_{\omega_-} = E\, e^{ik_R x}\, \mathbf{e}_y$, $\mathbf{E}_{\omega_+} = E\, e^{-ik_R x}\, \mathbf{e}_z$. This setup leads to an effective Zeeman magnetic field:

$$\mathbf{\Omega} = \delta\, \mathbf{e}_z + \Omega_R \left[\sin(2k_R x)\mathbf{e}_x - \cos(2k_R x)\mathbf{e}_y\right], \tag{2.10}$$

that couples with the total angular momentum $\hat{\mathbf{F}} = \hat{\mathbf{J}} + \hat{\mathbf{I}}$, with $\hat{\mathbf{J}}$ and $\hat{\mathbf{I}}$ the total electronic and nuclear angular momentum respectively. Hence, the atom-light hamiltonian reads:

$$H_{al} = \mathbf{\Omega} \cdot \hat{\mathbf{F}} = \delta\, \hat{F}_z + \left(\hat{F}_+\, e^{i2k_R x} + \hat{F}_-\, e^{-i2k_R x}\right) \Omega_R/2, \tag{2.11}$$

where $\hat{F}_\pm$ are the angular momentum ladder operators acting as $\hat{F}_+ \left|f, m\right\rangle = N(f,m)\ \left|f, m+1\right\rangle$, where $N(f,m) = \sqrt{f(f+1) - m(m+1)}$, $\left|f, m\right\rangle$ are the simultaneous eigenkets of $\hat{\mathbf{F}}^2$ and $\hat{F}_z$, with eigenvalues $\hbar^2 f(f+1)$ and $\hbar m$ respectively. Therefore, the Raman beams couple the different hyperfine levels providing a nearest neighbor hopping with open boundary condition (OBC) along the synthetic direction given by the spin degree of freedom. The derivation of the effective Zeeman field and all the details present in eqs.(2.10,2.11) that have been omitted are presented in Appendix(C). Note that there is no need for the two Raman beams to be counter propagating for obtaining the result in eq.(2.10). In the case of two Raman beams forming an angle θ with the x-axis as depicted in Fig.(2.7), the wave vector would change into $k_R = \frac{2\pi\cos(\theta)}{\lambda_R}$, where λ_R is the wavelength of the Raman beams.

As can be grasped from the Appendix(C), the derivation of the effective Zeeman field is thought for alkali atoms as for example ^{87}Rb, nevertheless the $f = 1$ three level

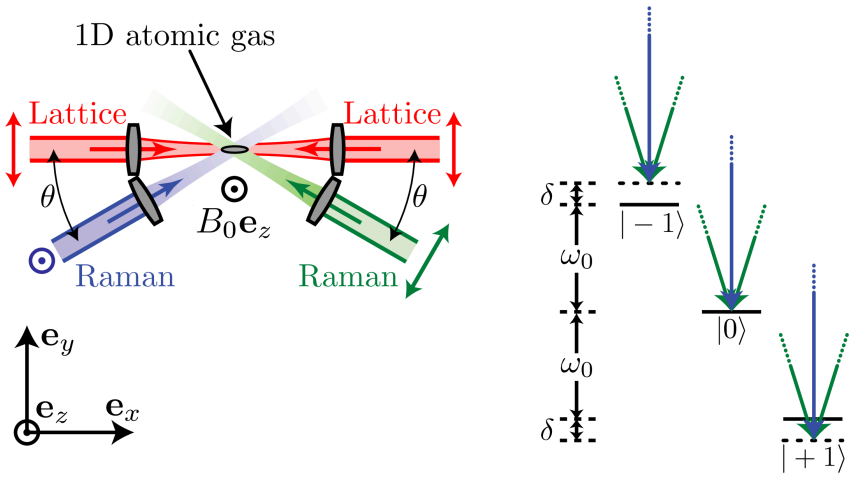

Figure 2.7: On the left, schematic representation of the experimental setup for simulating AGF in a one dimensional optical lattice as proposed in ref.[17]. On the right, physical level diagram for three-level total angular momentum $f = 1$, where $\hbar^2 f(f+1)$ are the eigenvalues of $\hat{\mathbf{F}}^2$.

systems in Fig.(2.7) can be realized also by coupling three spin states of fermionic ^{173}Yb [50]. In addition, periodic boundary condition (PBC) in the synthetic direction can be created by coupling the $m = \pm f$ states [17].

In an optical lattice, the atoms feel a periodic potential $V(\mathbf{r}+\mathbf{R}) = V(\mathbf{r})$, the many-body hamiltonian can be written as:

$$\hat{H} = \sum_{mm'} \int d\mathbf{x}\, \hat{\Psi}^\dagger_m(\mathbf{x}) \left[-\frac{\hbar^2\nabla^2}{2m}\delta_{mm'} + V(\mathbf{r})\delta_{mm'} + \mathbb{M}_{mm'}(\mathbf{x}) \right] \hat{\Psi}_{m'}(\mathbf{x}), \qquad (2.12)$$

$\mathbb{M}_{mm'} = \left[N(f,m)\,\delta_{m,m'-1} e^{i2\,\mathbf{k}_R\cdot\mathbf{x}} + \text{h.c.} \right] \Omega_R/2$ where $\mathbf{k}_R = (k_R, 0, 0)$, and $\hat{\Psi}(\mathbf{x})$ is the Fermi field. The second quantization expression of the kinetic term together with the periodic potential, expressed using the Wannier basis reads $\sum_{\mathbf{R}\mathbf{R}'} \sum_m t_{\mathbf{R}\mathbf{R}'}\, c^\dagger_{\mathbf{R}m} c_{\mathbf{R}'m}$, with $t_{\mathbf{R}\mathbf{R}'} = \int d\mathbf{x}\, w^*_{\mathbf{R}}(\mathbf{x}) \left[-\frac{\hbar^2\nabla^2}{2m} + V(\mathbf{x}) \right] w_{\mathbf{R}'}(\mathbf{x})$, is the hopping integral, and it is real in the case of inversion symmetry of the band.

It is useful to use the Bloch representation for the term of the hamiltonian proportional

to Ω_R:

$$\begin{aligned}
&\frac{\Omega_R}{2}\sum_{\mathbf{k}_1\mathbf{k}_2}\sum_{m_1m_2}\left[\int d\mathbf{x}\,\psi^*_{\mathbf{k}_1}(\mathbf{x})\,\mathbb{M}_{m_1m_2}(\mathbf{x})\,\psi_{\mathbf{k}_2}(\mathbf{x})\right]\,c^\dagger_{\mathbf{k}_1m_1}c_{\mathbf{k}_2m_2}+\text{h.c.}\\
=\;&\frac{\Omega_R}{2}\sum_{\mathbf{k}_1\mathbf{k}_2}\sum_{m}N(f,m)\left(\int d\mathbf{x}\,\psi^*_{\mathbf{k}_1}(\mathbf{x})\exp(i\boldsymbol{\varphi}\cdot\mathbf{x})\psi_{\mathbf{k}_2}(\mathbf{x})\right)\,c^\dagger_{\mathbf{k}_1m}c_{\mathbf{k}_2m-1}+\text{h.c.}\\
=\;&\frac{\Omega_R}{2}\sum_{\mathbf{k}}\sum_{m}N(f,m)c^\dagger_{\mathbf{k}m}c_{\mathbf{k}+\boldsymbol{\varphi}\,m-1}+\text{h.c.},
\end{aligned}\tag{2.13}$$

where $\boldsymbol{\varphi}=2\mathbf{k}_R$. This form of the hamiltonian can be justified by manipulating the integral in the positions:

$$\begin{aligned}
\int d\mathbf{x}\,e^{i\boldsymbol{\varphi}\cdot\mathbf{x}}\psi^*_{\mathbf{k}_1}(\mathbf{x})\psi_{\mathbf{k}_2}(\mathbf{x}) &= \sum_{\mathbf{R}}\exp\left[i\mathbf{R}\cdot(\boldsymbol{\varphi}-\mathbf{k}_1+\mathbf{k}_2)\right]\int_v d\,\mathbf{x}e^{i(\boldsymbol{\varphi}-\mathbf{k}_1+\mathbf{k}_2)\cdot\mathbf{x}}u^*_{\mathbf{k}_1}(\mathbf{r})u_{\mathbf{k}_2}(\mathbf{x})\\
&= \delta(\boldsymbol{\varphi}-\mathbf{k}_1+\mathbf{k}_2),
\end{aligned}\tag{2.14}$$

where v refers to the Wigner Seitz cell of the lattice, $u_{\mathbf{k}}(\mathbf{x})$ is the component of the Bloch function that is periodic in the lattice, i.e. $\psi_{\mathbf{k}}(\mathbf{x})=e^{i\mathbf{k}\cdot\mathbf{x}}u_{\mathbf{k}}(\mathbf{x})$. The term in eq.(2.13) can be expressed in the real space basis as following:

$$\sum_{\mathbf{R}}\Omega(f,m)\exp(i\boldsymbol{\varphi}\cdot\mathbf{R})\,c^\dagger_{\mathbf{R}m}c_{\mathbf{R}m-1}+\text{h.c.},\tag{2.15}$$

where $\Omega(f,m)=\Omega_R N(f,m)/2$. In the cases where only nearest neighbor hopping between lattice sites is considered, the final form of the many-body hamiltonian on the lattice reads:

$$\hat{H}=-t\sum_{\langle\mathbf{R}\mathbf{R}'\rangle}\sum_{m}c^\dagger_{\mathbf{R}m}c^\dagger_{\mathbf{R}'m}+\sum_{\mathbf{R}}\Omega(f,m)\exp(i\boldsymbol{\varphi}\cdot\mathbf{R})\,c^\dagger_{\mathbf{R}m}c_{\mathbf{R}m-1}+\text{h.c.},\tag{2.16}$$

The hamiltonian in eq.(2.16) besides the usual hopping term in real space, it contains also an hopping along the axis of the internal degrees of freedom, that is called synthetic dimension. Furthermore, a fermion that hops in the synthetic dimension acquires a phase, that depends on the lattice site.

In conclusion, exploiting light-matter interaction paves the way to the simulation of AGF on lattice models. In particular, using the scheme with two Raman beams shown in Fig.(2.7), it is possible to simulate a static magnetic field that couples the hyperfine levels of the atom, with a finite magnetic flux given by $\boldsymbol{\varphi}$.

2.4 Final remarks and brief plan of the thesis

The aim of this introduction was to resume briefly the wide range of possible configurations that can be achieved exploiting alkaline-earth and alkaline-earth like atoms and their interactions with light. Furthermore, a particular attention was paid to the parameters that can be controlled in the lab, mentioning some of the most recent goals achieved experimentally. In particular, it was shown that a wide class of Hubbard models can be simulated by the current state of the art of the cold-atomic experimental toolbox.

In the progress of the thesis, the most generic case, that was introduced for completeness will be not addressed. More specifically, the electronic (orbital) degree of freedom will be neglected. Nevertheless, the enlarged spin degeneration brought to the tunable number of fermionic species, together with the possibility of synthesizing gauge fields will be taken into account.

In the next chapter, it will be introduced in a more formal way the Hubbard model in its simplest configuration of two fermionic species in a single band, for introducing the issue related to the *Mott transition*: a metal to insulator transition brought by the strong interactions among fermions. For this purpose the concepts of *Fermi Liquid* and *Mott Insulator* will be given in order to achieve a full comprehension of the paramagnetic competing phases of the Hubbard-model. A systematic method for studying such a model is represented by the *Dynamical Mean Field Theory* (DMFT) that also will be introduced in the next chapter, and its application to the single-band Hubbard model will be reviewed.

In Chapt.(4), a generalization of the Mott transition in systems with an N-fold spin degeneration will be given. In the first part, it will be addressed the case of half-filling, that displays a Mott transition only when $N = 2M$. This is related to a fully symmetric spin-1/2 system with M degenerate orbitals. The case of odd values of N away from particle-hole symmetry also will be considered. In particular, the $SU(3)$-symmetric Hubbard model will be studied as a representative of this situation.

The main topic of Chapt.(5) focuses on the study of the multi-component Hubbard model in presence of artificial gauge fields. After an introductory discussion about a wide class of models that can be studied using DMFT, the specific case of $\boldsymbol{\varphi} = 0$ is addressed. In particular, it is considered the case of an artificial gauge field that acts as an hopping within the spin degree of freedom. This introduces the

concept of a *synthetic dimension* relative to the internal degrees of freedom of atoms. Furthermore, an analogy with multi-orbital systems that display different onsite energies for different orbitals is discussed. More specifically, a three component fermionic system is considered, in the case of a nearest neighbors hopping along the synthetic dimension with both open and periodic boundary conditions.

The last chapter of the thesis is devoted to the quantum magnetism arising from Hubbard models. In the first part, the two component Hubbard model is treated solving the DMFT equations generalized in oder to take into account long range antiferromagnetic solutions. The system is studied away from the half-filled configuration and at finite temperature. The second part focuses on the generalization of antiferromagnetism in the case of a three component systems in a tripartite lattice. After a brief introduction about the motivations for studying such a configuration, a mean-field analysis of the $SU(3)$-symmetric Hubbard model in the triangular lattice is provided. The possibility of treating such a system using DMFT is also discussed.

In the conclusions chapter the main results relative to the thesis will be briefly summarized and highlighted.

CHAPTER 3

THE HUBBARD MODEL AND DYNAMICAL MEAN FIELD THEORY

3.1 Introduction

One of the earliest triumphs of the band theory of solids has been to put on firm theoretical ground the distinction between metals and insulators. When electrons experience a periodic potential (due to the ions in a solid), their single-particle eigenvalues turn from the parabolic distortion of free electrons in vacuum into a series of energy bands $\epsilon_{\mathbf{k}\alpha}$ separated by energy gaps. If the mutual interaction between the particles is neglected, the many-body state can be simply built by progressively populating the energy levels, each with two electrons with opposite spin. If the number of electrons is such that a band is completely filled and the next one is empty, a gap for single-particle excitations opens and the system is an insulator, while in the case of a partially filled band, electrons can be excited with arbitrarily low energy and the system is a metal.

As a consequence, in a metal the single-particle density of states

$$g(\epsilon) = \frac{1}{N} \sum_{\mathbf{k}\alpha} \delta(\epsilon - \epsilon_{\mathbf{k}\alpha}) \tag{3.1}$$

at the Fermi energy is finite, while in an insulator the Fermi energy lies in the middle of the gap so that the density of states at that energy vanishes. One of the implications is that a necessary, but not sufficient, condition to have an insulator is that the number of electrons per atom is even.

All these simple results are however based on a single-particle picture, which is challenged when the interactions between the electrons are not negligible or they can not be described in terms of an effective single-particle potential. As matter of fact, already in the early decades of quantum mechanics, a series of experimental evidences has shown a clear and qualitative breakdown of this prediction. Indeed a number of oxides with a partially filled band have been experimentally found insulating. Consider for simplicity on the case where the valence band is half-filled, with one electron per orbital, in most cases, at low temperature, the insulating behavior is indeed accompanied by magnetic ordering with an antiferromagnetic pattern of the spins, whose direction alternates in every spatial direction.

This kind of ordering, which obviously spontaneously breaks the spin rotational symmetry, leads indeed to a doubling of the unit cell and doubles the number of bands in the reduces Brillouin zone. Therefore one of the two sub-bands becomes completely filled, while the other remains empty, leading to an effective band insulator. A similar picture can be also obtained within a static mean-field treatment of the interactions.

Yet, the magnetic symmetry breaking is not the end of the story in strongly correlated materials such as, V_2O_3 [46]. Indeed when the temperature is increased, the antiferromagnetic insulator turns into another insulating state which restores the magnetic symmetry and does not show signs of any alternative ordering. This insulating state defies any description in terms of a band picture, which means that the single-particle approximation breaks down calling for a fully non-perturbative treatment of the Coulomb interaction. Mott was indeed the first to blame electron-electron interactions for the breakdown of the band description and for the existence of interaction-driven insulators, which are therefore called "Mott insulators", while the transition between a metal and a Mott insulator as a function of any control parameter is called a "Mott transition".

The simplest theoretical framework to study and understand Mott insulators and Mott transition is the same Hubbard model we described in the previous chapter and that can be realized with ultracold atoms in optical lattices. Of course this model is

only a rough approximation of an actual material, but it is widely believed to contain the important physics to describe a Mott transition and the wealth of phenomena which stem from Mott physics.

The Hamiltonian is shown again here to make the manuscript more readable

$$H = -t \sum_{\langle \mathbf{R}\mathbf{R}' \rangle, \sigma} c^{\dagger}_{\mathbf{R}\sigma} c_{\mathbf{R}'\sigma} + U \sum_{\mathbf{R}} \hat{n}_{\mathbf{R}\uparrow} \hat{n}_{\mathbf{R}\downarrow} - \mu \sum_{\mathbf{R}\sigma} \hat{n}_{\mathbf{R}\sigma}, \tag{3.2}$$

where $c_{\mathbf{R}\sigma}$ is the destruction operator of a fermion with spin σ on the site $\mathbf{R}$, $\hat{n}_{\mathbf{R}\sigma} \equiv c^{\dagger}_{\mathbf{R}\sigma} c_{\mathbf{R}\sigma}$ is the number operator, t is the hopping amplitude, U the Hubbard on site repulsion and μ is the chemical potential. The parameters t and U can be expressed in terms of the electronic orbitals as following:

$$\begin{aligned} t &= \int d\mathbf{x}\, w_{\mathbf{R}}(\mathbf{x}) \left[-\hbar^2 \frac{\nabla^2}{2m} + V(\mathbf{x}) \right] w_{\mathbf{R}'}(\mathbf{x}) \\ U &= \int d\mathbf{x}\, d\mathbf{y}\, U(\mathbf{x}-\mathbf{y})\, w^2_{\mathbf{R}}(\mathbf{x}) w^2_{\mathbf{R}}(\mathbf{y}), \end{aligned} \tag{3.3}$$

where $V(\mathbf{x}+\mathbf{R}) = V(\mathbf{x})$ is the periodic potential that define the lattice, $\mathbf{R}$, $\mathbf{R}'$ are two nearest neighbor sites of the lattice, $U(\mathbf{x}-\mathbf{y})$ is the interaction term, and $w_{\mathbf{R}}(\mathbf{x})$ are the Wannier orbitals [3]. As mentioned above, the derivation of the model implies a number of approximations, from the neglect of multiorbital effects and related interactions to the absence of the lattice degrees of freedom and their coupling with the fermions and disorder effects.

In the case of a half-filled lattice (one fermion per lattice site), the model indeed describes rather naturally a metal in the non-interacting limit, where band theory holds, while in the opposite limit of vanishing hopping t (atomic limit) the energy is obviously minimized by placing one fermion per site. These fermions are indeed completely localized and describe the prototype of a Mott insulating state.

Despite the huge simplifications and the formal simplicity, the Hubbard model proved extremely resistent to theoretical investigations and exact solutions are known only in one dimension thanks to the Bethe ansatz [45], and in the limit of infinite dimension thanks to the Dynamical Mean-Field Theory [28], as it will be discussed in some more detials at the end of this chapter.

The reason why the Hubbard model is so hard to solve lies in the direct competition between two terms which tend to have opposite effects, and they are diagonal in two

conflicting representations. The hopping term, which gives rise to a kinetic energy for the lattice fermions, promotes delocalized metallic states and it can be diagonalizaed in momentum space, while the local interacting term tends to "freeze" the motion of the electrons and it is diagonal in real space. As it will be discussed in the following, this leads to a metallic solution in weak-coupling and to an insulating solution for strong coupling (and a half-filled shell). It is natural to expect a metal-insulator transition separting the two limiting cases, but it is not equally simple to obtain a reliable theoretical description of it. In the following the present discussion is expanded, highlighting some of the main properties of metallic and insulating solutions.

When the local interaction strength is nonzero and $U \ll t$ the system is expected to stay in a metallic phase and its low energy properties are well captured by the Fermi Liquid (FL) theory [60][7], that applies to systems whose spectrum of elementary excitations is similar to that one of a free Fermi gas. More precisely, within FL theory it is assumed a one to one correspondence between the states of a free Fermi gas and those of the interacting system. In other words, by switching on the interaction adiabatically, an eigenstate of the interacting system is obtained starting from an eigenstate of the non interacting system. This assumption does not hold in general, and in particular fails when bound states appear when the interaction is turned on. For example, a superconductor is not related in a direct way to the free Fermi gas, but rather to a coherent superposition of a large number of states of the non interacting system [7]. Nevertheless, FL theory succeeds to explain strong correlated metals, where the interactions ar responsible for mass enhancement as in the case of V_2O_3[38]. One of the basics of FL theory is the concept of quasi-particle. The equilibrium distribution of the non-interacting system is given by the Fermi-Dirac distribution function, therefore the number of particles of the ground-state are fixed by the chemical potential, in a grand-canonical picture. An elementary excitation of the system consists of adding one particle (hole) with momentum $\mathbf{p}$ outside (inside) of the Fermi surface. If interactions are adiabatically turned on, it is possible to obtain an elementary excitation of the interacting system of momentum $\mathbf{p}$, since momentum is conserved during collisions. Once the interaction is completely turned on, the added particle moves in an effective medium that is given by the surrounding particle distortion brought about the interactions. The particle is said to be dressed with a self-energy cloud, and the dressed particle is called quasiparticle. On the other hand, since quasi-particles undergo real collisions which leads to damping, any definition of elementary excitation is somewhat imprecise. Fortunately, close enough to the Fermi

Surface (FS), the life time of the quasi-particles becomes sufficiently long, and in pure system and at $T = 0$ it goes as the inverse square of the energy separation from the FS [60]. Therefore, FL theory states that close enough to the FS, it is possible to define coherent elementary excitations in a similar way that naturally happens in the non-interacting case.

A microscopic justification of FL can be obtained starting from the Hubbard model and studying the Green's function that is defined as:

$$G(\tau - \tau', \mathbf{R} - \mathbf{R}') \equiv -T_\tau \left\langle c_{\mathbf{R}\sigma}(\tau) c^\dagger_{\mathbf{R}'\sigma}(\tau') \right\rangle, \tag{3.4}$$

where translational and spin symmetry is assumed, and $c_{\mathbf{R}\sigma}(\tau) = e^{\tau H} c_{\mathbf{R}\sigma} e^{-\tau H}$ is the imaginary time evolution of the destruction operator.

In the non-interacting case, the model in eq.(2.2) reduces to a tight binding hamiltonian, that can be diagonalized by a Fourier transformation of the fields. Hence, at $U = 0$, the particles excitations are well described in momentum space by the energy dispersion $\epsilon_{\mathbf{k}}$ and by the Fermi-Dirac distribution function. In this case the Fourier transform of the Green's function is defined by

$$\mathcal{G}(i\omega_n, \mathbf{k}) = \frac{1}{i\omega_n - \xi_{\mathbf{k}}}, \tag{3.5}$$

where $\xi_{\mathbf{k}} = \epsilon_{\mathbf{k}} - \mu$, $i\omega_n = \frac{\pi}{\beta}(2n + 1)$ are the fermionic Matsubara frequencies with $\beta = 1/T$. In general, the Green's function in eq.(3.5), can be evaluated for a generic complex frequency, i.e. $\mathcal{G}(z, \mathbf{k}) = (z - \xi_{\mathbf{k}})^{-1}$, it has a pole in $\bar{z} = \xi_{\mathbf{k}}$ and:

$$\mathrm{Im}\mathcal{G}(\omega \pm i0^+) = \mp\pi\delta(\omega - \xi_{\mathbf{k}}). \tag{3.6}$$

From equations (3.6,3.1), it is clear how the DOS is related to the imaginary part of the non-interacting Green's function.

In the interacting case reads, the interacting Green's function can be obtained using the Dyson equation:

$$G(z, \mathbf{k}) = \frac{1}{z - \xi_{\mathbf{k}} - \Sigma(z, \mathbf{k})}, \tag{3.7}$$

where $\Sigma(z, \mathbf{k})$ is the self energy of the interacting quasi-particles [11][52]. At weak coupling, perturbation theory assures that Appendix():

$$\mathrm{Im}\Sigma(\omega + i0^+, \mathbf{k}) \propto \omega^2 \qquad \text{when} \;\; \omega \sim 0. \tag{3.8}$$

Therefore, in the weak coupling regime and for low energies, the green's function can be approximated as following:

$$G(\omega + i0^+, \mathbf{k}) \sim \frac{1}{\omega - \xi_{\mathbf{k}} - \mathrm{Re}\Sigma(\omega + i0^+, \mathbf{k})}. \tag{3.9}$$

The denominator of eq.(3.9) has a simple pole in $z = \tilde{\xi}_{\mathbf{k}}$, i.e. the self-energy is an analytic function in the complex plane, the residue of $G(z, \mathbf{k})$ can be calculated:

$$Z_{\mathbf{k}} \equiv \lim_{z \to \tilde{\xi}_{\mathbf{k}}} (z - \tilde{\xi}_{\mathbf{k}})\, G(z, \mathbf{k}) = \left(1 - \frac{\partial \mathrm{Re}\Sigma}{\partial z}\bigg|_{z=\tilde{\xi}_{\mathbf{k}}}\right)^{-1}. \tag{3.10}$$

To be consistent with the previous approximation on the imaginary part of the self energy in eq.(3.8), the pole of the Green's function must be close to the FS, i.e. $\tilde{\xi}_{\mathbf{k}} \sim 0$.

Therefore close the the Fermi-surface, the Green's function can be approximated by the first term of its power expansion around the simple pole in $z = \tilde{\xi}_{\mathbf{k}}$, namely

$$G(z, \mathbf{k}) \sim \frac{Z_{\mathbf{k}}}{z - \tilde{\xi}_{\mathbf{k}}}, \qquad \text{when} \quad z \sim 0. \tag{3.11}$$

This result obtained using many-body physics considerations, confirms what FL theory states, that for weak coupling, the system is expected to have coherent excitations close enough to the Fermi-surface. In general, as long as the condition in eq.(3.9) is fulfilled close to the FS, the Green's function can always be written as

$$G(z, \mathbf{k}) = \frac{Z_{\mathbf{k}}}{z - \tilde{\xi}_{\mathbf{k}}} + G_{inc}(z, \mathbf{k}) \tag{3.12}$$

where the second term on the RHS, is a reminder that takes into account the incoherent single-particle excitations, away from the Fermi surface. When this description is valid, the system is said to be in a FL state, where coherent excitations are defined close to the Fermi Surface.

If $\Sigma(z, \mathbf{k})$ does not depend on $\mathbf{k}$, $Z_{\mathbf{k}} \equiv Z$ gives the ratio between the free-electrons and the interacting electron masses, i.e.:

$$Z = m/m^*. \tag{3.13}$$

This result leads to the more physical interpretation of the FL, where the motion of a

quasi-particle with an energy very close to the FS can be approximated as the motion of a free electron but with an effective mass given by eq.(3.13).

Another feature of the FL state is that the Luttinger theorem holds [48]. In the case of a **k**-independent self-energy the theorem reads [28]:

$$n = \sum_{\alpha} \int_{-D}^{D} d\epsilon \, g(\epsilon) \, \theta(-\epsilon + \mu - \mathrm{Re}\Sigma(i0^+)). \tag{3.14}$$

In other words the density of the interacting system is the same of a non-interacting system whose chemical potential is $\tilde{\mu} = \mu - \mathrm{Re}\Sigma(i0^+)$.

Another important properties is that the imaginary part the of Green's function calculated at $\tilde{\mu}$ is independent on the interactions and matches its non-interacting value, called the pinning value:

$$-\frac{1}{\pi}\mathrm{Im}G(i0^+) = g(\tilde{\mu}). \tag{3.15}$$

This last property of the FL is easy to show, once it is assumed that $\mathrm{Im}\Sigma(\omega + i0^+) \propto \omega^2$, in fact, in the case of a **k**-independent self-energy :

$$\begin{aligned} \mathrm{Im}G(i0^+) &= \lim_{\eta \to 0^+} \int_{-D}^{D} d\epsilon \, g(\epsilon) \, \frac{1}{-\epsilon + \mu - \Sigma(i0^+) + i\eta} \\ &= -\int_{-D}^{D} d\epsilon \, g(\epsilon) \overbrace{\left[\lim_{\eta \to 0^+} \frac{\eta}{(-\epsilon + \mu - \Sigma(i0^+))^2 + \eta^2} \right]}^{\pi \, \delta(-\epsilon + \mu - \Sigma(i0^+))} \\ &= -\pi \, g(\tilde{\mu}) \, . \end{aligned} \tag{3.16}$$

On the other hand, when $U/t \gg 1$, the system is better described in real space, rather than in momentum space. At $t = 0$, the single band Hubbard model of N degenerate species of fermions $\alpha = 1, ..., N$ becomes a sum of disconnected single site models:

$$H = U \sum_{\mathbf{R}} \sum_{\alpha < \beta} n_{\mathbf{R}\alpha} n_{\mathbf{R}\alpha'} - \mu \sum_{\mathbf{R}\alpha} n_{\mathbf{R}\alpha} = \sum_{\mathbf{R}} h_{\mathbf{R}}, \tag{3.17}$$

where $h_{\mathbf{R}} = \sum_{\alpha < \beta} \hat{n}_{\mathbf{R}\alpha} \hat{n}_{\mathbf{R}\alpha'} - \mu n_{\mathbf{R}\alpha}$.

Since the full hamiltonian can be written as the sum of many local hamiltonians, the

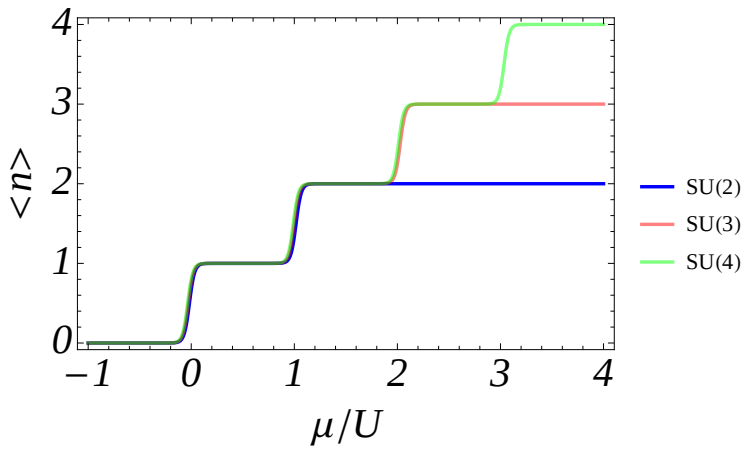

Figure 3.1: The average density calculated in the atomic limit as a function of the chemical potential at $\beta = 10$, for different spin degeneracies $N = 2, 3, 4$.

partition function of the system is given by the product of the local partition functions. Therefore, it is enough to analyze the local partition function at a generic site. The local hamiltonian can be written in terms of the total density $n = \sum_\alpha n_\alpha$:

$$h = \frac{U}{2}\hat{n}^2 - \left(\mu + \frac{U}{2}\right)\hat{n}. \tag{3.18}$$

Consequently the partition function reads:

$$\mathcal{Z} = \sum_n p(n) e^{-\beta h(n)}, \tag{3.19}$$

where n are the eigenvalues of $\hat{n}$, $p(n) = \begin{pmatrix} N \\ n \end{pmatrix}$ takes into account of the degeneracy of the sector at fixed density. The total density average value is given by the following relation:

$$\langle n \rangle = -\frac{1}{\beta \mathcal{Z}} \frac{\partial \mathcal{Z}}{\partial \mu}. \tag{3.20}$$

In Fig.(3.1) it is shown the behavior of $\langle n \rangle$ as a function of μ, for different values of β. It is clear that the system is in a insulating state at integer filling, since its compressibility vanishes in proximity of the density plateaus. In fact, the density remains fixed until the chemical potential fills the energy gap of the spectral function.

In order to grasp the deep difference between this insulating state and the FL-state mentioned above, it is worth to study the Green's function in the limit of strong

interactions. The Fourier transform of the Green's function, at $T = 0$, can be expressed via Lehmann representation:

$$G_\alpha(i\omega_n) = \frac{1}{\mathcal{K}} \sum_{|0\rangle} \sum_n \left[\frac{\overbrace{\left|\langle n| c_\alpha^\dagger |0\rangle\right|^2}^{p}}{i\omega_n + E_0 - E_n} + \frac{\overbrace{\left|\langle n| c_\alpha |0\rangle\right|^2}^{h}}{i\omega_n + E_n - E_0} \right], \tag{3.21}$$

where $\{|0\rangle\}$ is the many-body ground state manifold and $\mathcal{K}$ its cardinality, $E_0 - E_n$ is the energy difference between the ground state and the n-th excited state. The subscripts p and h label respectively the particle and hole contributions to the single particle propagator, connecting the ground state, that belong to the subspace with a total number of fermions M to the subspaces with total number of fermions $M \pm 1$.

Therefore, in the case of $N = 2$, with $\mu = \frac{U}{2}$, that correspond to $\langle n \rangle = 1$ the green's function reads

$$G_\alpha(i\omega_n) = \frac{1}{2} \left(\frac{1}{i\omega_n + \frac{U}{2}} + \frac{1}{i\omega_n - \frac{U}{2}} \right) = \frac{1}{i\omega_n - \frac{U^2}{4} \frac{1}{i\omega_n}}. \tag{3.22}$$

It is worth to notice that the self-energy of the system $\Sigma(i\omega_n) \propto 1/i\omega_n$ it is non-analytic at the origin of the complex plane and diverges. Furthermore the spectral function that is given by the formula:

$$A(\omega) = -\frac{1}{\pi} \mathrm{Im} G(\omega + i0^+), \tag{3.23}$$

has the form of two delta functions centered respectively in $\pm U/2$, with no spectral weight at the Fermi energy. When $U \gg t$, but U is not infinite, the hopping term broadens the two Dirac deltas yielding the so called Hubbard bands, that correspond to incoherent high energy excitations and the system is said to be in a Mott Insulator (MI) state.

In summary, in this introduction the main differences between the FL and MI states were pointed out. More specifically, it has been stated that the MI state cannot be obtained using perturbation theory since its self-energy it is not an analytic function at half filling.

In the next section will be presented the Dynamical Mean-Field Theory (DMFT), a powerful non-perturbative method that therefore provides a tool to study the evolution between the two limiting cases as a function of the ration U/t.

3.2 Dynamical Mean-Field Theory

DMFT is emerging in the few last decades as one of the reference method to treat strongly correlated systems. The main idea behind this method is to extend the mean-field concept, in which every position in the lattice is equivalent for the description of the physics, to a quantum domain. From a more formal point of view, DMFT is based on the construction of a *local* effective theory starting from a lattice model. The equivalence between the lattice model and the effective local theory is then enforce requiring that a dynamical observable, the single-particle Green's function computed in the local theory coincides with the local component of the lattice Green's function in the DMFT approximation. This is clearly a generalization of the static mean-field, where a static observable (e.g., the magnetization in a Ising model) is replaced by a dynamical (frequency dependent observable).

More specifically, in the case of the Hubbard model the effective theory is defined by the effective action (which it is written in imaginary time, but the same equations can be derived for real-time observables):

$$S_{eff} = \sum_{\sigma} \iint d\tau \, d\tau' \, \bar{\psi}_{\sigma}(\tau) \, \mathcal{G}^{-1}(\tau - \tau') \, \psi_{\sigma}(\tau) + U \int d\tau \, n_{\uparrow}(\tau) n_{\downarrow}(\tau), \tag{3.24}$$

where $\bar{\psi}_{\sigma}$, ψ_{σ} are grassman variables, τ is the imaginary time. $\mathcal{G}^{-1}$ is the so-called dynamical *Weiss field* which includes the effect of the rest of the lattice on the site that has been selected to build the local theory. The crucial approximation with respect to an exact treatment is that all the higher-order propagators have been neglected and the rest of the lattice acts like an effective bath which has to be determined self consistently as will be discussed later.

It is worth to notice that despite the approach neglects by construction any spatial fluctuation, nevertheless, since $\mathcal{G}^{-1}$ depends on time, the quantum dynamical fluctuations are fully taken into account without further approximations. Within DMFT the self-energy of the effective local theory, which is constructed as a site-independent quantity, plays the role of the lattice self-energy, namely:

$$\Sigma(\mathbf{k}, i\omega_n) \equiv \Sigma(i\omega_n), \tag{3.25}$$

where $\omega_n = (2n+1)\pi/\beta$ are the fermionic Matsubara frequencies.

Therefore, the main assumption made in DMFT consists in assuming a local form

of the self-energy that is a function of the frequencies only. Although this is a very strong assumption, nevertheless it is exact (in any space dimensions) both in the non-interacting and in the opposite atomic limit, and it allows for a faithful and rich description for both the Fermi liquid and Mott insulator phases with no bias in favor of one or the other. Furthermore, it gives the possibility of establish whether the system is in a Fermi liquid or in a Mott insulating state by studying the analytical properties of the self-energy and two study many relevant dynamical observables, as opposed to many other theoretical approaches.

3.2.1 Effective action and DMFT equations

In this section will be reviewed the basic derivation of DMFT using the cavity method. The partition function of the Hubbard model can be expressed in the path integral formulation as following:

$$Z = \int \prod_{\mathbf{R}\sigma} \mathcal{D}\bar{\psi}_{\mathbf{R}\sigma} \mathcal{D}\,\psi_{\mathbf{R}\sigma}\, \exp\left(-S\left[\bar{\psi},\psi\right]\right), \tag{3.26}$$

where the Hubbard model action reads:

$$\begin{aligned} S\left[\bar{\psi},\psi\right] &= \int d\tau \sum_{\mathbf{R}\mathbf{R}'\sigma} \bar{\psi}_{\mathbf{R}\sigma}(\tau)\left[(\partial_\tau - \mu)\,\delta_{\mathbf{R}\mathbf{R}'} - t_{\mathbf{R}\mathbf{R}'}\right]\psi_{\mathbf{R}'\sigma}(\tau) \\ &+ U \int d\tau \sum_{\mathbf{R}} n_{\mathbf{R}\uparrow}(\tau) n_{\mathbf{R}\downarrow}(\tau), \end{aligned} \tag{3.27}$$

where $\bar{\psi}_{\mathbf{R}\sigma}$, $\psi_{\mathbf{R}\sigma}$ are grassmannian variables, $t_{\mathbf{R}\mathbf{R}'}$ is hopping matrix, that is non zero only if $\mathbf{R}$ and $\mathbf{R}'$ are nearest neighbors. The effective action in eq.(3.24) is defined as

$$\frac{1}{Z_{eff}} \exp\left(-S_{eff}[\bar{\psi}_\sigma,\psi_\sigma]\right) \equiv \frac{1}{Z} \int \prod_{\mathbf{R}\neq\mathbf{0},\,\sigma} \mathcal{D}\bar{\psi}_{\mathbf{R}\sigma} \mathcal{D}\psi_{\mathbf{R}\sigma} \exp\left(-S[\bar{\psi},\psi]\right), \tag{3.28}$$

where all the fermions are integrated out except for $\psi_\sigma \equiv \psi_{\mathbf{R}=\mathbf{0}\,\sigma}$. It is worth to notice that the knowledge of S_{eff} allows for the calculations of all the *local* correlation functions relative to the original Hubbard model. This observation is valid for any number of dimensions. In order to proceed with the evaluation of the formal expression of S_{eff}, it is useful to split the full lattice action into three part: $S = S_{\mathbf{0}} + S^{(\mathbf{0})} + \Delta S$,

where $S^{(\mathbf{0})}$ is the lattice action in presence of the "cavity" in $\mathbf{R} = \mathbf{0}$, and

$$\begin{aligned} S_{\mathbf{0}} &= \int d\tau \sum_{\sigma} \bar{\psi}_{\sigma}(\tau)(\partial_{\tau} - \mu)\psi_{\sigma}(\tau) + U\, n_{\uparrow}(\tau)\, n_{\downarrow}(\tau), \\ \Delta S &= -\int d\tau \sum_{\mathbf{R}\sigma} t_{\mathbf{0R}} \left[\bar{\psi}_{\mathbf{R}\sigma}(\tau)\, \psi_{\sigma}(\tau) + \bar{\psi}_{\sigma}(\tau)\, \psi_{\mathbf{R}\sigma}(\tau) \right]. \end{aligned} \tag{3.29}$$

Here, $\eta_{\mathbf{R}} \equiv t_{\mathbf{0R}}\, \psi_{\sigma}$ can be consider as the source coupled to the field $\bar{\psi}_{\mathbf{R}\sigma}$, and it can be defined the following functional:

$$\mathcal{W}[\bar{\psi}, \psi, \bar{\eta}, \eta] \equiv \ln \left[\left\langle \exp\left(\int d\tau \sum_{\mathbf{R}\sigma} \bar{\eta}_{\mathbf{R}\sigma}(\tau)\, \psi_{\mathbf{R}\sigma}(\tau) + \bar{\psi}_{\mathbf{R}\sigma}(\tau)\, \eta_{\mathbf{R}\sigma}(\tau) \right) \right\rangle_{S^{(\mathbf{0})}} \right], \tag{3.30}$$

where the average value over the cavity action $S^{\mathbf{0}}$ of a generic operator $\mathcal{O}$ is defined as $\langle \mathcal{O} \rangle_{S^{(\mathbf{0})}} \equiv \frac{1}{Z^{(\mathbf{0})}} \int \prod_{\mathbf{R}\neq\mathbf{0},\sigma} \mathcal{D}\bar{\psi}_{\mathbf{R}\sigma} \mathcal{D}\psi_{\mathbf{R}\sigma} \left[\exp\left(-S^{(\mathbf{0})}\right) \mathcal{O} \right]$.
The functional in eq.(3.30) is the generating functional of the connected Green's function of system in presence of the cavity, that can be computed via its functional derivatives as:

$$G^{(\mathbf{0})}(\alpha_1, ..., \alpha_n | \alpha'_1, ..., \alpha'_n) \equiv \left. \frac{\delta^{2n} \mathcal{W}\left[\bar{\eta}, \eta\right]}{\delta\bar{\eta}(\alpha_1)...\delta\bar{\eta}(\alpha_n)\, \delta\eta(\alpha'_1)...\delta\eta(\alpha'_n)} \right|_{\bar{\eta}=0, \eta=0}, \tag{3.31}$$

where $\alpha_i \equiv (\tau_i, \mathbf{R}_i)$ is a composite index including imaginary time and position [52].
Therefore the effective action in eq.(3.28) can be expressed in the following way:

$$S_{eff} = S_{\mathbf{0}} + \mathcal{W} + \text{const.} \tag{3.32}$$

Hence, S_{eff} may be expanded in powers of the sources $\eta_{\mathbf{R}\sigma}$ using the relation in eq.(3.30)

$$S_{eff} = S_{\mathbf{0}} + \sum_{n} \sum_{\alpha_1 ... \alpha'_n} \bar{\eta}(\alpha_1)...\bar{\eta}(\alpha_n)\, \eta(\alpha'_1)...\eta(\alpha'_n)\, G^{(\mathbf{0})}(\alpha_1, ..., \alpha_n | \alpha'_1, ..., \alpha'_n), \tag{3.33}$$

where the notation of $\sum_{\alpha_1} \to \int d\tau_1 \sum_{\mathbf{R}_1}$ was adopted for the summation over the compact indices and the irrelevant constant factor was dropped. Now it can be exploited the limit of large coordination number. In fact, in this limit dimension the hopping terms must be rescaled to $t_{\mathbf{RR'}} \to d^{-\|\mathbf{R}-\mathbf{R'}\|/2}\, t^{*}_{\mathbf{RR'}}$, where d is the dimensionality of the system and $\|.\|$ is the Manhattan norm between two lattice sites. The n-th order of the expansion scales as d^{n-2} [28], so that only $n = 2$ survives in the

limit $d \to \infty$. Within this great simplification the effective action in infinite dimension reads as in eq.(3.24), where the Weiss field $\mathcal{G}^{-1}$ is given by the Fourier transform of

$$\mathcal{G}^{-1}(i\omega_n) = i\omega_n + \mu - \sum_{\mathbf{R}\mathbf{R}'} t_{\mathbf{0}\,\mathbf{R}}\, t_{\mathbf{0}\,\mathbf{R}'}\, G^{(\mathbf{0})}_{\mathbf{R}\mathbf{R}'}(i\omega_n). \tag{3.34}$$

This last expression is very important because it relates the Weiss field to the Green's function of the Hubbard model with one site removed. In order to obtain a closed set of equations one still needs to relate the Weiss field to the original lattice Green's function. In this case the limit of infinite dimension is very useful again, nevertheless this relation remains still complicated for a generic lattice. In the particular case of the *Bethe lattice* that corresponds to a Cayley tree with an infinite coordination number, the relation is easily obtained. In fact in this case, the summation in eq.(3.34) is restricted to $\mathbf{R} = \mathbf{R}'$, since neighbors of $\mathbf{0}$ are totally disconnected once the cavity has been introduced. Furthermore, one can exploit translational invariance symmetry that imposes $G^{(\mathbf{0})}_{\mathbf{R}\mathbf{R}} = G_{\mathbf{R}\mathbf{R}} = G_{\mathbf{0}\mathbf{0}} \equiv G$, where $G(i\omega_n)$ corresponds to the Green's function of the effective local hamiltonian, nameley: $G(i\omega_n) = \int_0^\beta d\tau\, e^{i\omega_n \tau} G(\tau)$, with $G(\tau - \tau') = -\left\langle \psi(\tau)\, \bar{\psi}(\tau') \right\rangle_{S_{eff}}$. The summation in eq.(3.34) becomes

$$G(i\omega_n) \sum_{\mathbf{R}} t^2_{\mathbf{0}\,\mathbf{R}} = t^2 G(i\omega_n) \overbrace{\left(d^{-1} \sum_{n.n.} \right)}^{1} = t^2 G(i\omega_n), \tag{3.35}$$

where $n.n.$ indicates the summation over the sites $\mathbf{R}$ that are nearest neighbors of the cavity, t is the rescaled hopping. Therefore, the DMFT equations in the case of infinite dimension and for a Bethe lattice read

$$\begin{aligned} \mathcal{G}^{-1}(i\omega_n) &= i\omega_n + \mu - t^2 G(i\omega_n) \\ G(\tau - \tau') &= -\left\langle \psi_\sigma(\tau) \bar{\psi}_\sigma(\tau') \right\rangle_{S_{eff}} . \end{aligned} \tag{3.36}$$

It is worth to notice that since G is the local Green's function of the Hubbard model it can be calculated using the local effective action defined in eq.(3.28).

For a generic lattice with an energy dispersion $\epsilon_{\mathbf{k}}$, whose non-interacting density of states is $g(\epsilon)$, the DMFT equations can be expressed in the following way:

$$\begin{aligned} G(i\omega_n) &= \sum_{\mathbf{k}} \frac{1}{i\omega_n + \mu - \epsilon_{\mathbf{k}} - \Sigma(i\omega_n)} = \int d\epsilon\, \frac{g(\epsilon)}{i\omega_n + \mu - \epsilon - \Sigma(i\omega_n)} \\ \Sigma(i\omega_n) &= G^{-1}(i\omega_n) - \mathcal{G}^{-1}(i\omega_n), \end{aligned} \tag{3.37}$$

where $\Sigma(i\omega_n)$ is the self-energy of the effective action. This equations couples the local Green's function of the lattice model obtained through a summation over $\mathbf{k}$ to the Weiss field of the effective action. These equations are exact in the limit of infinite dimension. In the case of finite dimensionality, the DMFT can be solved in the same way, nevertheless their solutions constitute an approximation of the real model. In general, when d is finite the self-energy depends on $\mathbf{k}$, while in $d = \infty$ it does not. Therefore, the main approximation brought by a DMFT scheme is to assume that $\Sigma(i\omega_n, \mathbf{k}) \sim \Sigma(i\omega_n)$, that is good for high dimensionality and it becomes less reliable at low dimensions. Nevertheless, it is worth to notice that when such an assumption has been done, one has full access to all non-local quantities that can be calculated through the self-energy. The most straightforward example of that is represented by the Green's function evaluated in $\mathbf{k}$ space, i.e. $G(i\omega_n, \mathbf{k}) = (i\omega_n + \mu - \epsilon_{\mathbf{k}} - \Sigma(i\omega_n))^{-1}$.

3.2.2 Solving the effective local theory

Once the DMFT equations have been set up, one still needs a method to solve the interacting effective action in eq.(3.24), in order to compute the Green's function (or equivalently the self-energy) starting from a generic form of the Weiss field. Then one has to obtain a Weiss field such that the corresponding Green's function of the effective local theory satisfies the self-consistency condition 3.37. This is customarily realized by iterative solution of the effective theory: starting from a guess for the Weiss field, the new Green's function is computed from the AIM and then used to produce a new Weiss field. The process is repeated until the old and the new Weiss fields coincide within a given accuracy.

For this reason, and also to obtain a better physical insight, it is very useful to represent the effective action in eq.(3.24) in a Hamiltonian form. The Anderson Impurity Model (AIM) introduces by P.W. Anderson [2] to study localized magnetic states in metal, constitutes a natural choice for this purpose. In particular, this model describes a bath of non-interacting fermions coupled via hybridization terms to a local interacting impurity. The hamiltonian of the AIM reads:

$$H_{AIM} = \sum_{\ell\sigma} \epsilon_{\ell\sigma}\, d^\dagger_{\ell\sigma} d_{\ell\sigma} + \sum_{\ell\sigma} V_{\ell\sigma} d^\dagger_{\ell\sigma} c_\sigma + \text{h.c.} + U n_\uparrow n_\downarrow - \mu \sum_\sigma n_\sigma \,, \tag{3.38}$$

where $c^\dagger_\sigma$ is the creation operator of a fermion on the impurity, $n_\sigma \equiv c^\dagger_\sigma c_\sigma$, $d^\dagger_{\ell\sigma}$ is the creation operator of a fermion of the the non-interacting bath. The parameters $\epsilon_{\ell\sigma}$, $V_{\ell\sigma}$

represent the energy levels of the bath and the hybridization amplitudes respectively and they are often called *Anderson parameters*. One can easily show by integrating out the bath degrees of freedom that this model indeed represents the effective action in eq.(3.24), and that in this representation the Weiss field assumes the following form:

$$\mathcal{G}_\sigma^{-1}(i\omega_n) = i\omega_n + \mu - \sum_\ell \frac{|V_{\ell\sigma}|^2}{i\omega_n - \epsilon_{\ell\sigma}}, \tag{3.39}$$

that corresponds to the inverse of the Green's function of the AIM at $U = 0$ (which has nothing to do with the non-interacting local component of the lattice Green's funtion). Hence the Anderson parameters determines the effective local theory.

Several methods have been proposed and used to study the AIM in the context of DMFT, which go under the collective name of "impurity solvers". Among the most powerful numerical methods, are mentioned the Continuous-Time Quantum Monte Carlo, the Numerical Renormalization Group and the Exact Diagonalization. Approximate analyical tools like different kinds of perturbation theory, slave-bosons and similar methods have been employed to reach a better analytical insight.

Here it will be presented in some detail the exact diagonalization algorithm that has been implemented by the author of this thesis. In order to use any exact diagonalization method the size of the Hilbert space must be finite and sufficiently small to be handled. For this purpose it is necessary to truncate the infinite series in eq.(3.39) to a finite number N_s, that physically translates into an AIM with a finite number of discrete energy levels in the bath. The cycle is initialized with a first choice of the Anderson parameters. After, the system is diagonalized and the spectral properties, i.e. the Green's function and the self-energy are calculated using the Lanczos technique. The self-consistence equation is used to compute the new Weiss field $\mathcal{G}_{new}^{-1}$. At this point it is necessary to infer from $\mathcal{G}_{new}^{-1}$ the new set of Anderson parameters through the minimization of the following function:

$$\chi\left(\{V_{\ell\sigma}\}, \{\epsilon_{\ell,\sigma}\}\right) \equiv \left(\sum_{i\omega_n} f(i\omega_n) |\mathcal{G}_{new}(i\omega_n) - \mathcal{G}_{Ns}(i\omega_n;\, \{V_{\ell\sigma}\}, \{\epsilon_{\ell\sigma}\})|^p \right)^{1/p}, \tag{3.40}$$

where

$$\mathcal{G}_{N_s}^{-1}(i\omega_n;\, \{V_{\ell\sigma}\}, \{\epsilon_{\ell\sigma}\}) \equiv i\omega_n + \mu - \sum_\ell^{N_s} \frac{|V_\ell|}{i\omega_n - \epsilon_\ell}\,. \tag{3.41}$$

and $f(i\omega_n)$ is a positive weight. The function χ represents a norm between two

functions of the Matsubara frequencies and it is not univocally defined, therefore the expression in eq.(3.40) constitutes just a possible choice. Once the new set of Anderson parameters is obtained a new iteration of the DMFT cycle starts and the loop closes when the convergence of the Weiss field is achieved.

3.3 Mott Transition at half filling.

The spectral weight at the fermi energy $A(\omega = 0)$ establishes whether the system is an insulator or not. Nevertheless, this quantity can assume only two values: $A(0) = g(0)$, where $g(\epsilon)$ is the DOS, in the FL, as stated in eq.(3.16), and $A(0) = 0$ in the insulator.

Therefore, it does not give any quantitative information about the correlations of the metal close to the MIT. Hence, other important quantities to study are the quasi-particle residue, the self-energy of the system as well as the whole spectral function $A(\omega)$, that contains also the high energy incoherent contributions introduced in eq.(3.12).

The DMFT equations in eq.(3.37) admit both metallic and insulating solutions. The latter exist when $U > U_{c1}$, while the metallic solution exists when $U < U_{c2}$. Numerical and analytical evidences [28] show that $U_{c1} < U_{c2}$, hence when $U_{c1} < U < U_{c2}$ the metallic and insulating solutions coexist, and a first order phase transition is expected at $U = U_c$, when the free energies relative to the two different solutions cross. Nevertheless, it is easy to show analytically that, at $T = 0$, $U_c = U_{c2}$, and in this specific case the MIT is a second order phase transition [51].

In Fig.(3.2) the spectral density $A(\omega)$ is shown for several values of U. This result has obtained using IPT method for solving the AIM [28][71]. For small U, the spectral function is similar to the non-interacting density of states, while for larger values of U, a narrow quasiparticle peak is formed at the Fermi level of width ZD and weight Z. At $U/D = 3$, the spectral weight at high energy (Hubbard Bands) is well separated from the quasi-particle peak that shrinks at fixed height. At $U/D = 4$ there is no spectral weight at the FS and the system is a MI.

Fig.(3.3) shows the quasi-particle weight as a function of the interaction strength and the imaginary part of the Green's function evaluated on the imaginary axis for different values of U, obtained using ED calculations with $N_s = 6$. The imaginary part

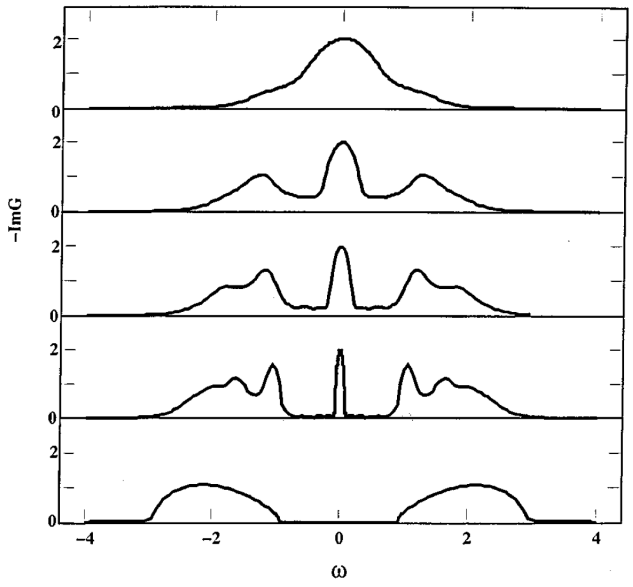

Figure 3.2: Sectral density at $T = 0$, for several values of U, obtained by the iterated perturbation theory approximation. The first four curves (from top to bottom, $U/D = 1, 2, 2.5, 3$) correspond to an increasingly correlated metal, while the bottom one ($U/D = 4$) is an insulator.

of the Green's function tends to the pinning value as long as the system is in a FL state, i.e. $\mathrm{Im}G(i0^+) = -2/D$ in the case of a semicircular DOS $g(\epsilon) = \frac{2}{D\pi}\sqrt{D^2 - \epsilon^2}$. On the other hand, when the system is in an insulating state $\mathrm{Im}G(i\omega_n) \propto \omega_n$ as in the atomic limit. It is worth to notice also, the differences between the correlated metal close to the MIT and the weak correlated metal. At weak coupling the Green's function is monotonic, it reaches the pinning value at $\omega_n = 0^+$ and it has a power law behavior at high frequencies. In the coexistence region, the Green's function shares the same asymptotic behavior for low and high frequencies as in the weak coupling case, nevertheless a local maximum at $\omega_n = \omega_{max}$ and a local minimum at $\omega_n = \omega_{min}$ appear, with $\omega_{max} \leq \omega_{min}$ and $\omega_{max}(U \to U_{c2}) = 0^+$. In this case, when $\omega_{max} < \omega_n < \omega_{min}$, the Green's function decreases as in the insulating cases. Therefore, also when evaluated on the imaginary axis, the Green's function of the correlated metal it is very similar to the Green's function of the Mott insulator, in a non-trivial range of intermediate frequencies.

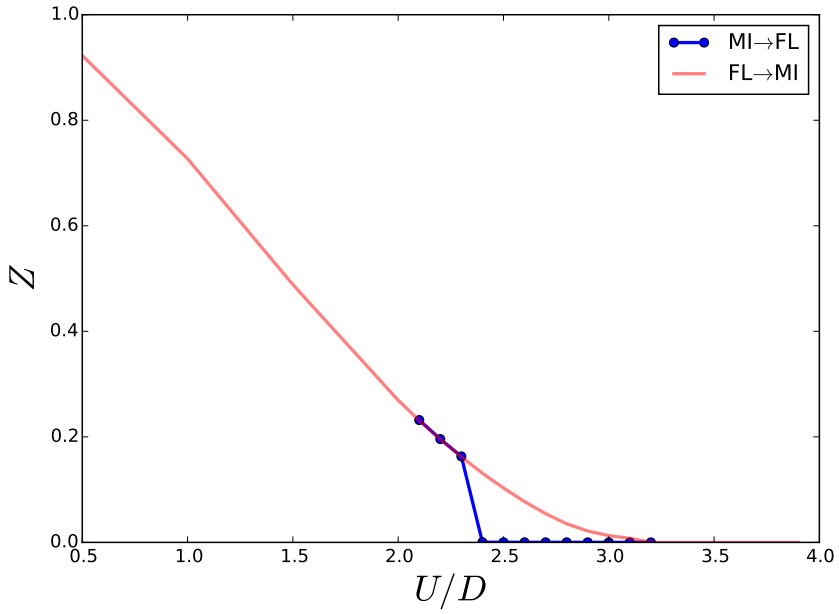

Figure 3.3: The quasiparticle weight as a function of the interaction strength U. The thick red line is relative to the DMFT solutions obtained starting from a FL initial state and by increasing the value of U. Instead, the blue dots are relative to the DMFT solutions obtained from a MI initial state and by decreasing the value of U.

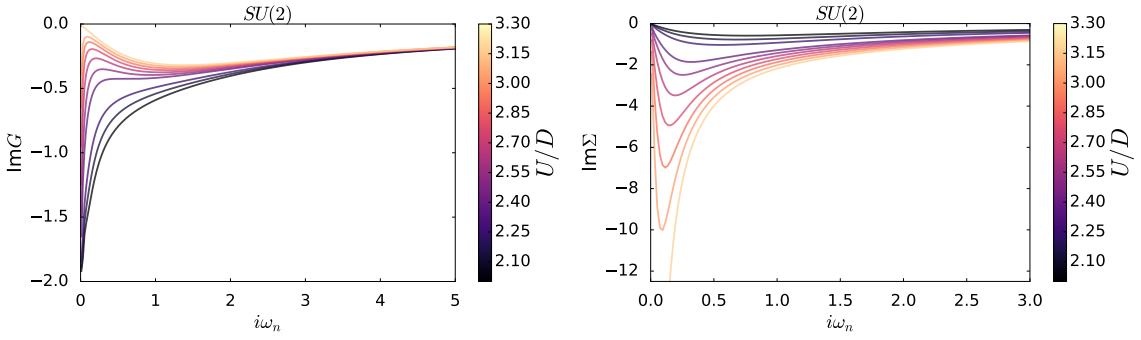

Figure 3.4: On the left side, the imaginary part of the Green's function evaluated on the imaginary axis for several values of the interaction strength. On the right side, the imaginary part of the self energy evaluated on the imaginary axis for several values of the interaction strength.

Part II

Results

CHAPTER 4

$SU(N)$-SYMMETRIC HUBBARD MODELS.

4.1 Introduction

This chapter is dedicated to the study of the Mott transition in $SU(N)$-symmetric Hubbard Models, that can be simulated using ^{173}Yb atoms in optical lattices. In particular, the Hubbard hamiltonian for a multi-component fermionic systems reads:

$$H = -t \sum_{\mathbf{R}\mathbf{R}'m} c^{\dagger}_{\mathbf{R}m} c_{\mathbf{R}'m} + U \sum_{\mathbf{R}} \sum_{m<m'} n_{\mathbf{R}m} n_{\mathbf{R}m'} - \mu \sum_{\mathbf{R}\,m} n_{\mathbf{R}m'}, \tag{4.1}$$

where $c_{\mathbf{R}m}$ is the destruction operator of the m-th fermionic component on the lattice site $\mathbf{R}$, and the m runs over the integer values $1, 2, .., N$.

First, it is considered the case of a half-filled configuration, which indeed can give a Mott transition only at $N = 2M$, where the $SU(N)$ model corresponds to a fully symmetric spin-1/2 system with M degenerate orbitals. For odd N a half-filled system has a non integer number of fermions per site and therefore cannot undergo full Mott localization. It is easy to realize that for symmetric bands the half-filling condition is obtained by imposing particle-hole symmetry, that in a bipartite lattice rads $c_{\mathbf{R}\,m} \to (-1)^{\mathbf{R}} c^{\dagger}_{\mathbf{R}\,m}$. The latter condition implying a specific value of the chemical

potential, that only under this condition can be written analytically as:

$$\mu = \frac{U\,(N-1)}{2}\,. \tag{4.2}$$

For this reason the chemical potential is often calculated respect to its particle-hole symmetric value, i.e. $\mu' = \mu + \frac{U\,(N-1)}{2}$.

$SU(2M)$ models have been already studied in refs.[26][53]. More specifically, it has been demonstrated analytically, that $U_{c1} \propto \sqrt{2M}$, and $U_{c2} \propto 2M$ [26], that corresponds to a broadening of the coexistence region. Fig.(4.1) shows the quasi-particle weight calculated for the $SU(4)$-Hubbard model for different values of the interaction strength, using the ED method with $N_S = 6$. The value of $U_{c2} \sim 5D$ is in a very good agreement with both references [26][53]. Fig.(4.2) shows the imaginary part of the self-energy and the imaginary part of the Green's function calculated both on the Matsubara frequencies for several values of U. It is evident that in the insulating phase the self-energy diverges as $1/i\omega_n$, and the Green's function goes linearly to zero when $\omega_n \to 0^+$, similarly to the already discussed $SU(2)$-symmetric case. Conversely, in the metallic phase the $\mathrm{Im}\Sigma(i\omega_n)$ goes to zero linearly and $\mathrm{Im}G(i\omega_n)$ tends to its pinning value when $\omega_n \to 0^+$. Therefore, in the case of the $SU(2M)$-Hubbard models the quasi-particle weight Z goes smoothly to zero at the critical point.

Now it will be discussed a more generic case, where the Mott transition does not occur in a particle-hole symmetric situation. This is the case of any integer filling different from $N/2$.

The difference between these two cases is due by the fact that in general, the real part of the self-energy does not diverge at $\omega = 0$ close to the transition, when the system is doped and it tends linearly to its static value. This can be shown using the self consistence relation, that for a semicircular DOS of half bandwidth D reads:

$$\mathcal{G}^{-1}(\omega + i0^+) = \omega + \mu - \frac{D^2}{4}\,G(\omega + i0^+). \tag{4.3}$$

In a Mott insulating state the spectral function has a gap, therefore $\mathrm{Im}G(\omega + i0^+) = 0$ when $\omega \sim 0$. Using the Dyson's equation $\mathcal{G}^{-1} - \Sigma = G^{-1}$, the real part of the self energy of a Mott insulator at low frequencies can be expressed as following:

$$\mathrm{Re}\Sigma(\omega + i0^+) = \omega + \mu - \frac{D^2}{4}\,\mathrm{Re}G(\omega + i0^+) - \mathrm{Re}G^{-1}(\omega + i0^+) \tag{4.4}$$

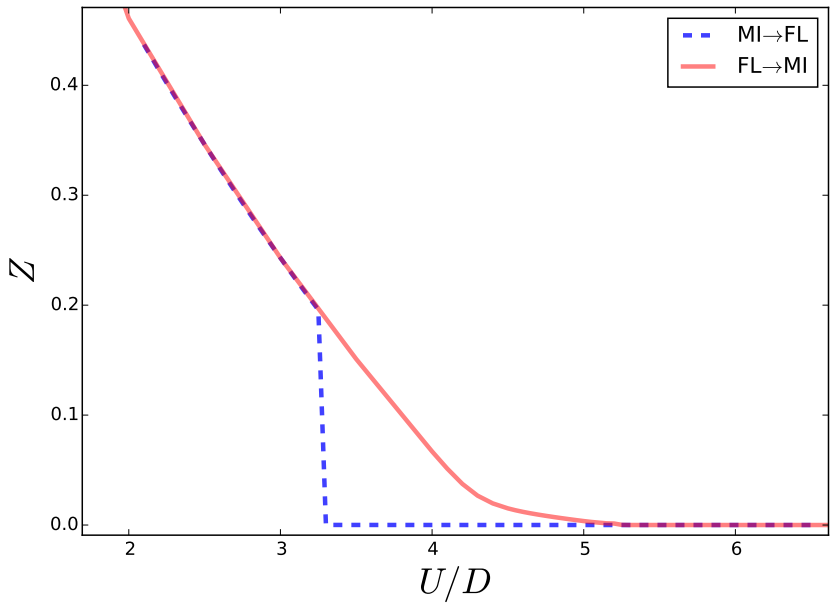

Figure 4.1: The quasiparticle weight as a function of the interaction strength U. The thick red line is relative to the DMFT solutions obtained starting from a FL initial state and by increasing the value of U. Instead, the blue dashed line is relative to the DMFT solutions obtained from a MI initial state and by decreasing the value of U.

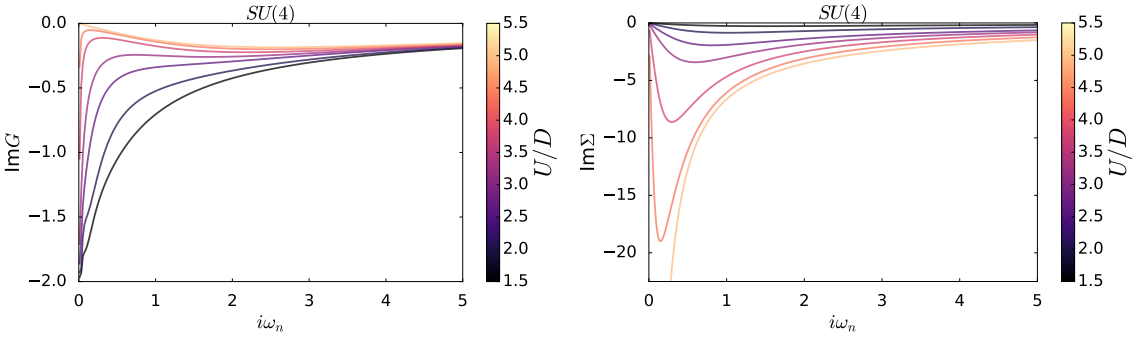

Figure 4.2: On the left side, the imaginary part of the Green's function evaluated on the imaginary axis for several values of the interaction strength. On the right side, the imaginary part of the self energy evaluated on the imaginary axis for several values of the interaction strength.

The real part of the Green's function can be obtained using the Kramers-Kronig relations, and expanding it at the first order in ω:

$$\begin{aligned} \mathrm{Re}\, G(\omega + i0^+) &= \frac{1}{\pi}\mathcal{P}\int_{-\infty}^{\infty} d\nu\, \frac{\mathrm{Im}\, G(\nu + i0^+)}{\nu - \omega} \\ &\simeq -\mathcal{P}\int_{-\infty}^{\infty} d\nu\, \frac{A(\nu)}{\nu} - \omega \int_{-\infty}^{\infty} d\nu\, \frac{A'(\nu)}{\nu} \\ &\equiv \rho_1 + \rho_2\, \omega\,. \end{aligned} \tag{4.5}$$

When $A(\omega)$ is an even function, as in the case of the $SU(2M)$-Hubbard models at half-filling, $\rho_1 = 0$ and $Re\,\Sigma(\omega + i0^+) \sim 1/\omega$ when $\omega \sim 0$. Instead, in a more generic case $\rho_1 \neq 0$ and the self-energy can be expanded in Taylor series :

$$\mathrm{Re}\,\Sigma(\omega + i0^+) = \Sigma(i0^+) + (1 - 1/\alpha)\,\omega + O(\omega^2), \tag{4.6}$$

where $1/\alpha = \rho_2/\rho_1^2 - \rho_1 D^2/4$.

Nevertheless, this result does not imply that the self-energy does not have poles for $\omega \neq 0$, how can be seen easily from the atomic limit. In fact, at $T = 0$, when $U < \mu < 2\,U$, the self-energy reads:

$$\Sigma(\omega + i0^+) \propto \frac{1}{\omega + \mu - \frac{U}{2}} - i\pi\delta\left(\omega + \mu - \frac{U}{2}\right), \tag{4.7}$$

therefore it has a pole at $\bar{\omega} = \frac{U}{2} - \mu$, and $1 - 1/\alpha \propto \left(\mu - \frac{U}{2}\right)^{-2}$.

Also at finite U in the insulating phase, the self-energy has in general a pole at $\omega \neq 0$, however its location is not fixed as in the atomic limit.

It is worth to note that, despite the quasi-particle weight and α are calculated in the same way, i.e. both can be written as $\left(1 - \frac{\partial \mathrm{Re}\Sigma}{\partial\omega}\Big|_{\omega=0}\right)^{-1}$, these two quantities have two different meanings. In fact, Z measures the quasi-particle fraction and it vanishes within the insulating phase, for its definition. Conversely, $\alpha \neq 0$ in the insulator and this implies that the real part of self-energy tends linearly to zero when $\omega \sim 0$. Therefore, α can be interpreted as a measure of the damping of the self-energy at low energies, since the latter increases its slope when α decreases and eventually diverges when $\alpha = 0$.

The same considerations hold, in the case of even N, where the insulator density is a integer number different from $N/2$. In fact, for a generic N there are $N - 1$ non

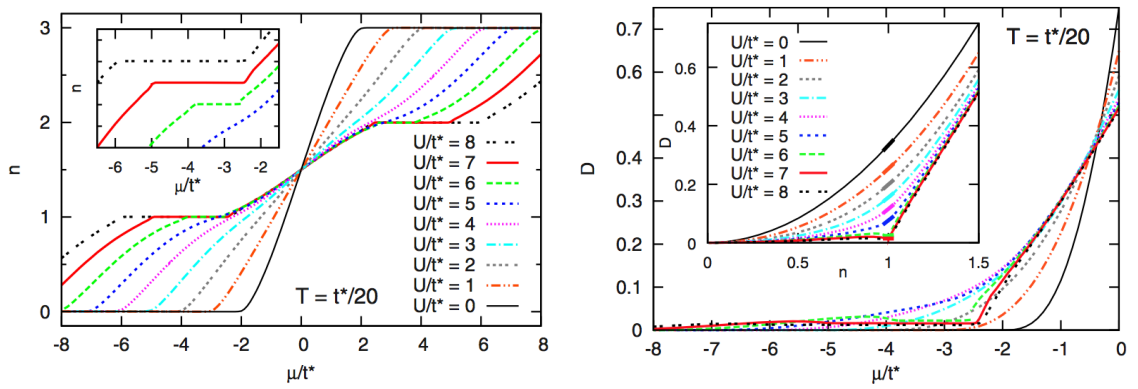

Figure 4.3: On the right side, HF-QMC estimates of particle density $n(\mu)$ at $T = D/40$ for various on-site interactions U. Plateaus at integer filling indicate localized Mott phases. On the left side, pair occupancy at $T = D/40$ vs chemical potential.

trivial insulating states with density $n = 1, 2, .., N-1$.

In the next section the case of $SU(3)$-Hubbard model will be addressed. A brief review of the literature [30] will be given, and the first original numerical results of this thesis will be shown.

4.2 Mott Transition of the $SU(3)$ model.

An early study of the $SU(3)$-Hubbard model has been carried out by Gorelik and Blümer [30], where the authors solve the DMFT equations using Hirsch-Fye QMC algorithm as impurity solver at finite temperature. Their main results are reported in Fig.(4.3). The left side shows the filling $n = \sum_\alpha \langle n_\alpha \rangle$ as a function of the chemical potential μ for a range of on-site interactions U. Initially, for $U = 0$, n varies smoothly and rapidly with μ from an empty band ($n = 0$) at $\mu/D \leq -1$ to a full band ($n = 3$) at $\mu/D \geq 1$. With increasing U, the slope generally decreases, but the curves remain smooth until, for $U/D \geq 3$, plateaus develop at integer fillings $n = 1$, $n = 2$, which signal the onset of localized Mott phase and correspond to gaps in the spectral function. No Mott phase is found at half filling, as expected.

The right side of Fig.(4.3), shows another fundamental property of Mott phases, that is the suppression of double occupancies, that in the case of the $SU(N)$-Hubbard model is straightforwardly generalized as $\mathcal{D} = \sum_{\alpha<\alpha'} \langle n_\alpha \, n_{\alpha'} \rangle$. The latter depends strongly on μ and U: the dependence on μ is mostly monotonic, except for the vicinity of plateaus $n = 1$ for $U/D \geq 3$. The impact of U is best understood at fixed density

n, see inset of Fig.(4.3): starting from the noninteracting limit $U = 0$, where $\mathcal{D} = \frac{2}{3}n$, $\mathcal{D}$ is suppressed with increasing U at all n. This suppression is strongly enhanced at $n = 1$ for $U/D \geq 3$.

If the work of Gorelik shows the evidences of the MIT away from half-filling in the $SU(3)$-Hubbard model, it lacks of a systematic study of the coexistence of the metallic and insulating phases. Furthermore, they do not show any phase diagram in the plane (U, μ) at $T = 0$, that would be unaccessible by exploiting the QMC technique, while it is suitable for the ED method. In the next section, this study is carried out and the $T = 0$ phase diagram of the DMFT paramagnetic solutions is shown.

4.2.1 Phase diagram in the (U, μ) plane.

Fig.(4.4) summarizes the phase diagram in the (U, μ) plane of the $SU(3)$-Hubbard model at $T = 0$ obtained using the ED method with $N_s = 6$. The case of particle doping, i.e. $\mu > 0$, has been addressed. Nevertheless, the phase diagram for the case of holes doping, i.e. $\mu < 0$, can be easily obtained from the one under consideration, if one performs a particle-hole transformation, i.e. $\mu \to -\mu$ and $n \to 3 - n$.

The phase diagram can be divided into three main regions: in the first one only metallic solutions exist, in the second the insulator is the only solution and in the third metallic and insulating phases coexist. Therefore, also in this case it is possible to identify two critical values of the interaction: $U_{c1} \sim 2.6\, D$, $U_{c2} \sim 3.5\, D$.

U_{c1} is defined as the greatest value of U such that only metallic solutions are found for all the values of the chemical potential before saturation, i.e. $n = 3$. In particular, for $U < U_{c1}$, the density is a smooth function of μ and no plateaus at integer filling are observed.

U_{c2} is defined as the lowest value of U such that no metallic solutions are found at integer filling. Hence, when $U > U_{c2}$, the density profiles $n(\mu)$ develop plateaus at $n = 2$. Furthermore, metallic solutions at $n \neq 2$ coexists with insulating solutions for a finite range of chemical potential values. More specifically, when $U > U_{c2}$, as shown in Fig.(4.4), there are four critical values of the chemical potential $\mu^{\pm}_{c1}(U)$ and $\mu^{\pm}_{c2}(U)$, that are ordered as following: $\mu^{-}_{c1} < \mu^{-}_{c2} < \mu^{+}_{c2} < \mu^{+}_{c1}$.

$\mu^{\pm}_{c1}$ is defined as the greatest (lowest) value of the chemical potential such that insulating solutions are found. Conversely, μ^{+}_{c2} and μ^{-}_{c2} are defined as the boundaries

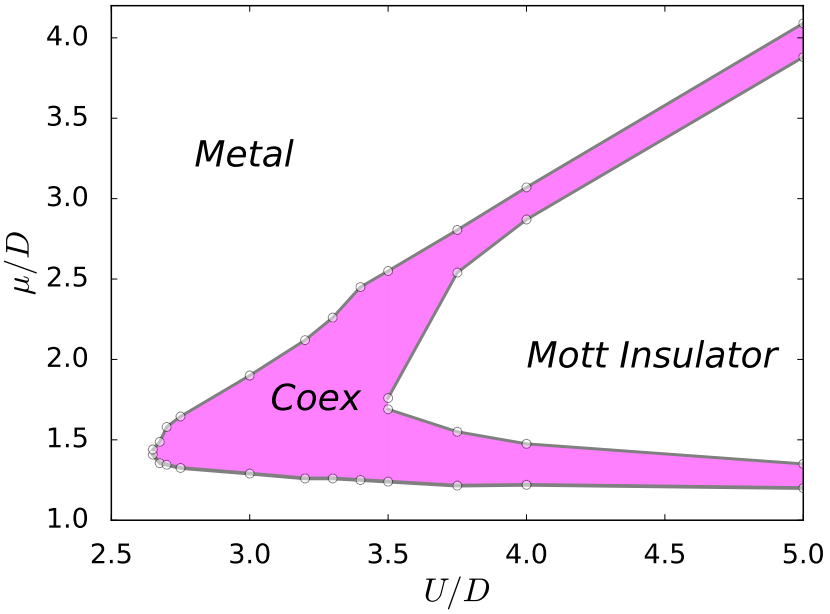

Figure 4.4: Phase diagram in the plane (U, μ) of the $SU(3)$-Hubbard model.

of the chemical potential interval where no metallic solutions are found. Hence, when $\mu < \mu_{c1}^{-} \vee \mu > \mu_{c1}^{+}$ the system is metallic and its density is respectively lower or greater than two. When $\mu_{c2}^{-} < \mu < \mu_{c2}^{+}$, the insulator is the only solution, while in the cases $\mu_{c1}^{-} < \mu < \mu_{c2}^{-}$ and $\mu_{c2}^{+} < \mu < \mu_{c1}^{+}$, an insulating solution at $n = 2$ coexists with a metallic one respectively with $n < 2$ and $n > 2$.

When $U_{c1} < U < U_{c2}$ metallic solutions are found for all the values of the chemical potential and insulating solutions exist in a finite portion of the phase diagram. In particular, there are two critical values of the chemical potential μ_{c1} and μ_{c2} such that insulating solutions are found in the interval $\mu_{c1} < \mu < \mu_{c2}$.

In the next sections, the numerical solutions relative to the three different regions of the phase diagram are discussed in detail.

$U < U_{c1}$.

The left side of Fig.(4.5) shows the density as a function of the chemical potential for $U/D = 2.25 < U_{c1}/D$. The density varies smoothly from $n(\mu = 0) = \frac{3}{2}$ until it reaches the saturation value for large values of μ. In DMFT, this quantity is evaluated directly from the AIM by averaging the number operator of the impurity over the ground state obtained in the last iteration. Furthermore, since the system is metallic, the Luttinger

theorem in eq.(3.14) must hold. Indeed, the panel on the right of Fig.(4.5) displays the density evaluated using eq.(3.14) as a function of the density obtained directly from the AIM, showing that the DMFT results are consistent with FL theory. The deviation between the two values is due to small numerical inaccuracies, in particular to the finite cut-off at low-energy introduced by the fictitious finite temperature $\beta = 300$, that is necessary for the ED method as explained in the previous chapter. Fig.(4.6) shows the ratio between the effective and bare masses, as a function of the density. It is evident that the effective mass has a peak when $n \sim 2$, signaling that the system is much more correlated close to integer filling than the half-filled case, where no MIT takes place.

The left side of Fig.(4.7) shows the spectral function for three values of the chemical potential with $U = 2.25\,D$. In the first case $\mu = 0$, the spectral density is that of a metal at half-filling, indeed it is symmetric under sign exchange of the frequencies $A(\omega) = A(-\omega)$. It is worth to notice, that the spectral weight gathers around the Fermi energy, and a small portion of it distributes at higher energy. The second panel it is relative to the case of a correlated doped metal, in fact the spectral function has a coherent peak at the Fermi energy, and a considerable portion of spectral weight distributes at higher energy constituting the Hubbard bands, that in this case can be distinguished very well. This last are not symmetric respect to the origin, since the system is away from half-filling, and since $n \sim 2.1 > 2$, the lower Hubbard band has a greater spectral weight than he upper band. The last panel shows the spectral density of a band insulator at $n = 3$, in fact its width equals $2\,D$ and no spectral weight can be seen at the Fermi energy.

When $U < U_{c1}$ the system is metallic, therefore FL theory implies that the spectral function evaluated at the Fermi energy reaches its pinning value, i.e. $\mathrm{Im}G(i0^+) = -\pi g(\tilde{\mu})$. Therefore, in the case of a semicircular density of states, as long as the system is in a FL state, $A(\omega = 0)$ is expected to decrease upon doping. The right side of Fig.(4.7) shows the imaginary part of the Green's function evaluated on the imaginary axis for several values of μ. In order to show the consistence of the DMFT solutions, the limiting values $-\pi g(\tilde{\mu})$ are drawn as thin horizontal lines and compared to the Green's function.

In conclusion in the metallic region, i.e. when $U < U_{c1}$, the system increases its correlations upon doping from half-filling until around integer filling, where the correlations have a maximum, and tends to a band insulator upon doping further.

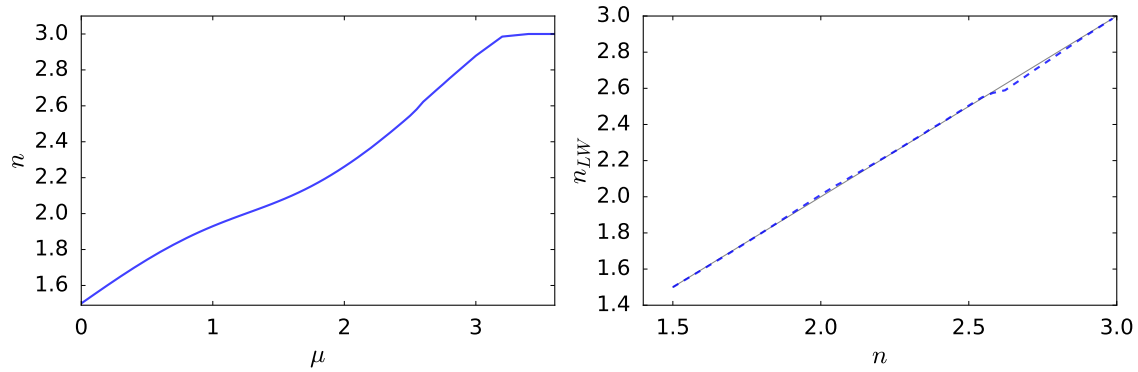

Figure 4.5: On the left side, the density as a function of the chemical potential for $U = 2.25\,D$. In the center, a comparison between the density obtained from the last DMFT iteration from the AIM with the value predicted by the Luttinger theorem.

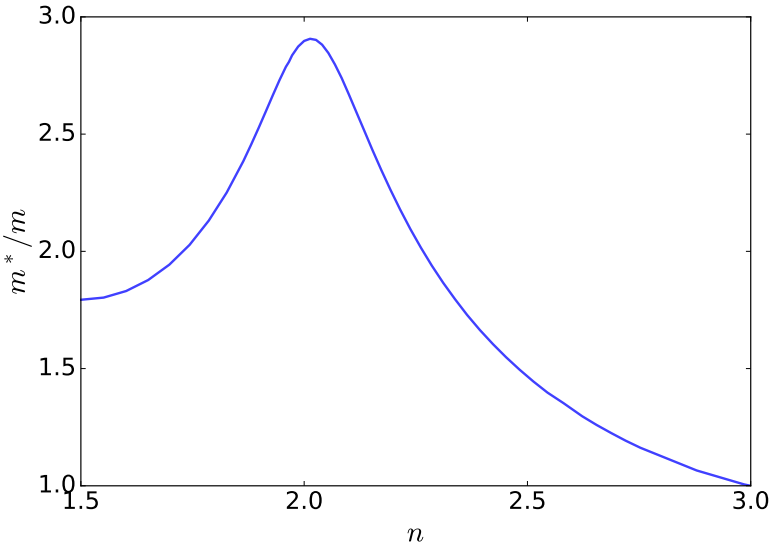

Figure 4.6: The ratio between the effective and the bare masses as a function of the density evaluated at $U = 2.25\,D$.

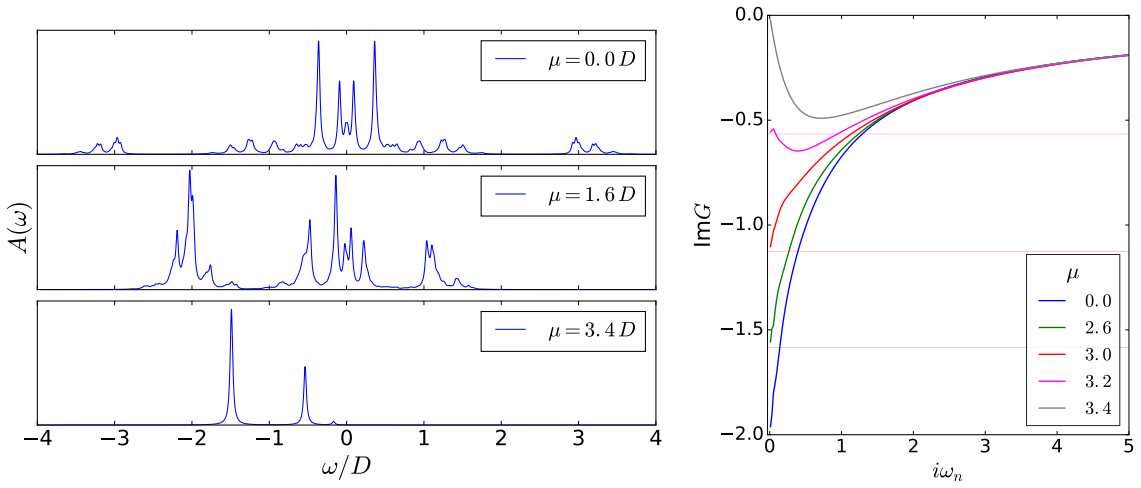

Figure 4.7: On the left side, the spectral function evaluated in the case of $U = 2.25\,D$ with $N_s = 6$ for three different values of the chemical potential $\mu = 0.0, 1.6\,D, 3.4\,D$ (from the top to the bottom). On the right side, the imaginary part of the Green's function evaluated on the imaginary axis, for several values of μ. The thin lines refer to the limiting value $\mathrm{Im}G(i0^+) = -\pi g(\tilde{\mu})$ predicted by FL theory.

$U > U_{c2}$.

The upper panel of Fig.(4.8) shows the density as a function of the chemical potential for $U = 3.65\,D > U_{c2}$. Metallic solutions are obtained for $\mu < \mu_{c2}^- \vee \mu > \mu_{c2}^+$, and the density relative to this kind of solutions tends to integer filling at the critical points, i.e. $n_{metal}(\mu_{c2}^{\pm}) = 2 \pm 0^+$. On the other hand, insulating solutions are found in the interval $\mu_{c1}^- < \mu < \mu_{c1}^+$, whose density is fixed at $n_{ins} = 2$. Therefore, in the intervals $\mu_{c1}^- < \mu < \mu_{c2}^-$ and $\mu_{c2}^+ < \mu < \mu_{c1}^+$, the two solutions coexist.

The lower panel of Fig.(4.8) displays the quasi-particle weight Z and the quantity α defined in eq.(4.6) as a function of μ. The quasi-particle weight decreases upon doping, until it jumps from a finite value to zero at the critical points $\mu_{c2}^{\pm}$. The quantity α vanishes at $\bar{\mu} \sim 2.32\,D$, that differs significantly from the value predicted in the atomic limit, that would be $1.825\,D$.

The left side of Fig.(4.9) shows the spectral function for three values of the chemical potential with $U = 3.65\,D$. In the first case $\mu = 0$, the spectral density is that one of a metal at half-filling, indeed it is an even function $A(\omega) = A(-\omega)$. The second panel is relative to the case of a doped correlated metal in the coexistence region, with $\mu_{c1}^- < \mu = 1.5\,D < \mu_{c2}^-$. In this situation, the quasi-particle residue is very small ($Z \sim 0.04$) and despite the spiky structure of the spectral function, the Hubbard bands

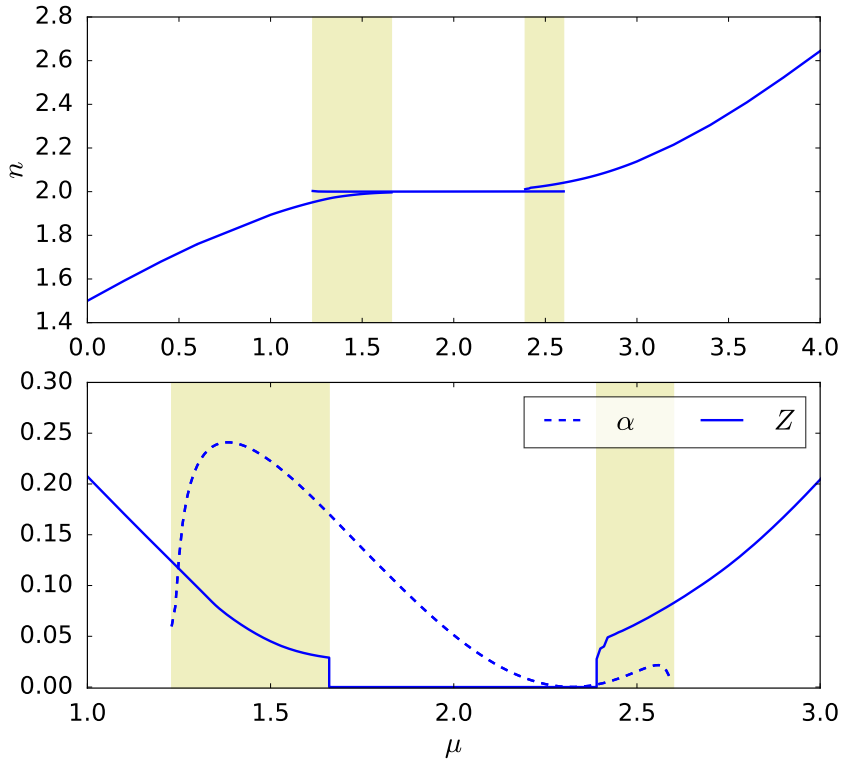

Figure 4.8: Upper panel, density as a function of the chemical potential relative to both insulating and metallic phases for $U = 3.65\,D$. Lower panel, the quasi-particle weight Z and the quantity α defined in eq.(4.6) as a function of μ. The green shaded areas illustrate the coexistence region.

are quite visible and well separated from the coherent peak at low energy. The last panel refers to the case of a Mott insulator, in fact the coherent peak has disappeared and the spectrum has a gap $\Delta \sim U$.

The right side of Fig.(4.9) illustrates the self-energy as a function of the real frequencies for three values of the chemical potential. It is evident that the self-energy has a pole in zero for $\mu = \bar{\mu} \sim 2.32\,D$ and that the pole is shifted to positive or negative values respectively for values of the chemical potential that are lower or greater than $\bar{\mu}$.

$U_{c1} < U < U_{c2}$.

When the interaction strength lies on the range $U_{c1} < U < U_{c2}$, both metallic and insulating solutions are allowed. Since metallic solutions are always allowed within this region, the quasi-particle residue as a function of μ has always a minimum and it

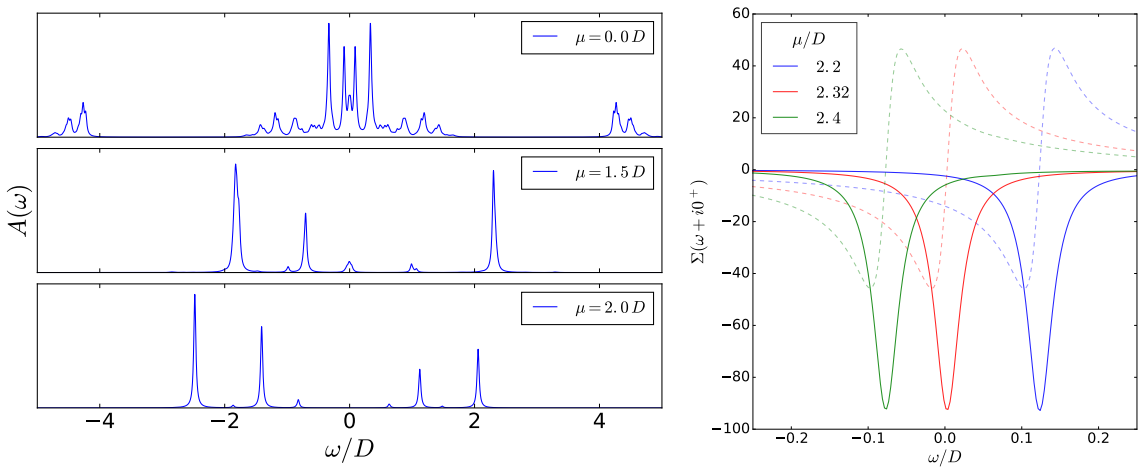

Figure 4.9: On the left side, the spectral function for three value of the chemical potential $\mu = 0,\ 1.5\,D,\ 2.0\,D$ (from the top to the bottom). On the right side, the self-energy for three different values of the chemical potential centered in $\mu = \bar{\mu}$. The thick lines refer to the imaginary part of the self-energy, while the dashed lines represent its real part.

does not vanish. On the other hand, it has been shown that the Z has a finite jump as a function of μ when $U > U_{c2}$. Therefore, the quasi-particle weight is expected to vanish smoothly as a function of the chemical potential only at $U = U_{c2}$.

Fig.(4.10) shows the behavior of the effective mass as a function of the chemical potential for different values of the interaction strength. It is clear that the mass diverges in the limit $U \to U_{c2}$. This limit could be consider as a more quantitative definition of U_{c2}.

4.3 Conclusions

This chapter was dedicated to the metal to insulator transition displayed by the $SU(N)$-symmetric Hubbard models.

In the previous chapter, it was argued that a MI state cannot be obtained in a perturbative manner starting from a FL. In fact, perturbation theory assures that at low energy the self-energy is an analytic function around the FS, while in the case of a MI there is always a point where the self-energy has a pole at low energy. Therefore, the need of a non perturbative method as DMFT in order to study the MIT was pointed out.

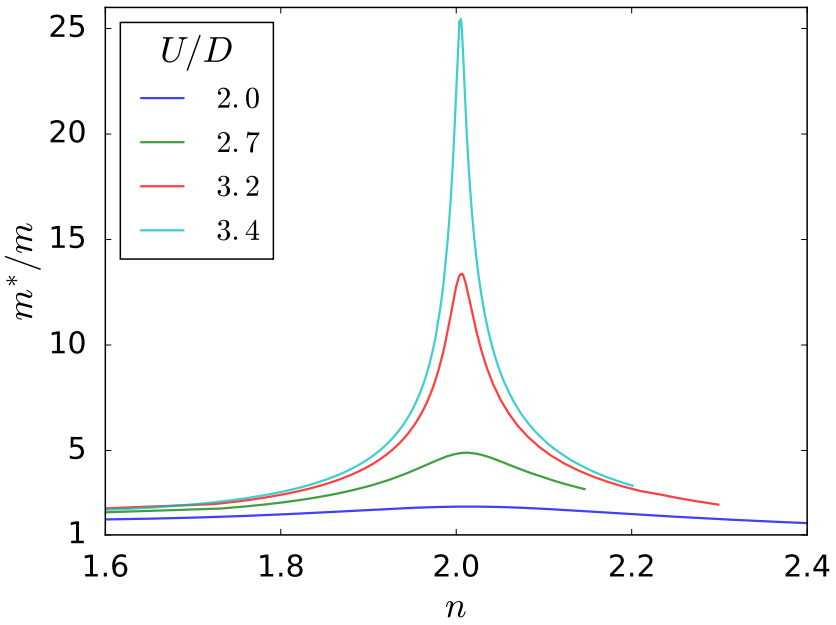

Figure 4.10: Effective mass as a function of the density for several vales of the interaction strength U.

In the first part of this chapter, the case of half-filled configurations has been addressed. It was pointed out that in this configuration the MIT can occur only at $N = 2M$, where the $SU(N)$ model corresponds to a fully symmetric spin-1/2 system with M degenerate orbitals. Some of the well known results of refs. [28][26][53] were obtained again, in order to benchmark the code *SU_N.py*, written by the author. An excellent quantitative agreement with all the main previous results has been found.

The last section focused on the MIT in the case of the $SU(3)$-Hubbard model. The presence of an odd number of internal degrees of freedom implies that the system cannot be found in a MI state at half-filling. Therefore, the MIT is expected to occur away from particle-hole symmetry and the chemical potential becomes an essential parameter. After a brief review of the previous results of Gorelik and Blümer [30], the phase diagram in the plane (U, μ) was presented and discussed. A careful analysis of the insulating and metallic solutions has been carried out, with a particular attention posed on the dynamical quantities as the spectral function, the self-energy and so on. The coexistence region between the metallic and insulating solutions has been shown in the phase diagram, and the two spinodal values of the interaction strength has been determined, i.e. $U_{c1} \sim 2.6\,D$ and $U_{c2} \sim 3.5\,D$.

In particular, the quasi-particle weight in the metallic and coexistence regions has a

minimum as a function of the density at $n \sim 2$ and goes to zero only for $U = U_{c2}$ at $n = 2$. Instead, for $U > U_{c2}$, Z is a discontinuous function of μ and jumps to zero at the critical values $\mu_{c2}^{\pm}$.

It was also pointed out, that the lack of particle-hole symmetry implies a shift of the self-energy pole in the insulating phase. The insulating solutions have been characterized studying the quantity $\alpha(U, \mu)$, that measures such a shift and signals the divergence of $\Sigma(\omega + i\,0^+)$ at the Fermi level when it vanishes.

CHAPTER 5

HUBBARD MODELS WITH ARTIFICIAL GAUGE FIELDS.

5.1 Introduction

In the first chapter of this thesis, it was shown how to simulate $SU(N)$-symmetric Hubbard models, exploiting the nature of the ^{173}Yb electronic ground state. Combining this with the possibility of simulating AGF gives the unique opportunity of simulating lattice model in presence of AGF where the onsite interactions between fermions become relevant.

In particular, the generic hamiltonian relative to the multi-component Hubbard model in presence of AGF reads:

$$H = \sum_{\mathbf{R}\mathbf{R}',m} t_{\mathbf{R}\mathbf{R}'}\, c^{\dagger}_{\mathbf{R}m} c_{\mathbf{R}'m'} + \sum_{\mathbf{R},\,mm'} (\mathbb{M}_{\mathbf{R}})_{mm'}\, c^{\dagger}_{\mathbf{R}m} c_{\mathbf{R}m'} + \frac{U}{2} \sum_{\mathbf{R}} n_{\mathbf{R}}(n_{\mathbf{R}} - 1), \qquad (5.1)$$

where $n_{\mathbf{R}} = \sum_m n_{\mathbf{R}m}$, $\mathbb{M}_{\mathbf{R}}$ is the AGF matrix. A more convenient spinorial notation will be used from now on, therefore the multi flavor fermionic spinors are defined:

$$\psi^\dagger_{\mathbf{R}} \equiv \left(c^\dagger_{\mathbf{R}1}, c^\dagger_{\mathbf{R}2}, \ldots, c^\dagger_{\mathbf{R}N}\right), \qquad \psi_{\mathbf{R}} \equiv \begin{pmatrix} c_{\mathbf{R}1} \\ c_{\mathbf{R}2} \\ \vdots \\ c_{\mathbf{R}N} \end{pmatrix}. \tag{5.2}$$

Hence, the many body hamiltonian can be written in terms of the spinors as following:

$$H = \sum_{\mathbf{R}\mathbf{R}'} t_{\mathbf{R}\mathbf{R}'}\, \psi^\dagger_{\mathbf{R}} \mathbb{1} \psi_{\mathbf{R}'} + \sum_{\mathbf{R}} \psi^\dagger_{\mathbf{R}} \mathbb{M}_{\mathbf{R}} \psi_{\mathbf{R}} + \frac{U}{2} \sum_{\mathbf{R}} \psi^\dagger_{\mathbf{R}} \mathbb{1} \psi_{\mathbf{R}} \left[\psi^\dagger_{\mathbf{R}} \mathbb{1} \psi_{\mathbf{R}} - 1\right], \tag{5.3}$$

where $\mathbb{1}$ is the $N \times N$ identity matrix.

The AGF matrix depends on the lattice site, therefore the system is not homogenous. Nevertheless, as can be grasped from eq.(2.16), the spatial dependence of $\mathbb{M}_{\mathbf{R}}$ enters as a phase, and two matrices calculated in two different lattice sites are related to each other by a unitary transformation. Namely, if $\mathbf{R}_1 = \mathbf{R} + \mathbf{R}_2$

$$\mathbb{M}_{\mathbf{R}_1} \quad = \quad \Phi_{\mathbf{R}} \mathbb{M}_{\mathbf{R}_2} \Phi^\dagger_{\mathbf{R}}, \tag{5.4}$$

where $\Phi_{\mathbf{R}} = \exp\left(-i\, \mathbb{G}\, \mathbf{R} \cdot \boldsymbol{\varphi}\right)$ is the unitary transformation, and $(\mathbb{G})_{mm'} = \delta_{mm'} m$ is the generator of the transformation. This condition implies that the eigenvalues of $\mathbb{M}_{\mathbf{R}}$ do not depend on $\mathbf{R}$. Therefore, it is possible to rotate the reference frame using the unitary transformation $\Phi_{\mathbf{R}}$:

$$H = \sum_{\mathbf{R}\mathbf{R}'} t_{\mathbf{R}\mathbf{R}'}\, \phi^\dagger_{\mathbf{R}} \left[\Phi^\dagger_{\mathbf{R}} \Phi_{\mathbf{R}'}\right] \phi_{\mathbf{R}'} + \sum_{\mathbf{R}} \phi^\dagger_{\mathbf{R}}\, \mathbb{M}\, \phi_{\mathbf{R}} + \frac{U}{2} \sum_{\mathbf{R}} \phi^\dagger_{\mathbf{R}} \mathbb{1} \phi_{\mathbf{R}} \left[\phi^\dagger_{\mathbf{R}} \mathbb{1} \phi_{\mathbf{R}} - 1\right], \tag{5.5}$$

where, $\mathbb{M} \equiv \mathbb{M}_{\mathbf{R}=0}$, $\phi_{\mathbf{R}} = \Phi^\dagger_{\mathbf{R}} \psi_{\mathbf{R}}$. Now, it is possible to perform the unitary transformation, that diagonalizes $\mathbb{M}$:

$$H = \sum_{\mathbf{R}\mathbf{R}'} t_{\mathbf{R}\mathbf{R}'}\, \widetilde{\phi}^\dagger_{\mathbf{R}}\, \rho_{\mathbf{R}\mathbf{R}'}\, \widetilde{\phi}_{\mathbf{R}'} + \sum_{\mathbf{R}} \widetilde{\phi}^\dagger_{\mathbf{R}}\, \lambda\, \widetilde{\phi}_{\mathbf{R}} + \frac{U}{2} \sum_{\mathbf{R}} \widetilde{\phi}^\dagger_{\mathbf{R}} \mathbb{1} \widetilde{\phi}_{\mathbf{R}} \left[\widetilde{\phi}^\dagger_{\mathbf{R}} \mathbb{1} \widetilde{\phi}_{\mathbf{R}} - 1\right], \tag{5.6}$$

where $\lambda = \mathcal{U}\, \mathbb{M} \mathcal{U}^\dagger = \mathrm{diag}(\lambda_1, \lambda_2, ..., \lambda_N)$, $\widetilde{\phi}_{\mathbf{R}} = \mathcal{U}\, \phi_{\mathbf{R}}$, and $\rho_{\mathbf{R}\mathbf{R}'} = \mathcal{U}\, \Phi_{\mathbf{R}'-\mathbf{R}}\, \mathcal{U}^\dagger$ depends only on the difference of $\mathbf{R} - \mathbf{R}'$. Therefore, the hamiltonian in eq.(5.6) is the one of an homogenous system. Nevertheless, the fields have been rotated via unitary operators that depends on $\mathbf{R}$. Since these operators have a simple form and are known explicitly,

it is possible to evaluate generic observables of the original system calculating them as an expectation value over the fields $\widetilde{\phi}_{\mathbf{R}}$ and subsequently get back to the original reference frame via unitary transformations. This scheme gives the advantage of using methods that are suitable for homogenous systems. Therefore, the DMFT can be safely used in its simplest single site formulation, with no need of invoking its real space extension. Nevertheless, cluster extensions of the DMFT [49][42] can be used for improving the description of the system in **k**-space especially if unconventional superconducting states are sought.

Therefore, the cavity method can be applied to the hamiltonian in eq.(5.6), and relative to the effective AIM reads:

$$\begin{aligned} H_{eff} &= \sum_{\ell} \chi_{\ell}^{\dagger}\, \Theta_{\ell}\, \chi_{\ell} + \sum_{\ell} \phi^{\dagger}\, \Xi_{\ell}\, \chi_{\ell} + \text{h.c.} \\ &+ \phi^{\dagger}\, \lambda\, \phi + \frac{U}{2} \phi^{\dagger} \mathbb{1}\, \phi \left(\phi^{\dagger} \mathbb{1}\, \phi - 1 \right), \end{aligned} \tag{5.7}$$

where $\chi_{\ell} = (d_{\ell 1}, d_{\ell 2}, ...d_{\ell N})$ is the ℓ-th spinor of the effective bath, $\phi = (c_1, c_2, ..., c_N)$ is the spinor relative to the interacting impurity, $(\Xi_{\ell})_{mm'}$ is the hybridization matrix that couples the ℓ-th spinor of the bath with the impurity and $(\Theta_{\ell})_{mm'}$ represents the energy levels of the effective noninteracting bath. It is worth to notice that in general both Θ_{ℓ} and Ξ_{ℓ} are not diagonal matrices in the spin indices since the kinetic term itself in the hamiltonian in eq.(5.6) it is not.

In the specific case of $\boldsymbol{\varphi} = 0$, many simplification arise from the fact that the matrix $\rho_{\mathbf{R}-\mathbf{R}'}|_{\boldsymbol{\varphi}=0} = \mathbb{1}$. This implies that the matrices $\Theta_{\ell} = \epsilon_{\ell m} \delta_{mm'}$ and $\Xi_{\ell} = V_{\ell m} \delta_{mm'}$ are also diagonal in the spin indices, and the effective theory is simplified. Hence, the effective hamiltonian reads:

$$\begin{aligned} H_{eff} &= \sum_{\ell m} \epsilon_{\ell m} d_{\ell m}^{\dagger} d_{\ell m} + \sum_{\ell m} V_{\ell m} d_{\ell m}^{\dagger} c_m + \text{h.c.} \\ &+ U \sum_{m<m'} \hat{n}_m \hat{n}_{m'} + \sum_{m} (\lambda_m - \mu) \hat{n}_m, \end{aligned} \tag{5.8}$$

where $\hat{n}_m = c_m^{\dagger} c_m$ is the number operator of the impurity, μ is the chemical potential, that has been added in order to study the system in the gran-canonical ensemble.

Given the effective AIM in eq.(5.8), the DMFT equations in the case of a semicircular

DOS $g(\epsilon) = \frac{2}{\pi D}\sqrt{D^2 - \epsilon^2}$ read:

$$\begin{aligned} G_m(\tau) &= -T_\tau \left\langle c_m(\tau) c_m^\dagger(0) \right\rangle_{H_{eff}} \\ \mathcal{G}_m^{-1}(i\omega_n) &= i\omega_n + \mu_m - \frac{D^2}{4} G_m(i\omega_n), \end{aligned} \tag{5.9}$$

where $\mu_m = \mu - \lambda_m$, $G_m(i\omega_n) = T\sum_{i\omega_n} e^{-i\omega_n\tau} G_m(\tau)$ and $\mathcal{G}_m^{-1}$ is the Weiss field relative to the fermionic bath that couples with the m-th fermionic component of the interacting impurity. The Weiss field as a function of the Anderson's parameters reads:

$$\mathcal{G}_m^{-1}(i\omega_n) = i\omega_n + \mu_m - \sum_\ell \frac{|V_{\ell m}|^2}{i\omega_n - \epsilon_{\ell m}}. \tag{5.10}$$

The DMFT equations are solved using the ED method discussed in Chapt.(3), therefore the infinite series that runs over ℓ is truncated at the N_s-th index. In this simple case, the DMFT cycle is very similar to the one in the symmetric case, with the only difference that three different Green's functions must be evaluated and three different fits of the Weiss Field have to be carried out. The simplicity of this case lies on the fact that the hybridization function is diagonal in the spin indices.

5.2 The case at $\boldsymbol{\varphi} = 0$

As anticipated in the introduction, the point of view adopted in this work is slightly different with respect to many studies of cold-atom systems in the presence of Raman processes mimicking a gauge field. The main focus of this thesis is in fact to study models which generalize multi-component models of condensed matter systems.

For this reason the case of $\boldsymbol{\varphi} = 0$ is addressed, where all the matrix elements of the matrix $\mathbb{M}$ are real. Even with this restriction, different analogies may be used to interpret the results that will be presented later.

If the N spin components are interpreted as local orbitals of a synthetic atom, the diagonal matrix elements act as different energy levels for the various orbitals, while the off-diagonal terms are local hybridizations between them. This analogy can be used to establish a connection with solid state systems with orbital-selective properties. Of course the analogy would be stronger for an even N in the case the levels remain degenerate in pairs, mimicking spinful orbitals in a solid. Nonetheless, it will be shown that interesting "flavour-selective" physics can take place also in the absence of a

residual degeneracy.

A second analogy consists in viewing the internal spin degree of freedom as a sort of synthetic dimension with a discrete nature. In this language, the diagonal elements of $\mathbb{M}$ play the role of different local energies for the sites in the extra dimension, while the off-diagonal elements are the equivalent of hoppings in the synthetic dimension.

Finally, treating the N components as a physical $SU(N)$ spin the matrix $\mathbb{M}$ can be viewed as a generalized magnetic field. This latter language highlights an important property. Since the interaction is $SU(N)$ symmetric, it is always possible to diagonalize the matrix $\mathbb{M}$ while keeping the interaction invariant. This amounts to use the direction of the magnetic field as the quantization axis.

This simple observation suggests that the physics of the problem will be determined by the eigenvalues of $\mathbb{M}$ which will appear as diagonal energies for the different spin components in the new basis that diagonalizes the "magnetic field". In the simplest and somewhat peculiar, $N = 2$ case, only the symmetric disposition $\pm\lambda$ is allowed. This is due to the fact that the generators of the $SU(2)$ algebra can be represented by the Pauli matrices $\{\sigma_\alpha\}$, that can be mapped to each other using the unitary transformations $\exp\left(\frac{-i\boldsymbol{\sigma}\cdot\boldsymbol{\theta}}{2}\right)$. More physically, the generators of the algebra correspond to the angular momentum operators, and since the system is isotropic, its response to an external magnetic field does not depend on its orientation.

Instead, in the case of $N > 2$, multiple dispositions of the eigenvalues are allowed, since the $SU(N)$ algebra generators are $N^2 - 1 > 3$, i.e. the cardinality of the generators is greater than the spatial dimensionality. This implies that, along a given axis, there can be different kind of magnetic fields, because of the increased number of spin permutations. In general, the system will have different responses to different matrices $\mathbb{M}$ that are not connected through unitary transformations. In this work, it is considered the $SU(3)$ case and in particular the two matrices

$$\mathbb{M}_1 = -\begin{pmatrix} 0 & \tau & 0 \\ \tau & 0 & \tau \\ 0 & \tau & 0 \end{pmatrix} \qquad \mathbb{M}_2 = -\begin{pmatrix} 0 & \tau & \tau \\ \tau & 0 & \tau \\ \tau & \tau & 0 \end{pmatrix}, \tag{5.11}$$

whose eigenvalues are $\boldsymbol{\lambda}_1 = \tau\{-\sqrt{2}, 0, \sqrt{2}\}$, $\boldsymbol{\lambda}_2 = \tau\{-2, 1, 1\}$. From the point of view of actual cold-atom systems, these choices would require some fine tuning of the Raman processes. The first case would require only Raman processes connecting "successive" spin projections differing of one spin quantum, which have to be tuned to

be identical. The second case would require also a next-neighbor process. Here it has been choosen to take all these matrix elements to simplify the theoretical description. However, the most important results obtained do not depend on this symmetric choice.

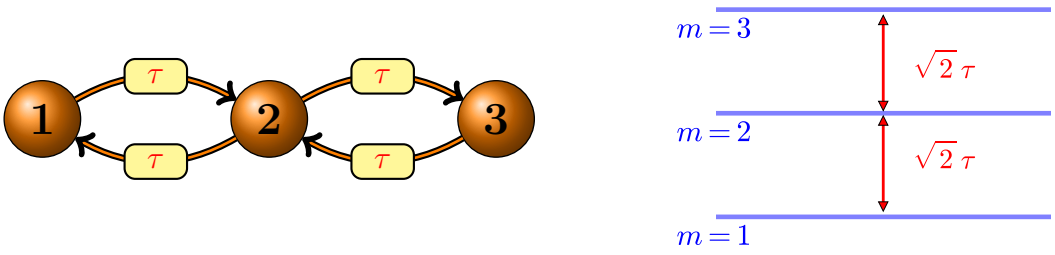

(a)

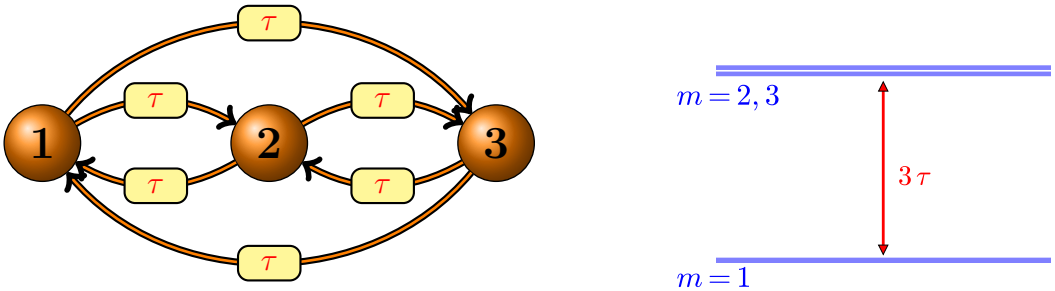

(b)

Figure 5.1: Schematic representation of two synthetic hopping processes along the synthetic dimension and their associated energy levels in the $SU(3)$ case. In particular, (a) represents graphically the AGF matrix $\mathbb{M}_1$ that corresponds to a nearest-neighbor hopping with OBC, whose eigenvalues are non degenerate and equally spaced from each other with an energy difference of $\sqrt{2}\tau$. Instead, (b) represents the AGF matrix $\mathbb{M}_2$, that corresponds to a nearest-neighbor hopping with PBC. In this case, the eigenvalues are doubly degenerate and their energy difference is 3τ.

Using the "synthetic dimension" language, the two matrices correspond respectively to a three-site hopping with open boundary conditions (OBC) and periodic boundary conditions (PBC), respectively. The two situations are quite different because in the PBC case a residual $SU(2)$ symmetry survives in a two-component manifold, while the OBC completely break the $SU(3)$ symmetry.

In the progress of this chapter, the differences between these two cases, that are depicted schematically in Fig.(5.1), will be extensively discussed, and the distinct

physical situations emerging from these differences will be highlighted.

Before entering the discussion of the original results of the present chapter for the $SU(3)$ case, some important aspect of the $SU(2)$ case are reviewed, which will prove useful to analyze the higher-N results.

DMFT studies of the single-band Hubbard model show a dramatic enhancement of the magnetization as a function of the intensity of an external magnetic field [6][5][58][35][43], in the intermediate coupling regimes. This behavior deviates significantly from the smooth trend predicted in the MF approximation. This is due to the tendency of the system to create a long range antiferromagnetic order via the super-exchange interaction induced by the Hubbard U. This can be understood following the original idea of Landau [44], who suggested that an antiferromagnet can be described as a stack of ferromagnetically ordered layers whose magnetization alternates from layer to layer. If the interlayer coupling is weak enough, it can be argued that a magnetic field of relatively small intensity would be sufficient to modify the mutual orientation of the moments in each layer. This leads to deviations from the linear dependence of the total moment on the field, i.e., to an anomalous increase of the susceptibility, and finally, at high fields, to a saturation of the magnetization.

Furthermore, for intermediate couplings, the quasi-particle effective mass is enhanced as a function of the external magnetic field and increases critically just before the system polarizes completely becoming a band insulator, where the band of the majority spin is totally filled [6][5]. This is an additional feature of the correlated system that cannot be grasped using the MF approximation, where the masses do not renormalize. Because of its anomalous response to an external magnetic field, such a system is said to be *metamagnetic* and it is often characterized by concave magnetization, i.e. $\frac{\partial^2 m}{\partial h^2} > 0$, just before its completely polarization.

In the next sections, the solutions of the DMFT equations in eq.(5.9), obtained using the ED method, will be shown and discussed. It is worth to notice, that in the present work antiferromagnetic long range order is neglected.

5.2.1 Synthetic hopping with OBC

This section focuses on the case of a synthetic hopping with OBC, i.e. the AGF matrix is given by $\mathbb{M}_1$ that corresponds to the case depicted in Fig.(5.1). In this situation, the magnetic field splits the Zeeman levels in a symmetric fashion around zero. Therefore,

in the rotated basis which diagonalizes $\mathbb{M}_1$, the m-th flavor feels an effective chemical potential $\mu_m = \mu - \lambda_m$ with $\{\lambda_m\} = \tau \left\{-\sqrt{2}, 0, \sqrt{2}\right\}$.

The numerical results are presented first in the rotated basis. The occupation number relative to the rotated m-th fermion component is labeled as $n_m \equiv \left\langle c_m^\dagger c_m \right\rangle$, while in general a tilde and greek indices are used for denoting quantities relative to the original fermions. This last are shown in order to provide a more direct benchmark to cold atoms experiments, where measurements are performed in the original basis.

As can be grasped from the previous chapter, the chemical potential represents an essential parameter in order to study the three components system. In the next sections it will be addressed the $\mu > 0$ case, which correspond to density values in the range $3/2 - 3$, where a Mott transition occurs at $n = 2$. However this case contains also the information relative to negative values of μ, because of the symmetrical dispositions of the eigenvalues $\{\lambda_m\}$. Indeed, after a particle hole transformation, i.e. $c_{\mathbf{R}m} \to (-1)^{\mathbf{R}} c_{\mathbf{R}m}^\dagger$ and the exchange of the flavor indices $1 \leftrightarrow 3$ the rotated hamiltonian is mapped onto itself with $\mu \to -\mu$.

In the weak coupling regime, the system can be studied using the mean field (MF) approximation, that constitutes a benchmark for the DMFT calculations when the values of the interaction strength U is small enough.

For stronger couplings, the mean field approximation becomes inadequate, since the correlations among fermions increase and start to play a central role. Furthermore, for $U/D > 1/g(\mu)$, the Stoner's criterion of ferromagnetism[1] applies, and very different results are expected in the case where a method or the other is used.

In the atomic limit, i.e. $t = 0$, the system is an insulator at integer filling. In particular, when $n = 2$, the ground state of the system is given by the product state $|\psi\rangle = |1\rangle_1 \otimes |1\rangle_2 \otimes |0\rangle_3$, where $|1\rangle_m = c_m^\dagger |0\rangle_m$, where m refers to the m-th fermionic component. Therefore, the system is expected to be completely polarized in the limit of large U/t.

Weak Coupling

At weak coupling, the MF approximation is expected to give a reliable description of the evolution of the system as a function of the parameters τ, U and μ. In general,

[1] The Stoner's criterion applies in general for any values of N [16].

one can proceed with the Hartree approximation, that consists in writing the number operator of the m-th fermionic component as $\hat{n}_m = n_m + \delta\hat{n}_m$, where $\delta\hat{n}_m \equiv \hat{n}_m - n_m$, substituting this expression into the hamiltonian in eq.(5.6) and keeping only the linear terms in $\delta\hat{n}_m$. This approximation is consistent as long as the correlations among the different fermionic components are weak enough, that is certainly true at weak coupling. The effective hamiltonian obtained within this approximation reads:

$$H_{eff} = \sum_{\mathbf{k}m} (\epsilon_{\mathbf{k}} - \tilde{\mu}_m)\, \hat{n}_{\mathbf{k}m}, \tag{5.12}$$

where $\tilde{\mu}_m = \mu - \lambda_m - U \sum_{m' \neq m} n_{m'}$ it is an effective chemical potential felt by the m-th fermionic flavor. This leads to a self consistent set of coupled equations for the occupation numbers of the different fermionic species, that in the case of a semicircular DOS reads:

$$\begin{aligned} n_m &= \frac{2}{D\pi} \int_{-D}^{\tilde{\mu}_m} d\epsilon \sqrt{1 - \left(\frac{\epsilon}{D}\right)^2} \\ &= \frac{1}{2} + \frac{1}{\pi} \left[\frac{\tilde{\mu}_m}{D} \sqrt{1 - \left(\frac{\tilde{\mu}_m}{D}\right)^2} + \sin^{-1}\left(\frac{\tilde{\mu}_m}{D}\right) \right]. \end{aligned} \tag{5.13}$$

The set of equations in eq.(5.13) is solved numerically and its results are compared with DMFT calculations.

Fig.(5.2) shows the total density as a function of μ for several values of τ. The density profile is smooth until the field reaches the critical value τ_c, such that for $\tau > \tau_c$ plateaus develop at $n = 2$. It is worth to notice that the density profile changes its shape smoothly as a function of τ. This corresponds to a smooth opening of a gap of the spectral function at the Fermi level. The upper panel of Fig.(5.3) shows the occupation numbers of the three fermionic components as a function of the chemical potential for several values of τ. It is evident that in the regions where the total density is a flat function of μ, the configuration of the occupation numbers is given by $n_1 = n_2 = 1$, $n_3 = 0$ and the system is a band insulator where the bands relative to the flavors "1" and "2" are totally occupied, while the 3rd flavor's band is empty. The lower panel of Fig.(5.3) shows the occupation numbers as functions of the total density. It is clear that the trend of $n_m(n)$ does not change very much as a function of τ and that it is almost linear except for $n_m \neq 1, 0$ where plateaus develop. DMFT results are compared with the MF data and a good agreement is obtained between these two different methods in this regime.

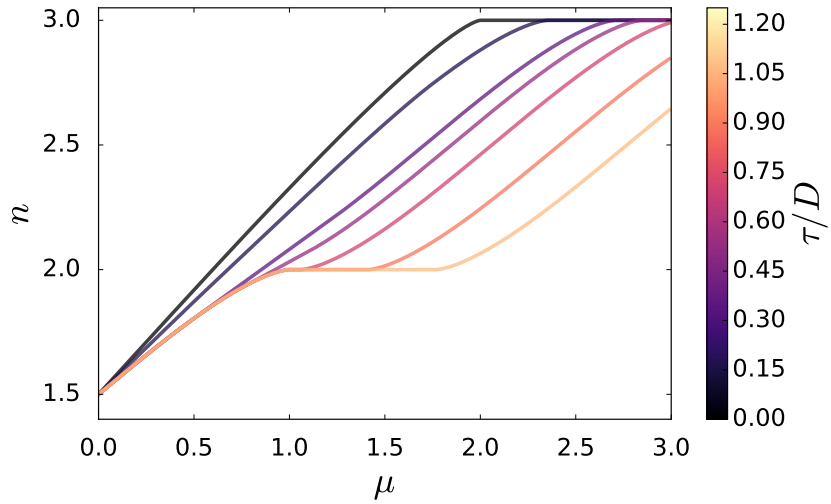

Figure 5.2: Total density as a function of the chemical potential for several values of τ and $U = 1\,D$. The color bar indicates the intensity of the external field τ in units of half-bandwidth. The plots refer to the numerical solution of the MF equations in eq.(5.13).

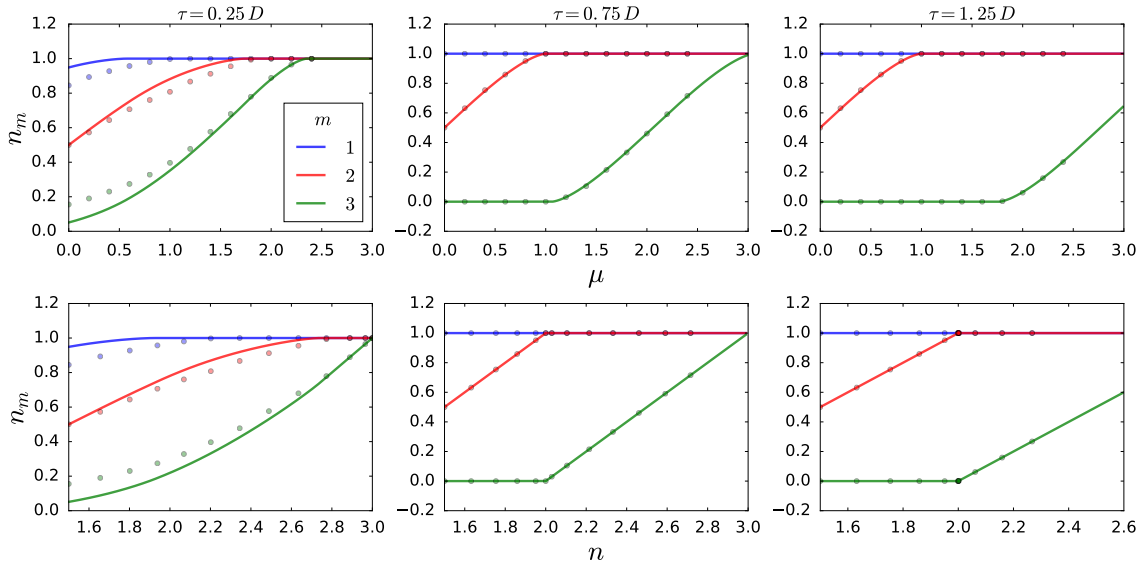

Figure 5.3: (Upper panel) Occupation numbers relative to the different fermion species as functions of the chemical potential for $\tau = 0.25\,D$, $0.75\,D$, $1.25\,D$ at $U = 1D$. (Lower panel) Occupation numbers relative to the different fermion species as functions of the total density for $\tau = 0.25\,D$, $0.75\,D$, $1.25\,D$ at $U = 1D$. The dots refer to the values of n_m evaluated with DMFT.

Intermediate Coupling

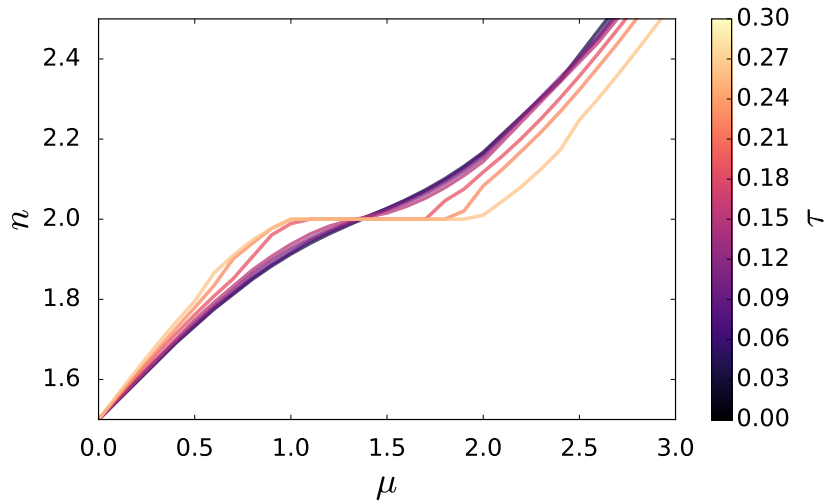

Figure 5.4: Total density as a function of the chemical potential for several values of τ and for $U/D = 2.5$.

Fig.(5.4) shows the total density as a function of the chemical potential, for several values of the field τ, for $U = 2.5\,D < U_{c1}(\tau = 0)$. The density profile does not change very much as a function of τ until the field reaches the critical value τ_c, such that for $\tau > \tau_c$ plateaus develop at $n = 2$. Therefore, for $\tau < \tau_c$, $A(\omega)$ has a finite spectral weight at the Fermi energy for any value of the chemical potential, while when $\tau > \tau_c$, there is a finite range of values of μ such that the spectral function is gapped at the Fermi level and the system is an insulator. The evolution of the spectral function for several values of τ, at $U = 2.5\,D$ is displayed in Fig.(5.5), where it is evident that for $\tau > \tau_c$ the ground state is a band insulator, as in the case of weak coupling. The band should recover the non-interacting DOS for any flavor index. The discretization of the effective bath used in the ED scheme for solving the AIM hides the result, nevertheless the frequency range is clearly the correct one for every band.

Despite the trivial nature of this insulating state, the approach to this state as a function of μ, τ and U is far from trivial.

As a first evidence of this last statement, it is worth to observe the abrupt change of the density profile $n(\mu)$ as a function of the external field, implying that the gap of the spectral function opens quite abruptly as a function of τ. Another non-trivial feature of the system is given by the distinct behaviors of the occupation numbers relative to different fermionic species as functions of τ and μ. The upper panel of Fig.(5.6) shows

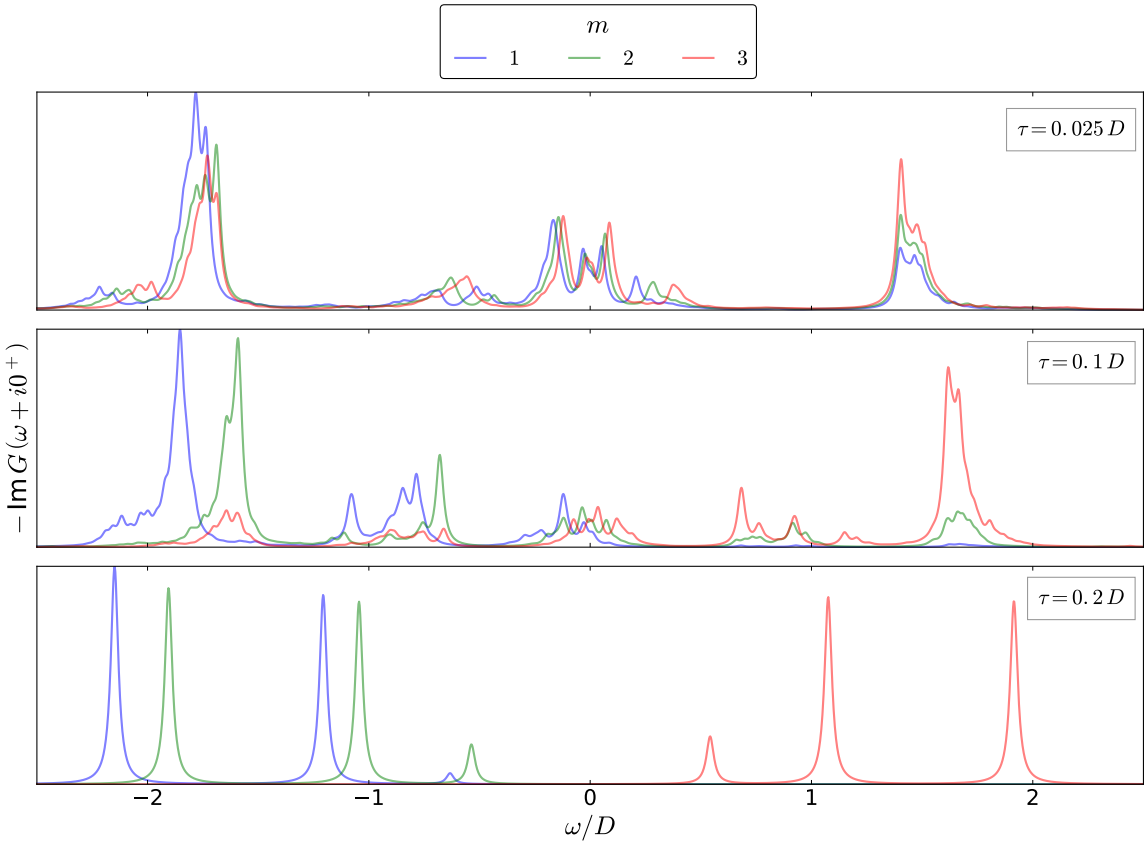

Figure 5.5: Spectral function relative to the three different flavor components for $\tau = 0.025\,D,\ 0.1\,D,\ 0.2D$ at $U = 2.5\,D$ and $n = 2$.

the occupation numbers of the fermionic components as a function of the chemical potential for several values of τ at $U = 2.5\,D$. As a direct consequence of the energy levels disposition shown in Fig.(5.1), the occupation numbers order in the following way $n_1 < n_2 < n_3$. When $\tau \ll \tau_c$, the trend of the occupation number relative to the m-th component is very similar to the symmetric case at $\tau = 0$. When $\tau < \tau_c$ but it is close to the critical value, the occupation numbers display a non-monotonic trend as a function of μ, that is very different from the behavior in the symmetric case. For values of $\tau > \tau_c$, the system polarizes at $n = 2$, i.e. there is a finite range of values of μ such that $n_1 = n_2 = 1$ and $n_3 = 0$. Also in this case, $n_3(\mu)$ and $n_2(\mu)$ assume a non-monotonic behavior when the system is close to its full polarization. The lower panel of Fig.(5.6), shows the occupation numbers as a function of the total density. Here, it is clear that the non-monotonic behavior of $n_{2/3}$ occurs when $n \sim 2$.

The lower panel of Fig.(5.7) shows the renormalized masses relative to the m-th component of the quasi-particle, labeled as m^*_m, as a function of the total density for several values of τ at $U = 2.5\,D$. Until $\tau < \tau_c$, the QP masses are continuous function of n and they have a maximum for $n \sim 2$ for every flavor index. It is worth to notice that for $\tau = 0.1\,D$, that is close to the critical value $\tau_c \sim 0.115\,D$, the renormalized masses of the fermionic species $2, 3$ are much greater than m^*_1. This difference is emphasized when $\tau > \tau_c$, where m^*_1/m_1 tends continuously to the unity when $n \to 2$, while $m^*_{2/3}$ jump to their bare values almost discontinuously at $n = 2$.

Fig.(5.8) shows the renormalized correlation relative to the different couples of fermionic species, that is defined as $D_\delta \equiv |\,\langle n_m n_{m'}\rangle - \langle n_m\rangle\,\langle n_{m'}\rangle\,|/\,\langle n_m n_{m'}\rangle + \langle n_m\rangle\,\langle n_{m'}\rangle$, where $\delta = (m, m')$. D_δ shows a selectivity of the correlations between the fermionic species $(2, 3)$, i.e. $D_{(2,3)} \gg D_{(1,2)}, D_{(1,3)}$ for $n \sim 2$ and $\tau \sim \tau_c$. In a typical cold atomic experiment, the probabilities for n-fold occupancy can be easily measured. D_δ depends on the double occupancies and the single occupation numbers, therefore it is a quantity related to the experiments in a more direct way respect to the quasi-particle masses.

Fig.(5.9) displays the occupation numbers of the different fermionic species separately as functions of the chemical potential for several values of τ. It is evident that while $n_1(\mu)$ tends continuously to its saturation value along both τ and μ axes, the same statement does not hold for $n_2(\mu)$ and $n_3(\mu)$. This is much clearer looking at the plots of $n_{2/3}$ as a function of the total density. Indeed, $n_{2/3}(n = 2)$ jumps discontinuously from a finite value in the range $[0, 1]$ to $1(0)$ at $\tau = \tau_c$. This is resumed in Fig.(5.12), where the occupation numbers are plotted as functions of τ at fixed density. The trend

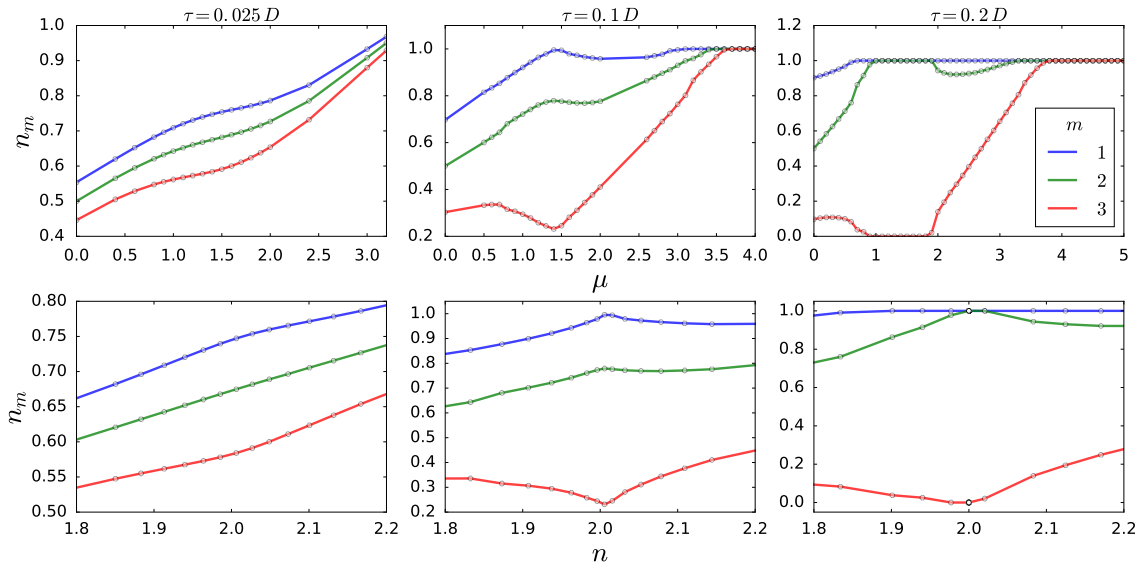

Figure 5.6: (Upper panel) Occupation number of the m-th fermionic component as a function of μ for $\tau = 0.025\,D,\ 0.1\,D,\ 0.2D$ at $U = 2.5\,D$. (Lower panel) Occupation number of the m-th fermionic component as a function of n for $\tau = 0.025\,D,\ 0.1\,D,\ 0.2D$ at $U = 2.5\,D$.

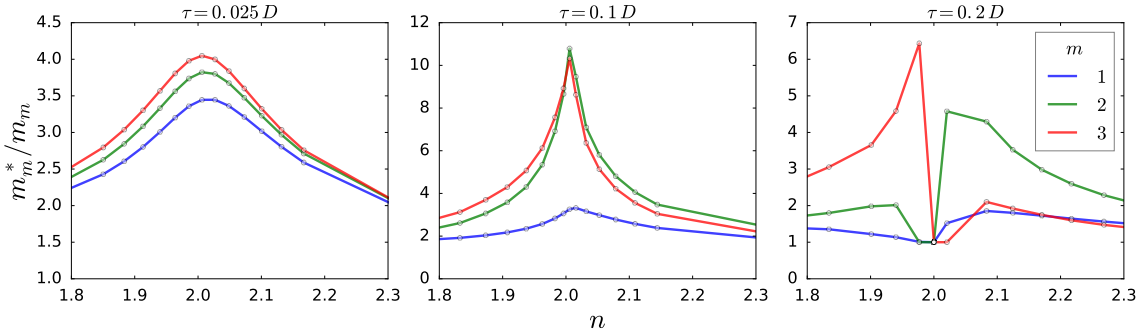

Figure 5.7: Ratio between the renormalized and bare mass of the m-th quasi-particle component as a function of n for $\tau = 0.025\,D,\ 0.1\,D,\ 0.2D$ at $U = 2.5\,D$.

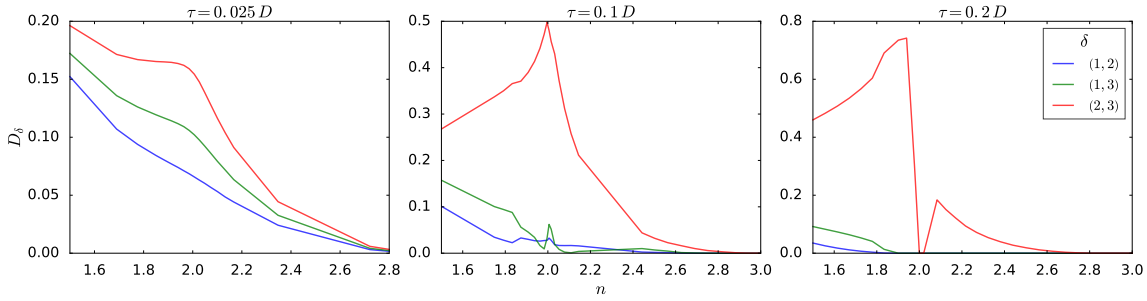

Figure 5.8: Renormalized correlation relative to the different couples of fermionic species $\delta = \{(1,2),\ (1,3),\ (2,3)\}$ as a function of n for $\tau = 0.025\,D,\ 0.1\,D,\ 0.2D$ at $U = 2.5\,D$.

of the occupation numbers curves $n_{2/3}(n=2)$ it is similar to what is observed in the single band Hubbard model in presence of an external magnetic field at intermediate coupling [6][5], where the system displays a metamagnetic behavior. Conversely $n_1(n=2)$ tends continuously to its saturation value, with a trend similar to the one obtained in the weak coupling regime. Therefore, the system shows an exotic selective metamagnetic behavior, mixing two different trends that usually occur in a distinct fashion. This selective metamagnetism is confirmed by the behavior of the effective masses of the fermion components as a function of the chemical potential and the magnetic field, as displayed in Fig.(5.10). Indeed, also the renormalized mass of the m-th quasi-particle component, has a selective trend. In general, when $\tau < \tau_c$, $m^*_m(n)$ is a continuous function and has a peak at $n \sim 2$ for all the flavor indices. Nevertheless, m^*_1 decreases as a function of τ, while $m^*_{2/3}$ are dramatically enhanced when τ approaches its critical value. When $\tau > \tau_c$, as already mentioned above, the effective masses are no more continuous functions of the total density, since at $n = 2$ the system is a band insulator and $m^*_m = m_m$ for all the flavor indices. However, when $n \neq 2$ the ground state is still metallic, and the quasi-particle renormalized masses has a divergent trend for the indices $m = 2, 3$, when the $n \sim 2$ and $\tau \sim \tau_c$. This trend is lost for $\tau \gg \tau_c$, and it is never observed for m^*_1.

Also the non-trivial feature encountered in this regime relative to the non-monotonic behavior of the occupation numbers as a function of the chemical potential is accentuated when $\tau \sim \tau_c$ and $n \sim 2$.

For completeness the occupation numbers relative to the fermionic components in the original basis are reported in Fig.(5.9). The unitary transformation that relates the two reference frames, mix the occupation numbers in such a way that $\tilde{n}_1 = \tilde{n}_3 > \tilde{n}_2$. The polarized state is now described by the configuration $\tilde{n}_1 = \tilde{n}_3 = 3/4$, $\tilde{n}_2 = 1/2$. Furthermore, it is worth to notice that the selective metamagnetic behavior is totally hidden in this basis, where both $\tilde{n}_1$ and $\tilde{n}_2$ have a finite jump at $n = 2$ at $\tau = \tau_c$.

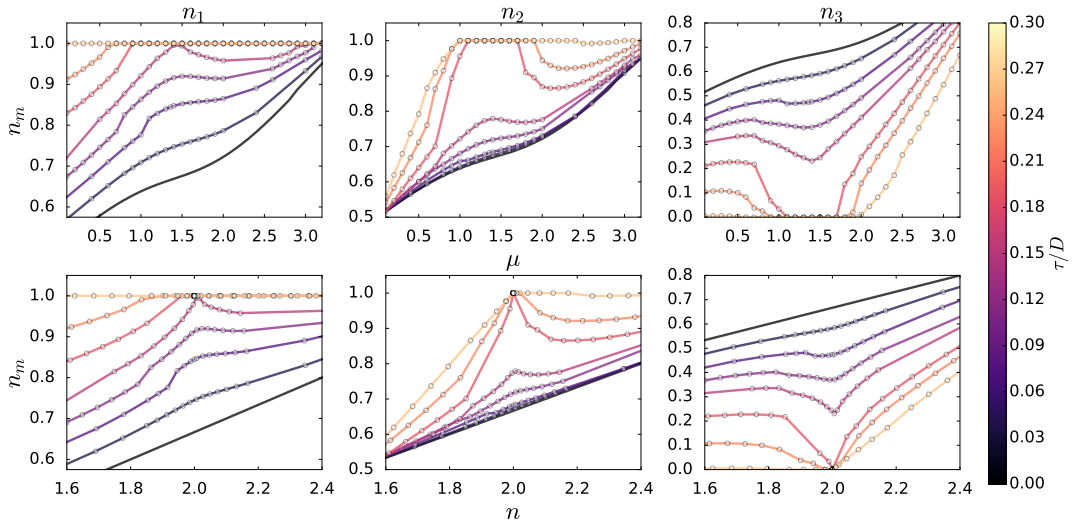

Figure 5.9: Occupation numbers of the three fermionic components $m = 1, 2, 3$ (from left to right) in the rotated basis as function of the chemical potential (upper panel) and the total density (lower panel) for several values of τ and for $U/D = 2.5$.

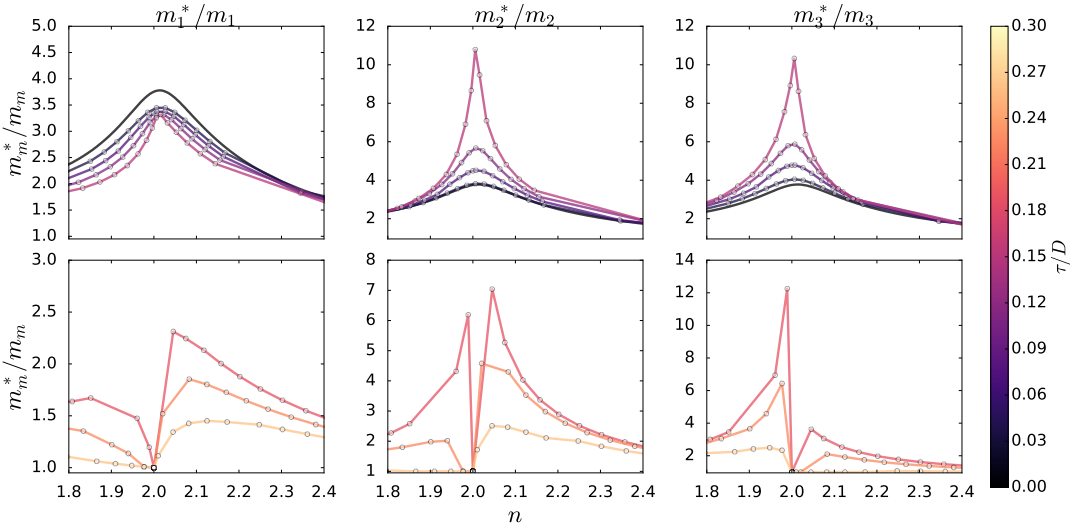

Figure 5.10: Effective masses of the three fermionic components $m = 1, 2, 3$ (from left to right) in the rotated basis as function of the total density for several values of τ and for $U/D = 2.5$. The upper and the lower panels refer to data relative to the cases where $\tau < \tau_c$ and $\tau > \tau_c$ respectively .

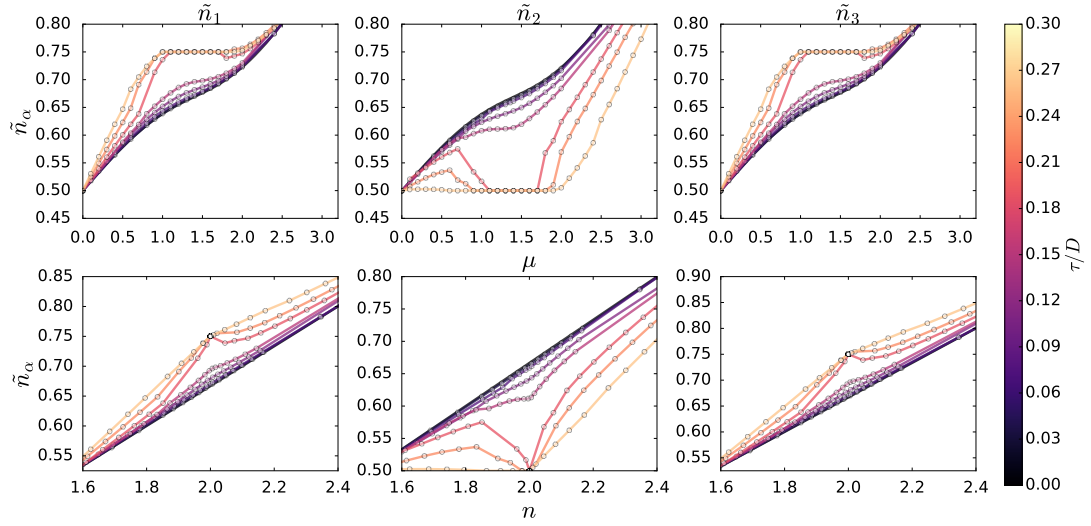

Figure 5.11: Occupation numbers of the three fermionic components $m = 1, 2, 3$ (from left to right) in the original basis as function of the chemical potential (upper panel) and the total density (lower panel) for several values of τ and for $U/D = 2.5$. In the specific case of a synthetic hopping with OBC, $\tilde{n}_1 = \tilde{n}_2$.

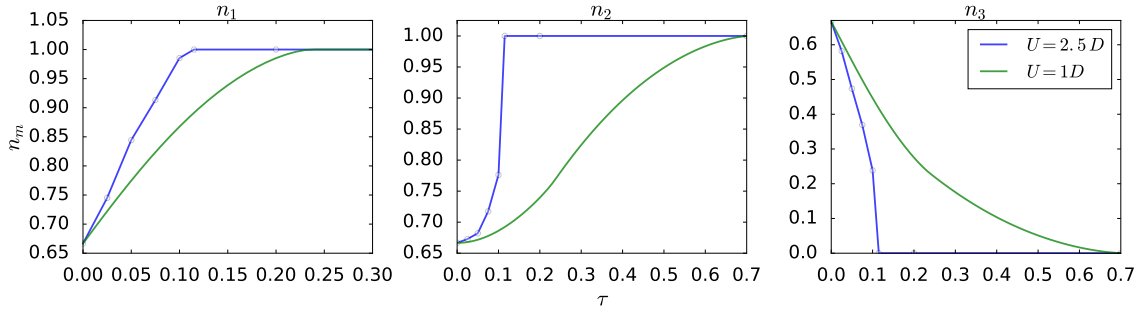

Figure 5.12: Occupation number of the m-th fermionic component as a function of the field τ evaluated at fixed total density $n = 2$. The data are reported for two different values of the interaction strength $U = 1\,D$, $2.5\,D$.

Strong Coupling

In the coexistence region where $U_{c1} < U < U_{c2}$, solutions of the DMFT equations are not found for all the values of the parameters μ and τ. Furthermore, when $U > U_{c2}$ no FL phases are found at $n = 2$ and insulating states are found only for large values of τ.

Fig.(5.13) shows the occupation numbers as a function of the total density for several values of the external field at $U = 3.3\,D$, both in the rotated and original basis. Metallic solutions at $n = 2$ are found only for small values of τ. It is worth to notice that in this regime n_1 and n_3 assume a non-monotonic trend as a function of n, while n_2 is very close to the symmetric solution at $\tau = 0$. Fig.(5.14) shows the effective masses as a function of the total density for different values of τ. A similar behavior as in the intermediate coupling regime is found: m_1^* decreases as a function of τ, while $m_{2/3}^*$ increase. Nevertheless, it is difficult to state whether the system has a selective metamagnetic behavior or not, because of the numerical difficulties encountered in this regime for higher values of τ, therefore τ_c could not be determined.

Also in this case the occupation numbers relative to the fermionic species in the original basis are reported on the right side of Fig.(5.13). It is worth to notice that in this basis the non-monotonic behavior it is not observed and that the occupation numbers have a linear trend as a function of n.

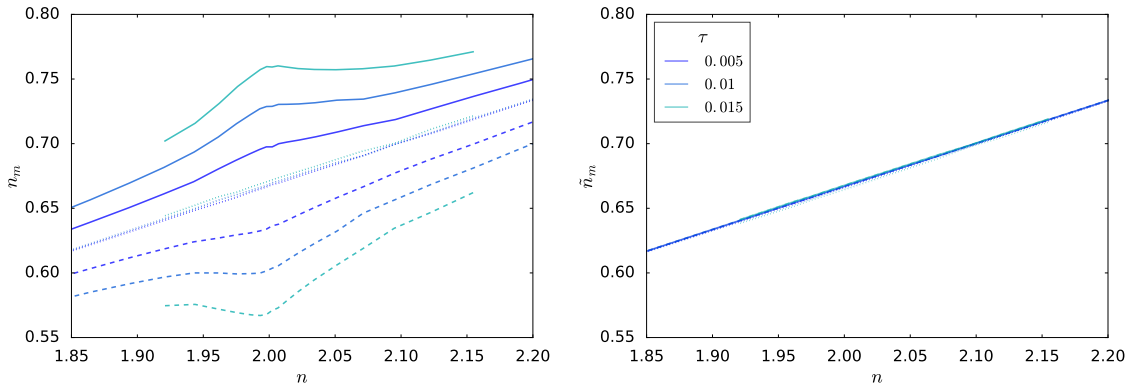

Figure 5.13: Occupation numbers of the three fermionic components in the rotated (left side) and original (right side) basis as a function of the total density for different values of the magnetic fields at $U = 3.3\,D$. The thick lines refer to n_1, the dashed lines to n_2 while the dotted ones to n_3.

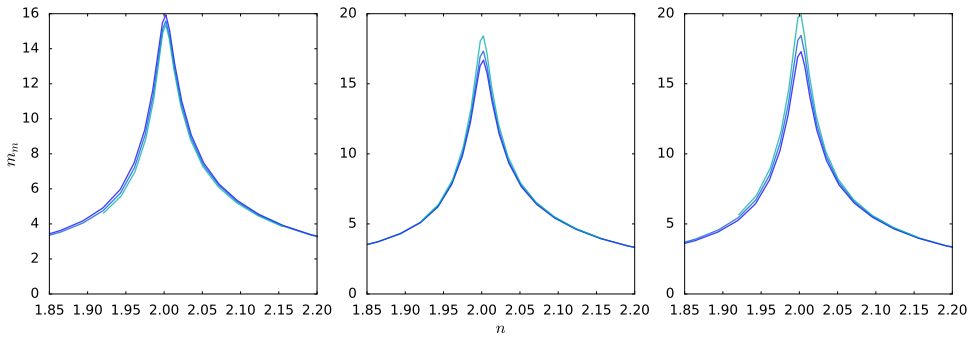

Figure 5.14: Effective masses of the rotated quasi-particles as a function of the density for different values of the field at $U = 3.3\,D$. The panels refer from left to right to the flavor indices $m = 1, 2, 3$.

Fig.(5.15) resumes the main results discussed so far about the DMFT solutions of the Hubbard model in presence of a nearest neighbor hopping along the synthetic dimension with OBC. In fact, it shows the density plots of the effective masses relative to the three fermionic components on the plane (U, τ) at $n = 2$. The symbols drawn over the density plots refer to the trend of the occupation numbers as a function of the chemical potential: the circles (triangles) stand for a monotonic (non-monotonic) trend. The critical line $\tau_c(U)$ represents a transition line between a FL and a band insulator for $U \leq 2.5\,D$ and the greatest value of the magnetic field such that metallic solutions are found for $U > 2.5\,D$. The masses have a singularity at the point $(U_{c2}, 0)$. Furthermore, the selective metamagnetic behavior of the system can be understood observing the trend of the masses of different flavor indices along the τ axis: m_1^* decreases, while $m_{2/3}^*$ increases. In addition, while for $m = 1, 3$ an increase of the effective masses corresponds to the appearance of a non-monotonic trend of the occupation numbers, the same statement does not hold for the flavor index $m = 2$. In fact, the non-monotonic behavior of n_2 disappears close to U_{c2}. A possible explanation of that could rely on the fact that at strong coupling FL solutions at $n = 2$ are found only for very small values of τ and the system is still in the linear response regime. Therefore, $m = 2$ does not feel any shift of the chemical potential, i.e. $\mu_{m=2} = \mu$, and the behavior of $n_2(\mu)$ is very close to the one obtained in symmetric case at $\tau = 0$.

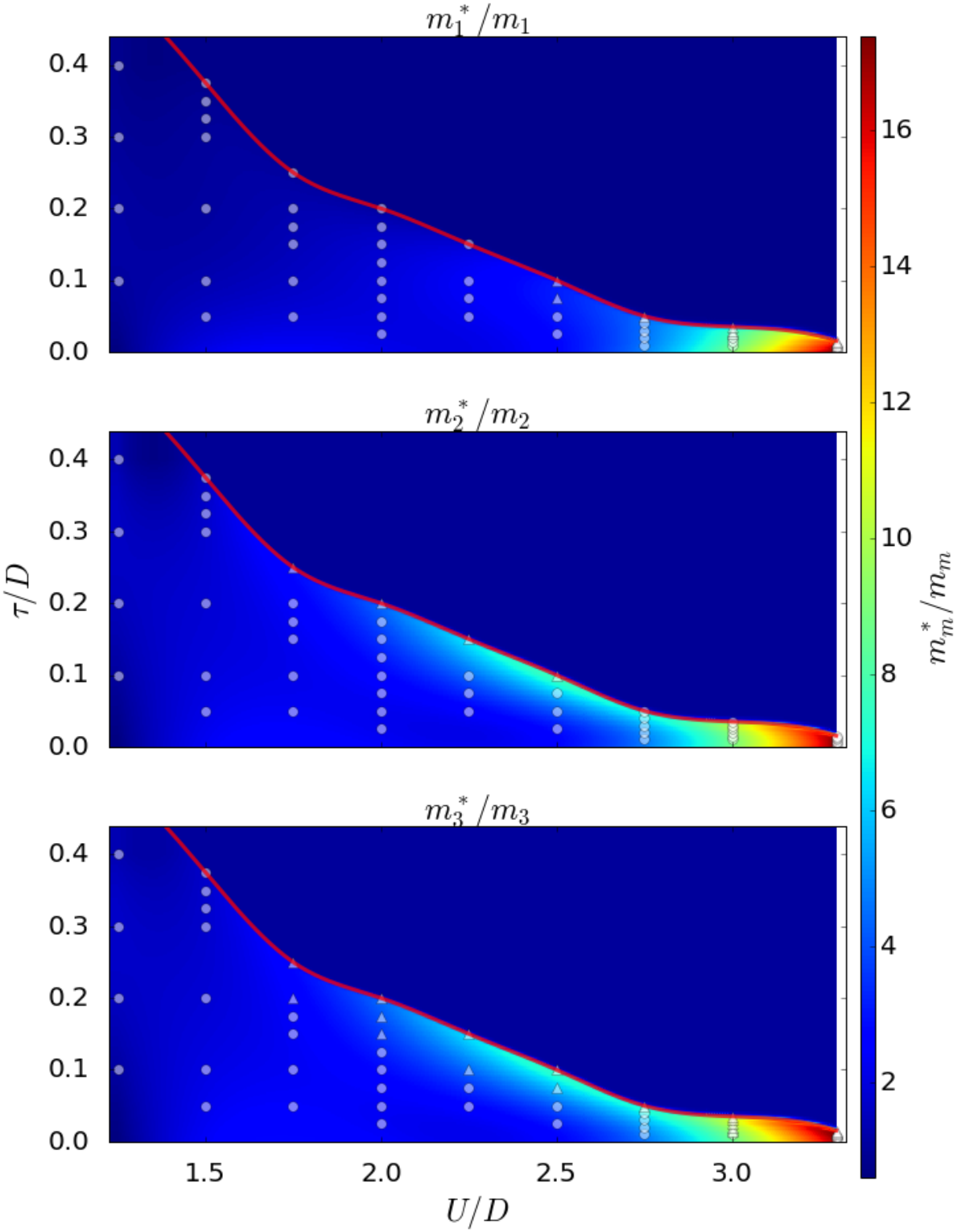

Figure 5.15: Density plots of the effective masses of the three fermionic components evaluated at $n = 2$ on the plane (U, τ). Symbols are drawn over the density plots, indicating whether the occupation number has a monotonic (circles) or non-monotonic (triangles) trend as a function of μ.

5.2.2 Synthetic hopping with PBC

In the case of a nearest neighbors hopping along the synthetic dimension with PBC, the eigenvalues of the AGF matrix reads $\{\lambda_m\} = \tau\{-2, 1, 1\}$. Therefore, a residual $SU(2)$ symmetry is preserved since the system is invariant under the permutation of the flavor indices $2 \leftrightarrow 3$.

In the atomic limit, i.e. $t = 0$, the system is an insulator at integer filling. In particular, when $n = 2$, the ground state of the system is given by the product state $|\Psi\rangle = |1\rangle_1 \otimes |\Phi\rangle_{23}$, where $|1\rangle_1 = c^\dagger_{m=1}|0\rangle_1$ and Φ_{23} belongs to the bi-dimensional degenerate subspace spanned by the kets $\{|1\rangle_2 \otimes |0\rangle_3, |0\rangle_2 \otimes |1\rangle_3\}$. Therefore, the system is simultaneously a paramagnetic Mott insulator made up by the fermionic components with flavor indices $m = 2, 3$ and a "band" insulator formed by the flavor index $m = 1$. Therefore, in this limit $n_1 = 1$ and $n_2 = n_3 = 0.5$.

Furthemore, for small values of τ, it is reasonable to expect that the phase diagram sketched in Fig.(4.4) does not vary very much its boundaries even though the nature of the insulating state is now totally altered respect its $SU(3)$-symmetric counterpart. Hence, when $U < U_{c1}$ the ground state of the system is metallic for any value of the total density, for $U_{c1} < U < U_{c2}$ the composite insulator coexists together with the FL phase, and finally for $U > U_{c2}$ only insulating solutions exist at $n = 2$.

Fig.(5.16) shows the density and the occupation numbers of the fermionic components as a function of the chemical potential, for $U = 3.0\,D$ for several values of the field. Since $U_{c1} < U < U_{c2}$, both metallic and insulating solutions coexist in a finite range of the chemical potential. The density profile relative to the FL solutions, becomes more flat in the coexistence interval increasing the external field. This is due to the fact that for large values of τ, the on site energy separation between the flavor components $m = 1, 2$ (or $m = 1, 3$) is very large, therefore n_1 tends to its saturation value very rapidly as a function of μ and the interactions between these components can be neglected. Since, in this regime only the interaction between the fermionic components $m = 1, 2$ is expected to be relevant, the physics of the system is very similar to the one of the single band Hubbard model at half-filling.

On the other hand, for small values of the field, the system has the very peculiar feature that the difference between the two values of the m-th component occupation number relative to the metallic and insulating solutions, i.e. $\Delta_m = n_m^{metal} - n_m^{ins}$ is much greater than the difference between the values of the density, i.e. $\Delta = n^{metal} - n^{ins}$.

This is due to the strong tendency of the system to fill the band relative to the $m = 1$ component and consequently to open a gap in the spectral function relative to the $m = 2, 3$ components. This discrepancy is reduced increasing the intensity of the magnetic field. It is worth to notice, that for intermediate values of the field, i.e. $\tau/D = 0.05$, n_m reaches its saturation value abruptly and its trend is very similar to the metamagnetic behavior discussed in the previous section in the case of OBC. Furthermore, for $\tau/D = 0.02, 0.05$ it is observed a non-monotonic trend for all the flavor occupation numbers.

Fig.(5.17) shows the density and the occupation numbers of the three fermionic components as a function of the chemical potential, for several values of τ at $U = 3.65\,D$. Since $U > U_{c2}$ no FL phases are found at $n = 2$ as expected. In particular there are two finite ranges of the chemical potential where a FL phase with density $n^{metal} \sim 2$ coexists together with the insulating solution. Also in this case, for relative small values of the field, a non-monotonic behavior of the occupation numbers as a function of μ and a metamagnetic trend of the component $m = 1$ are observed . All these peculiarities are lost when the magnetic field is high enough for the reasons already discussed above.

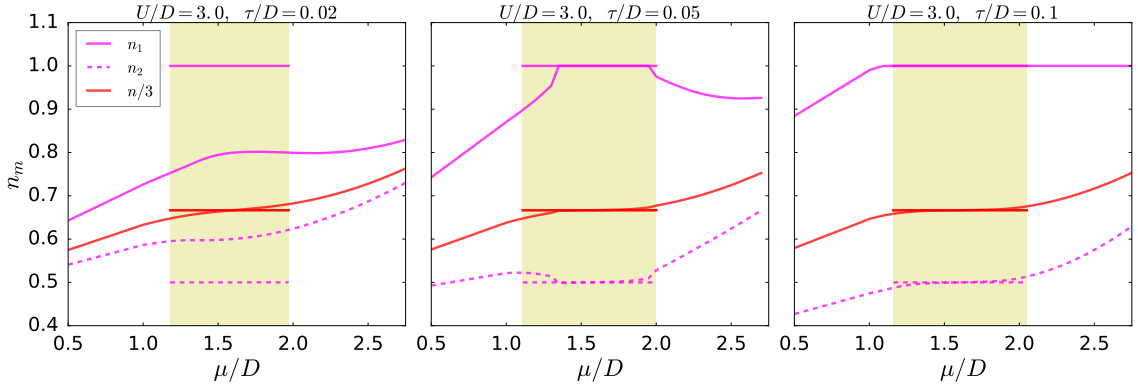

Figure 5.16: Density profiles and occupation numbers of the three fermionic components ($n_2 = n_3$) as a function of the chemical potential for several values of the magnetic field τ at $U = 3.0\,D$.

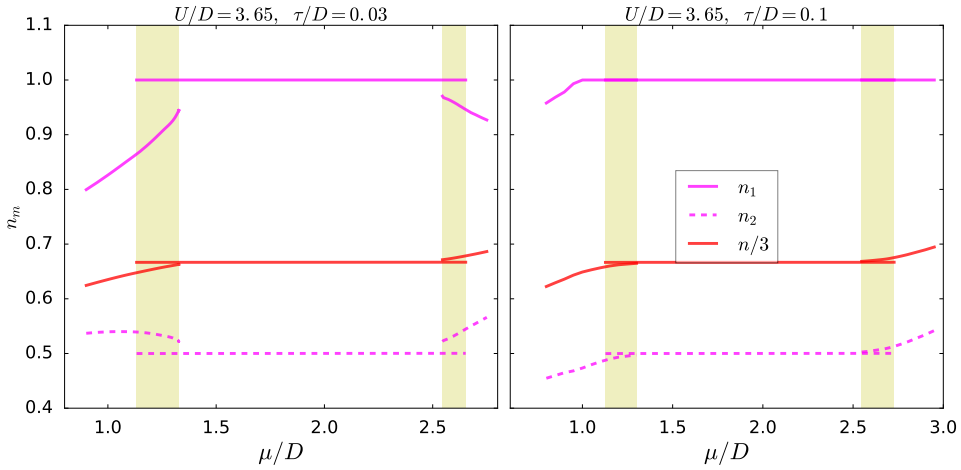

Figure 5.17: Density profiles and occupation numbers of the three fermionic components ($n_2 = n_3$) as a function of the chemical potential for several values of the magnetic field τ at $U = 3.65\,D$.

5.3 Toward the realization of a two component non-equilibrium state

It is interesting to wonder if the novel property relative to the non-monotonic trend of $n_m(\mu)$ could be exploited in order to provide a genuine non-equilibrium many body state composed by two fermionic components. In fact, while the total compressibility is always positive, i.e. $\kappa \equiv \frac{\partial n}{\partial \mu} \geq 0$, the same statement does not hold for the flavor compressibility defined as $\kappa_m \equiv \frac{\partial n_m}{\partial_\mu}$. The latter does not represent a thermodynamical quantity, and the stability of the system only relies on κ. Nevertheless, if an experimental setup could be arranged in order to suddenly get rid of one of the fermionic components, the system could be found in a state composed by two fermionic species whose overall compressibility is negative.

More formally, the procedure for eliminating one of the fermionic components, corresponds to a projection of the ground state of the system onto a subspace of the original Hilbert space. The many body ground state of the three components system $|\Psi\rangle$ belongs to the Hilbert space $\mathcal{H}$ that can be partitioned into $\mathcal{H} = \mathcal{H}_1 \otimes \mathcal{H}_2 \otimes \mathcal{H}_3$, where the subscript is relative to the flavor index. Therefore, $\mathcal{H}_m$ is the space spanned by the many-body states $|\Psi_m\rangle = \prod_\alpha c^\dagger_{\alpha m} |0\rangle$, where α could be the lattice site $\mathbf{R}$ or the wave vector $\mathbf{k} \in BZ$. The projector onto $\mathcal{H}_1 \otimes \mathcal{H}_2 \equiv \mathcal{H}_{12}$ can be written formally as $P_{12} = \left(\sum_i |i\rangle \langle i| \right) \otimes |0_3\rangle \langle 0_3|$, where $\{|i\rangle\}$ corresponds to an orthonormal basis of

$\mathcal{H}_{12}$ and $|0_3\rangle$ is the vacuum state belonging to $\mathcal{H}_3$. Therefore, the projected wave function now reads $|\Phi\rangle = P_{12}\,|\Psi\rangle$. Since the hamiltonian contains interactions among the three different flavors, the original ground state cannot be written as product of many body states that belong separately to the $\mathcal{H}_m$ spaces, i.e. $|\Psi\rangle \neq \prod_m |\Psi_m\rangle$, where $|\Psi_m\rangle \in \mathcal{H}_m$. This implies that, the average values of operators acting on $\mathcal{H}_{12}$ change after the projection, as for the case of the occupation numbers $n_{1/2}$, i.e. $\langle\Phi|\,\hat{n}_{1/2}\,|\Phi\rangle \neq \langle\Psi|\,\hat{n}_{1/2}\,|\Psi\rangle$. Therefore, it is not assured that if $\kappa_m < 0$ when calculated for the ground state of the three components system, it will be still negative after the projection.

5.4 Conclusions

The combined possibility of simulating $SU(N)$-symmetric interactions and synthesizing local gauge potentials, exploiting both the electronic structure of alkali and alkaline-earth like atoms and their interactions with light, can give rise to many interesting and exotic physical phenomena.

In particular, the scheme presented in the introduction of two Raman beams incident on a optical lattice, is suitable for simulating an effective hopping along the synthetic dimension, given by the flavor degree of freedom. In addition, a Pierles phase $\exp(\pm i\,\boldsymbol{\varphi}\cdot\mathbf{R})$ dependent on the lattice site can be impressed upon fermions that hop along the synthetic dimension. It has been discussed that the inhomogeneity brought to the system by a non-zero magnetic flux is trivial as long as two AGF matrices $\mathbb{M}_{\mathbf{R}}$ and $\mathbb{M}_{\mathbf{R}'}$ are connected to each other by a unitary transformation that depends only on the difference $\mathbf{R}-\mathbf{R}'$. Therefore, methods suitable for studying homogenous systems, as single site DMFT, can be used in order to study this class of systems. Furthermore, the symmetry of the interactions under $SU(N)$ unitary transformations simplifies very much the calculations and the numerical protocols that must be adopted for solving the resulting multi-component Hubbard Model.

The increased number of possible permutations of the flavor indices, gives the possibility of studying novel problems also in the limit of $\boldsymbol{\varphi} = 0$. For instance, for $N = 3$, a nearest neighbor hopping along the synthetic dimension can be simulated with both OBC and PBC. These two cases correspond respectively to the AGF matrix $\mathbb{M}_1$ and $\mathbb{M}_2$ presented in eq.(5.11). The differences between the spectra of these two simple 3×3 matrices lead to distinct physical results.

In the case of a synthetic hopping with OBC, the system shows a flavor selective metamagnetic behavior at intermediate couplings. In particular, $n_1(n = 2)$ goes to its saturation value continuously as a function of τ, while $n_2(n = 2)$ and $n_3(n = 2)$ has a finite jump from a value in the range $[0, 1]$ to 1 and 0 respectively, at the critical value $\tau = \tau_c$. Furthermore the effective masses of the quasi-particle component $m = 1$ decreases as a function of τ, while $m^*_{2/3}$ increases dramatically when $\tau \sim \tau_c$.

This two distinct behaviors have been shown to occur in the single band Hubbard model in presence of a magnetic field, but always separately. Therefore, this exotic mixed magnetic behavior can be consider as a novelty brought by the increased flavor degeneration. In the main text, the renormalized correlation D_δ relative to the different couples of fermionic species as a function of n is also reported, in order to link the theoretical description in a more direct way to experiments. Furthermore, since all the quantities of interest were calculated as functions of the chemical potential, it is possible with the presented data to take into account of the harmonic trap of a cold atomic experiment using the *Local Density Approximation*, therefore constructing the spatial profiles of the occupation numbers.

Afterwards, the case of a synthetic hopping with PBC has been addressed. The $SU(2)$ residual symmetry preserved by the $\mathbb{M}_2$ matrix, allows for an insulating mixed state made up of a "band" insulator and a paramagnetic Mott insulator. More in detail, the spectral function of this new insulating state is composed by a totally filled band relative to the flavor index $m = 1$ and a gapped distribution relative to the flavor components $m = 2, 3$. Also in this case non-monotonic trends of the occupation numbers as a function of μ is observed for intermediate and small values of τ.

In addition a non-monotonic trend of the occupation numbers as a function of the chemical potential has been observed for intermediate values of τ. This novel feature inspired the idea of constructing a genuine non-equilibrium state obtained as a projection of the GS of the three-component system onto a subspace of the original Hilbert space. In particular, the possibility of obtaining a two component system with a negative overall compressibility has been discussed.

CHAPTER 6

QUANTUM MAGNETISM IN THE MULTI-COMPONENT HUBBARD MODEL

The previous chapters were focused on the Mott transition in the paramagnetic sector, where any magnetic ordering has been neglected. Nevertheless, at very low temperature in the case of three dimensional systems, and at $T = 0$ for two dimensional systems, some kind of magnetic ordering is expected at least in the strong coupling regime, where the electrons become localized spins. In the particular, it is well known that in the large-U regime and for a half-filled system, the single-band Hubbard model is mapped onto the Heisenberg model, i.e.:

$$H = J \sum_{\mathbf{R}\mathbf{R}'} \mathbf{S}_{\mathbf{R}} \cdot \mathbf{S}_{\mathbf{R}'}, \tag{6.1}$$

where $S^{\mu}_{\mathbf{R}} = \sum_{\alpha\beta} c^{\dagger}_{\mathbf{R}\alpha} \left(\sigma^{\mu}\right)_{\alpha\beta} c_{\mathbf{R}\beta}$ are the local spin components along the directions $\mu = x, y, z$ and $J = 2t^2/U$ is the effective spin coupling obtained using second order perturbation theory. The Néel temperature in the Heisenberg limit is $T_N \propto J$, therefore it scales as the inverse of the interaction strength U.

In the opposite limit of weak interactions, the Néel temperature is exponentially

small as a function of U for a bipartite nested lattice, as can be shown by a simple Hartree mean field analysis of the Hubbard model. This can be understood through considerations about the response of the system to an external field. In the mean field approximation the response of the system to an external potential is given by its susceptibility that reads $\chi(\mathbf{q},\omega) = \chi_0/(1+U\chi_0)$, where $\chi_0(\mathbf{q},\omega)$ is the non-interacting susceptibility. As will be explicitly shown in the next chapter, if the energy dispersions satisfy the nesting property for a particular vector $\mathbf{Q}$, i.e. $\epsilon_{\mathbf{k}+\mathbf{Q}} = -\epsilon_{\mathbf{k}}$, as in the case of an hyper-cubic lattice in d-dimension for $\mathbf{Q} = \overbrace{(\pi,\pi,...,\pi)}^{d}$, $\mathrm{Re}\chi_0(0,\mathbf{Q}) \sim -\ln(\Lambda/T)$, where Λ is an energy cutoff. Therefore, the Néel temperature can be calculated as $1 + U\mathrm{Re}\chi_0(0,\mathbf{Q}) = 0 \Longrightarrow T_N \propto \exp(-D/U)$.

The weak and strong coupling regimes are connected by a smooth crossover and the Néel temperature displays a peak at intermediate couplings. This is illustrated in Fig.(6.1) that shows T_N calculated using DMFT as a function of the interactions.

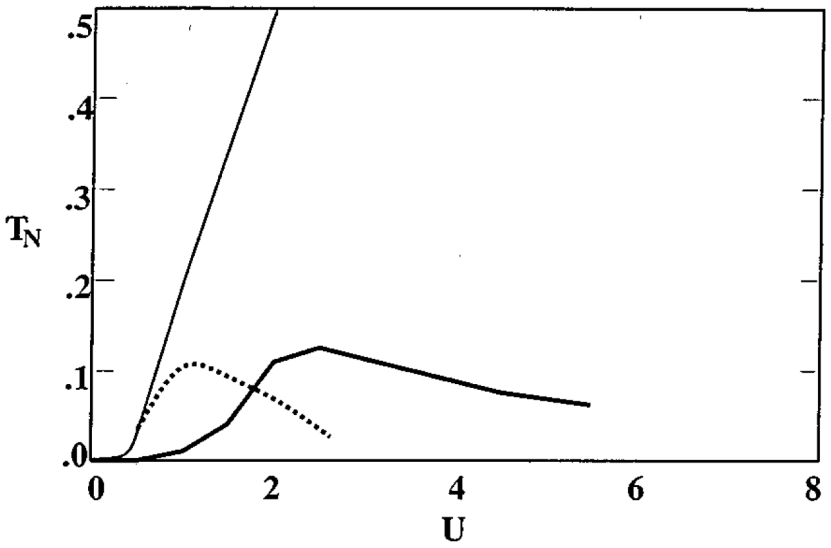

Figure 6.1: Néel temperature T_N as a function of the interaction strength U/D evaluated using DMFT in the case of a bipartite Bethe lattice at half-filling. The bold line refers to QMC calculations, the thin line is obtained using static mean-field theory, while the dotted line displays data obtained through IPT [28].

An alternative way to recover the broken symmetry consists in doping the system at a fixed temperature. In the gran canonical ensemble, this is achieved by a variation the chemical potential from its particle-hole symmetric value, how shown in the previous

chapters. In fact, a similar analysis of the system in the case of $\mu \neq 0$ in the weak coupling regime at zero temperature yields $\mathrm{Re}\chi_0(0, \mathbf{Q}) \sim -\ln(\Lambda/\mu)$.

Indeed, the first part of this chapter is dedicated to the analysis of a doped antiferromagnetic system at finite temperature, in the particular case of the single-band Hubbard model.

In the more generic case of N-fold flavor degeneration, spin hamiltonians can be derived from the hamiltonian in eq.(2.6) in the large-U limit. The increased number of possible spin and orbital permutations gives rise to a larger spectrum of the hamiltonian also in the atomic limit, whose energy manifolds are fixed by the $SU(N) \times U(1)$ symmetry. Therefore, the large-U limit provides different spin models belonging to different atomic energy manifolds. In this chapter, the case of one atom in its ground state per lattice site is considered. This corresponds in terms of the irreducible representations of $SU(N)$ to one Young tableaux per each site of the lattice and the $SU(N)$-Heisenberg hamiltonian reads:

$$H = J \sum_{\langle \mathbf{R}\mathbf{R}' \rangle} S^m_{m'}(\mathbf{R}) S^{m'}_m(\mathbf{R}') \tag{6.2}$$

where $J = \frac{2t^2}{U}$ is the super-exchange coupling and the $S^m_{m'}$ are the $N^2 - 1$ generators of the $SU(N)$ Lie algebra that obey the following commutation relation:

$$[S^m_{m'}, S^n_{n'}] = S^n_{m'}\delta^m_{n'} - S^m_{n'}\delta^n_{m'} \,. \tag{6.3}$$

In the case of $N = 2$ the Heisenberg model in eq.(6.1) is recovered, where its ground state in a bipartite lattice is an AFM. In general with $N > 2$, and in a generic lattice the situation can be far more complicated.

In the second part of this chapter, the case of $N = 3$ in the triangular lattice is addressed. References [4],[65] may be considered as a starting point of the further developments of this section. Here, it has been shown, that for $N = 3$ in the Heisenberg limit, the ground state in the square and the triangular lattices with one fermion per site is a tripartite AFM. The model in eq.(6.2) has been treated in the mean field approximation plus harmonic quantum fluctuations in the thermodynamic limit, and with ED and Density Matrix Renormalization Group (DMRG) methods in finite clusters. The mean field analysis of the $SU(3)$-Heisenberg model that has been carried

out is based on a site factorized ansatz on the many-body wave function:

$$|\Psi\rangle = \prod_{\mathbf{R}} \left(d_{A\,\mathbf{R}} \, |A\rangle_{\mathbf{R}} + d_{B\,\mathbf{R}} \, |B\rangle_{\mathbf{R}} + d_{C\,\mathbf{R}} \, |C\rangle_{\mathbf{R}} \right), \tag{6.4}$$

where A, B, C stands for the three different flavors state and the vectors $\mathbf{d_R} = (d_{A\mathbf{R}}, d_{B\mathbf{R}}, d_{C\mathbf{R}})$, are variational parameters to be optimized in order to minimize the mean field energy expectation value, that reads:

$$E_{MF} = \frac{\langle \Psi | \, H \, | \Psi \rangle}{\langle \Psi | \, \Psi \rangle} = J \sum_{\langle \mathbf{R}\mathbf{R}' \rangle} |\mathbf{d_R} \cdot \mathbf{d}^*_{\mathbf{R}'}|^2 \, . \tag{6.5}$$

Since $J > 0$, any configuration where the vectors $\mathbf{d_R}$ are orthogonal among nearest neighbors yields the ground state energy. The increase of internal degrees of freedom leads, at the mean field level, to an higher degeneration of the ground state respect to the common situation with $N = 2$. For example, in the case of the square lattice, the ground state is double degenerate when $N = 2$, while for $N = 3$ the degeneration space of the ground state is proportional to the size of the system. Nevertheless, the quantum fluctuations selects a tripartite order in the square lattice shown in Fig.(6.2).

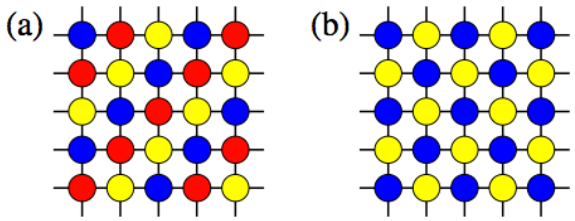

Figure 6.2: Schematic representation of a three sub-lattice (a) and a two sub-lattices antiferromagnetic state of the $SU(3)$ Heisenberg model in the square lattice. The degeneration of the two configuration at the mean field level is lifted by adding quantum fluctuations [65].

Linear flavor wave theory (LFWT), that is an extension of the usual spin wave theory of the $SU(2)$ Heisenberg model, formulated in the case of $SU(3)$-symmetry in Refs.[56][57], may be used in order to take into account of quantum fluctuations. Therefore, the quantum $SU(3)$ spin operator can be represented in the following way:

$$S^m_{m'}(\mathbf{R}) = b^\dagger_{m'}(\mathbf{R}) b_m(\mathbf{R}), \tag{6.6}$$

where $b_m(\mathbf{R})$ is the boson destruction operator relative to the m-th flavor at site $\mathbf{R}$. The ground state of the system can be now fixed, choosing a particular irreducible representation of $SU(3)$ group at each site. In this case of interest the representation corresponds to M Young Tableaux disposed horizontally per each site. This corresponds to fix the number of the Schwinger bosons at M for every site:

$$\sum_{\alpha} b_m^{\dagger}(\mathbf{R}) b_m(\mathbf{R}) = M. \tag{6.7}$$

The LFWT corresponds to let M to be large enough, in order to allow a large-M expansion. It should be noted that the right representation that corresponds to the physical situation of interest, i.e. on particle per site, it is given by $M = 1$, with the large-M expansion corresponding to a semiclassical treatment of the Heisenberg Model.

In the following, the case of an antiferromagnetic ordered state, where the spins on the site l, which belongs to the sub-lattice Λ_α, point the α-direction is considered. Hence, starting from the ordered state the following expansion for the $S_\beta^\alpha(\mathbf{R})$ operators can be used:

$$\begin{aligned} S_\alpha^\alpha(\mathbf{R}) &= M - \sum_{\beta \neq \alpha} b_\beta^{\alpha\dagger}(\mathbf{R}) b_\beta^\alpha(\mathbf{R}) \\ S_\beta^\alpha &\sim \sqrt{M}\, b_\beta^{\alpha\dagger} \\ S_\alpha^\beta &\sim \sqrt{M}\, b_\beta^\alpha \\ S_\beta^{\beta'} &= b_\beta^{\alpha\dagger}\, b_{\beta'}^\alpha, \quad \text{with} \quad \beta, \beta' \neq \alpha. \end{aligned} \tag{6.8}$$

The superscript α indicates that the boson operators act on the sub-lattice Λ_α, where the bosons on the $\alpha-$axis condensate, i.e. $b_\alpha^\alpha, b_\alpha^{\dagger\alpha} \sim \sqrt{M}$. Using eq.(6.8) the exchange term between two sites $\mathbf{R} \in \Lambda_\alpha$ and $\mathbf{R}' \in \Lambda_{\alpha'}$ reads:

$$\begin{aligned} &\sum_{\beta\gamma} S_\beta^\gamma(\mathbf{R}) S_\gamma^\beta(\mathbf{R}') = \\ &M \left[b_{\alpha'}^{\dagger\alpha}(\mathbf{R}) b_{\alpha'}^\alpha(\mathbf{R}) + b_\alpha^{\dagger\alpha'}(\mathbf{R}') b_\alpha^{\alpha'}(\mathbf{R}') + b_{\alpha'}^{\dagger\alpha}(\mathbf{R}) b_\alpha^{\dagger\alpha'}(\mathbf{R}') + b_\alpha^{\alpha'}(\mathbf{R}') b_{\alpha'}^\alpha(\mathbf{R}) \right]. \end{aligned} \tag{6.9}$$

The last equation can be plugged into eq.(6.2) and after a Fourier transform of the boson fields (defined in the sub-lattices) and a Bogoliubov transformation, the

Heisenberg Hamiltonian finally reads:

$$H = -\frac{z}{2} J\, M\, N_\Lambda + M \sum_{\mathbf{k}\in RBZ} \sum_{\alpha} \sum_{\beta\neq\alpha} \omega_{\alpha\beta}(\mathbf{k}) \left[\tilde{b}^{\alpha\dagger}_{\beta,\mathbf{k}} \tilde{b}^{\alpha}_{\beta,\mathbf{k}} + \frac{1}{2} \right], \tag{6.10}$$

where $\tilde{b}^{\alpha}_{\beta,\mathbf{k}}$ is the quasi-particle destruction operator, N_Λ is the total size of the system, z the lattice coordination number, and $\omega_{\alpha\beta}(\mathbf{k})$ represents the energy associated to the quasi-particle fluctuations along the β-axis in the Λ_α sub-lattice.

In the case of the triangular lattice, assuming a tripartite order, the fluctuations are degenerate and reads $\omega(\mathbf{k}) = \sqrt{1-|\gamma_\mathbf{k}|^2}$, with $\gamma_\mathbf{k} = \frac{1}{3}(e^{i\,k_x} + 2e^{-i\,k_y/2}\cos(\sqrt{3}k_y/2))$. The ordered moment is reduced from the unity by quantum fluctuations, yielding $\langle S^\alpha_\alpha(\mathbf{R})\rangle = M - \left\langle \frac{1}{\omega(\mathbf{k})} - 1 \right\rangle_{BZ} \sim 0.484$, therefore the tripartite order is stable under quantum fluctuations [4].

In the square lattice, as can be understood from eq.(6.5), the classical ground state is highly degenerate. The tripartite and bipartite order shown in Fig.(6.2) are both admitted. Actually a more generic helical order state is admitted by the mean field calculations, that is given by the following relation:

$$\mathbf{d}_{l+2} = \cos\theta\, \mathbf{d}_l + \sin\theta\, \mathbf{d}_l \times \mathbf{d}_{l+1}, \tag{6.11}$$

where the subscript l stands for lattice sites belonging to the l-th diagonal. The bipartite and tripartite order are obtained from the last equation respectively for $\theta = 0, \frac{\pi}{2}$. In ref. [65] has been shown that the tripartite system is the one with lowest zero point energy, once quantum fluctuations are added, and therefore is the actual ground state. Nevertheless, the quantum fluctuations in this case diverges and the ordered moment cannot be calculated using LFWT. Therefore, ED and DMRG calculations are been performed, showing that the tripartite order is stable.

The Heisenberg model in eq.(6.2) is a very good representative of quantum magnetism emerging from the Hubbard Model at strong coupling, but it is not reliable in the case of weak and intermediate coupling. Therefore, all the results shown in this introduction can be taken as benchmarks and inspiration for the upcoming sections of this chapter, where the magnetic solutions of the $SU(N)$ Hubbard model are studied at weak and intermediate coupling, using Hartree-Fock method.

6.1 DMFT analysis of a doped AFM.

In order to take into account of the antiferromagnetic solutions of the Hubbard model using a DMFT scheme, the self-consistence equations in eq.(3.37) must be generalized in the way a long range order may take place.

In general a bipartite lattice can be partitioned into two sub-lattices A and B. Therefore the non-interacting hamiltonian may be expressed in terms of these two sub-lattices as following:

$$H_0 = \sum_{\sigma} \sum_{\mathbf{k} \in RBZ} \epsilon_{\mathbf{k}} \left(c^{\dagger}_{A\mathbf{k}\sigma} c_{B\mathbf{k}\sigma} + c^{\dagger}_{B\mathbf{k}\sigma} c_{A\mathbf{k}\sigma} \right), \tag{6.12}$$

where the summation over $\mathbf{k}$ has to be carried out over the reduced Brillouin zone because of the doubling of the lattice spacing. The Green's function of the interacting lattice model can be obtained by inverting the following matrix:

$$G^{-1}(i\omega_n, \mathbf{k}) = \begin{pmatrix} \xi_{A\sigma} & -\epsilon_{\mathbf{k}} \\ -\epsilon_{\mathbf{k}} & \xi_{B\sigma} \end{pmatrix}, \tag{6.13}$$

with $\xi_{A\sigma} = i\omega_n + \mu - \Sigma_{A\sigma}(i\omega_n)$ and $\xi_{B\sigma} = i\omega_n + \mu - \Sigma_{B\sigma}(i\omega_n)$. In the relation in eq.(6.13) it is clear that a local form of the self-energy has been assumed, since $\Sigma(i\omega_n)$ is diagonal in the sub-lattice indices. Therefore, the local Green's function of the lattice model reads:

$$G_{\alpha\sigma} = \xi_{\bar{\alpha}\sigma} \int_{-\infty}^{\infty} d\epsilon \frac{g(\epsilon)}{\xi_{A\sigma}\xi_{B\sigma} - \epsilon^2}. \tag{6.14}$$

In the current case, where no external magnetic fields are considered, the system is symmetric under the composite transformation of a translation $A \to B$ plus a π rotation. This amounts to impose that $G_{B\sigma} = G_{A\bar{\sigma}}$, that allows for studying the original lattice model using only the local effective action relative to the sub-lattice A. In this case, the self consistence relations are spin-dependent and in the case of a Bethe lattice read:

$$\mathcal{G}^{-1}_{\sigma}(i\omega_n) = i\omega_n + \mu - t^2 G_{\bar{\sigma}}(i\omega_n), \tag{6.15}$$

whose physical meaning consists in the fact that the effective retarted potential felt by the $\uparrow$ fermion is given by the effective bath of the $\downarrow$ fermions.

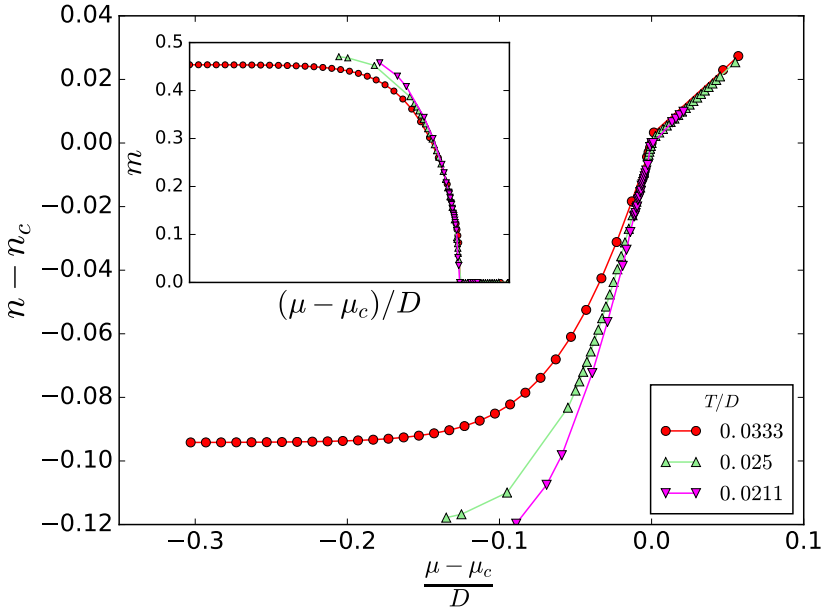

Figure 6.3: Density and staggered magnetization as functions of the chemical potential for several values of the temperature at $U = 4D$.

6.1.1 Thermodynamic instabilities of the doped AFM

The system is expected to display a second order phase transition as a function of the chemical potential at high enough temperatures. Therefore in this regime, there exists a critical value $\mu = \mu_c(T)$ that depends on the temperature such, that a transition between an antiferromagnet to a paramagnet occurs and the staggered magnetization vanishes. Since the second order character of the transition, the charge compressibility of the system κ is expected to have a discontinuity when the transition occurs. Furthermore, in Ref.[12] a dramatic enhancement of the charge compressibility as a function of the temperature was reported. Nevertheless, since the high temperature regime, it was not possible for the authors to establish whether the system was going toward a divergency of κ or not.

Fig.(6.3) shows the magnetization and the density as functions of the chemical potential for several values of the temperature T at $U = 4D$. The data were computed using an ED solver at finite temperature with $N_s = 6$. At $\mu = \mu_c$, the staggered magnetization m vanishes continuously and $\kappa \equiv \frac{\partial n}{\partial \mu}$ has a discontinuity, as expected. The trend of the density curves increases its slope more and more as a function of the temperature and a divergent behavior of $\kappa(\mu_c, T)$ is observed as a function of T. This permits to estimate a critical temperature T_c such that such a divergency occurs. Fig.(6.4) shows

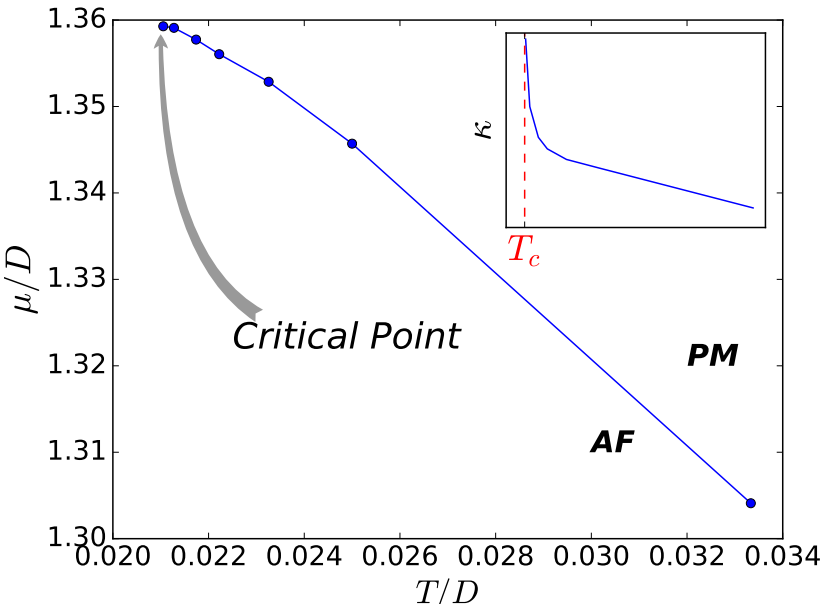

Figure 6.4: Phase diagram in the plane (T, μ) evaluated at $U = 4D$. The inset shows the divergent behavior of $\kappa(\mu_c, T)$ evaluated on the critical line.

the phase diagram in the plane (T, μ) for $U = 4D$. The critical line $\mu_c(T)$ separates the antiferromagnetic region from the paramagnetic one where $m = 0$. The inset in the figure, shows the divergent behavior of the compressibility $\kappa(\mu_c(T), T)$ calculated on the critical line. It was possible to estimate the critical temperature T_c through a logarithmic fit of the compressibility. For $T < T_c$, the DMFT cycle does not converge for any value of the chemical potential. Conversely, a finite range of "forbidden" values of μ opens in correspondence of the critical point shown in the phase diagram.

Even though no solutions are found n correspondence of the "forbidden" region, it interesting to analyze the details relative to the DMFT cycle. In particular, Fig.(6.5) shows the the density, the magnetization and the convergence test χ as a function of the DMFT iteration i, at $U = 4D$ and $T < T_c$, for three different values of $\mu = 1.34\,D$, $1.35\,D$, $1.36\,D$ that correspond to three different regimes. In the first one ($\mu = 1.34D$), after a certain number of iterations the system achieves convergence. In the second regime ($\mu = 1.35D$), the system takes a very long iteration time to find an homogenous solution. Furthermore, the observables m and n displays a damped oscillating dynamics as a function of the iteration time. Finally the third regime ($\mu = 1.36D$) is characterized by a conservative oscillation trend of the observables as a function of i, and no convergence is achieved. More specifically, the density oscillates

between two values n_- and n_+ with $n_- < n_+$, that correspond to an antiferromagnetic and a paramagnetic state respectively. It is interesting to wonder if it is possible to grasp some physical insights from this additional informations relative to the cycle dynamics. In particular, this intriguing oscillatory behavior between two states with different densities, together with the divergence of the charge compressibility would suggest that the system is moving toward a phase separation, where puddles of an antiferromagnetic phase alternates with paramagnetic ones. This would be consistent with the following interpretation of the DMFT cycle. At the iteration time i the site $\mathbf{R}_i$ of the original lattice is treated as the interacting impurity of the effective action S_{eff}. Afterwards this last is solved and $\mathcal{G}_i^{-1}$ is computed through the self-consistence equation. Therefore, a new iteration starts at the time $i+1$, and the site $\mathbf{R}_{i+1}$, that belongs to the nearest neighbors of $\mathbf{R}_i$, is selected as the new impurity of the effective action, feeling an effective potential $\mathcal{G}_i^{-1}$ induced at the time i by its nearest neighbors. Then, another iteration starts and the cycle proceeds in this way moving from one site to its nearest neighbors. Following this interpretation, the period relative to the undamped oscillations observed in the DMFT cycle, could be thought as an effective length that measures the distance between the centers of the magnetic and paramagnetic puddles. In this case the data reported in Fig.(6.5) would suggest a characteristic length of the order of hundreds of the lattice spacing.

Fig.(6.6) shows the critical temperature T_c as a function of U. The curve displays a maximum at intermediate coupling and decreases at stronger and weaker couplings. The trend of T_c seems to mimick the Néel temperature behavior in the Heisenberg limit and at intermediate coupling. At weaker couplings, the iteration time necessary to achieve convergence increases dramatically.

In this case, rather than estimating T_c as a logarithmic fit of the charge compressibility $\kappa(\mu_c(T), T)$ as for the specific case of $U = 4D$, the values reported in figure were estimated in a different manner. In particular, T_c has been defined as the greatest value of the temperature such that undamped oscillations appear in the DMFT cycle. More in detail, the dots plotted in Fig.(6.6) were computed as the average $\frac{T_c^+(U)+T_c^-(U)}{2}$, where $T_c^+(U)$ represents the lowest value of T such that DMFT solutions were found for arbitrary values of μ, while $T_c^-(U)$ is the greatest value of T such that oscillations in the DMFT cycle appear for a finite range of μ. The error bars were computed as the relative error between $T_c^{\pm}(U)$. It is worth to notice that the values of T_c evaluated in the two different manners for $U = 4D$ are in a very good quantitative agreement.

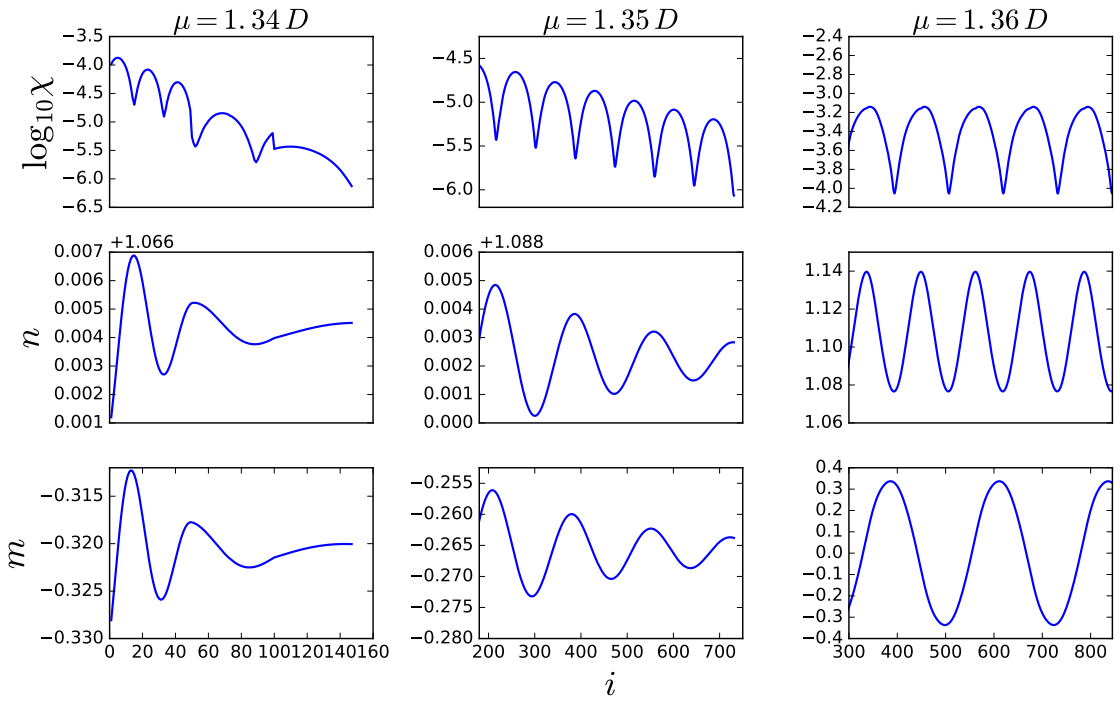

Figure 6.5: Plot of the staggered magnetization, density and convergence test as functions of the iteration time i. Different columns are relative to different values of the chemical potential, that correspond to the three different regimes of the cycle dynamics commented in the main text.

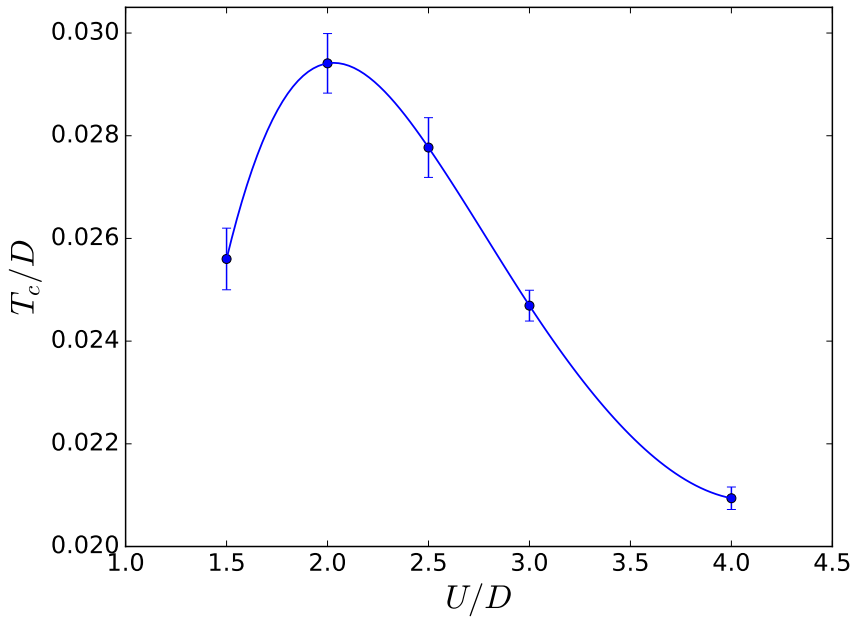

Figure 6.6: Critical value of the temperature T_c as a function of the interaction strength U.

6.2 SU(3) AFM in the triangular lattice

Three flavors can be arranged in a lattice that can be divided into three sub-lattices, in order to form an antiferromagnetic configuration. Straightforwardly, the triangular lattice seems to be a perfect candidate to display an antiferromagnetic order of this kind. Nevertheless, the situation is different from the case of the $SU(2)$ Hubbard model in the square lattice, where perfect nesting occurs.

This section is organized in three parts. In the first, the non-interacting gas instability in the particle-hole channel is studied by means of RPA approximation. In the second part the Hartree-Fock method is used for studying the emergence of the ordered phase. In the last part, it is discussed a possible extension of DMFT for a tripartite lattice in order to study the tripartite antiferromagnetic order and to take into account, in a non perturbative way, the local quantum fluctuations.

6.2.1 RPA susceptibilities

In order to understand if is there any instability under the action of a magnetic field in the particle-hole channel, it is useful to compute the RPA susceptibility. For this purpose, consider the interacting part of the Hubbard hamiltonian:

$$H_{int} = U \sum_{\alpha<\beta} \int d^d x \, \rho_\alpha(x) \, \rho_\beta(x). \tag{6.16}$$

The flavor density can be rewritten as $\rho_\alpha = \delta\rho_\alpha + \langle\rho_\alpha\rangle$, where $\delta\rho_\alpha = \rho_\alpha - \langle\rho_\alpha\rangle$. In case of small fluctuations, the interacting hamiltonian can be linearized in the flavor densities, i.e. discarding quadratic terms in $\delta\rho_\alpha$. The linearized hamiltonian reads

$$H_{int} \sim U \int d^d x \sum_{\alpha\neq\beta} \langle\rho_\beta\rangle \, \rho_\alpha - \frac{1}{2} \langle\rho_\alpha\rangle \langle\rho_\beta\rangle \ . \tag{6.17}$$

The density of the flavor α is now decoupled from the others, but is subjected to an effective external field created by the other flavor densities.

Linear response theory gives a formula for calculating the density average of the system under the action of an external field V_{ext}. In the case of a non interacting gas, the formula reads:

$$\langle\rho_\alpha(\omega, \mathbf{q})\rangle = V_{ext}(\omega, \mathbf{q}) \, \chi_0(\omega, \mathbf{q}) \, . \tag{6.18}$$

In the case the interactions are turned on the noninteracting χ_0 must be replace by the interacting one and the equation reads:

$$\langle \rho_\alpha(\omega, \mathbf{q}) \rangle = V_{ext}(\omega, \mathbf{q})\, \chi(\omega, \mathbf{q})\,. \tag{6.19}$$

Calculating χ is not an easy issue, in general. However, when U is small enough, the interaction can be treated in the mean field approximation as discussed above. In this case the particles don't interact with each others but they feel an effective external field to be summed up to V_{ext} in eq.(6.18), in order to calculate $\langle \rho_\alpha \rangle$ consistently.

Therefore:

$$\langle \rho_\alpha(\omega, \mathbf{q}) \rangle = \left(V_{ext}(\omega, \mathbf{q}) + V^\alpha_{eff}(\omega, \mathbf{q}) \right) \chi_0(\mathbf{q}, \omega), \tag{6.20}$$

that is a system of coupled algebraic equations in $\langle \rho_\alpha \rangle$, and can be reformulated in a more convenient matrix form, as following:

$$\begin{pmatrix} \rho_1 \\ \rho_2 \\ \rho_3 \end{pmatrix} = U\chi_0 \begin{pmatrix} 0 & 1 & 1 \\ 1 & 0 & 1 \\ 1 & 1 & 0 \end{pmatrix} \begin{pmatrix} \rho_1 \\ \rho_2 \\ \rho_3 \end{pmatrix} + \chi_0 \begin{pmatrix} V^{(1)}_{ext} \\ V^{(2)}_{ext} \\ V^{(3)}_{ext} \end{pmatrix}. \tag{6.21}$$

Now the interacting RPA susceptibility, will be calculated for two kind of external fields:

$$V_{\lambda_1} = V \begin{pmatrix} 1 \\ -1 \\ 0 \end{pmatrix} \qquad V_{\lambda_2} = V \begin{pmatrix} 1 \\ 1 \\ -2 \end{pmatrix} \tag{6.22}$$

The components of the external fields are chosen to be the same of the diagonal elements of the Cartan subalgebra matrices of $SU(3)$.

The solution of the system in eq.(6.21) is:

$$V_{\lambda_1} : \begin{cases} \rho_1 = \dfrac{\chi_0}{1 + U\chi_0} V \\ \rho_2 = -\dfrac{\chi_0}{1 + U\chi_0} V \\ \rho_3 = 0 \end{cases} \qquad V_{\lambda_2} : \begin{cases} \rho_1 = \dfrac{\chi_0}{1 + U\chi_0} V \\ \rho_2 = \dfrac{\chi_0}{1 + U\chi_0} V \\ \rho_3 = -2\dfrac{\chi_0}{1 + U\chi_0} V \end{cases} \tag{6.23}$$

and consequently the interacting χ reads:

$$\chi = \frac{\chi_0}{1 + U\chi_0}\,. \tag{6.24}$$

The non interacting susceptibility

In the mean field approximation the interacting susceptibility depends explicitly on χ_0, therefore the interacting system can be understood by means of the analytic properties of χ_0, that can be written using the Lindhard formula:

$$\chi_0(\omega, \mathbf{q}) = \frac{1}{\Omega} \sum_{\mathbf{k}} \frac{n_F(\xi_{\mathbf{k}}) - n_F(\xi_{\mathbf{k}} + \mathbf{Q})}{\xi_{\mathbf{k}} - \xi_{\mathbf{k}+\mathbf{Q}} + \omega + i0^+}, \tag{6.25}$$

where $\xi_{\mathbf{k}} = \epsilon_{\mathbf{k}} - \mu$ is the lattice energy dispersion measured respect to the chemical potential.

Hence, the dimensionality together with the lattice topology and filling play a crucial role, as for instance, in the case of the hypercubic lattice in d dimension at half-filling, where the band dispersion satisfies the nesting property:

$$\xi(\mathbf{k} + \mathbf{Q}) = -\xi(\mathbf{k}), \tag{6.26}$$

with $\mathbf{Q} = (\pi, \pi, .., \pi)$. This property leads to a singularity of χ_0 at the Fermi surface, and in particular it can be shown that

$$\mathrm{Re}\chi_0(0, \mathbf{Q}) \sim -\ln(1/T). \tag{6.27}$$

This implies that there exists a temperature for any arbitrary small interaction $U > 0$, such that the denominator of the RPA susceptibility vanishes, i.e $U\chi_0 = -1$. This is the reason why, at zero temperature there is always an antiferromagnetic ordering for arbitrary small values of U.

In the case of the triangular lattice in two dimensions, the situation is different. Indeed, there is no nesting property of the lattice energy dispersion, at least not for the antiferromagnetic wave vector $\mathbf{Q} = \frac{4\pi}{3}(1, 0)$, that was calculated in the previous section. This is the reason why the antiferromagnetic transition occurs at a finite value of the interaction strength U in the tripartite triangular lattice.

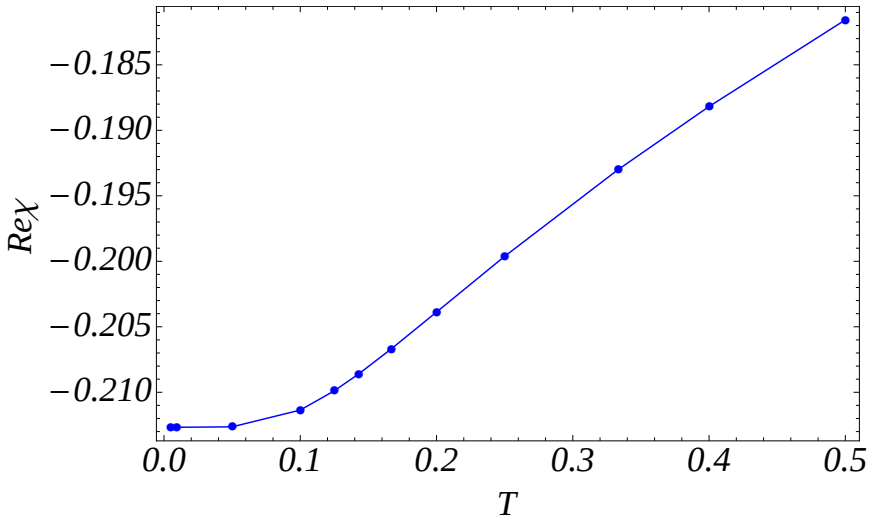

Figure 6.7: Temperature behavior of the function $\mathrm{Re}\chi_0(\omega = 0, \mathbf{Q}, T)$ in the case of the triangular lattice, with one fermion per site. The function clearly does not diverge and saturates in the limit of $T = 0$ to a constant value, from which the critical value of the interaction strength can be extrapolated, i.e. $U_c^{RPA}/D = 1/\mathrm{Re}\chi_0(\omega = 0, \mathbf{Q}, T = 0) \sim 1.05$.

Nesting properties

This section is dedicated to the nesting property of the Fermi surface and more in detail, eq.(6.27) is proved. Finally the same computation is carried out for a generic filling, showing that no divergency of the χ_0 occurs.

Let us consider the expression in eq.(6.25), in the case eq.(6.26) is fulfilled. In this specific case the Lindhard function, at $\omega = 0$ reads:

$$-\frac{1}{\Omega}\sum_{\mathbf{k}} \frac{\tanh\left(\frac{\beta\xi_{\mathbf{k}}}{2}\right)}{\xi_{\mathbf{k}}} = -\int_{-\infty}^{+\infty} d\xi\, g(\xi)\, \frac{\tanh\left(\beta\xi/2\right)}{\xi}. \tag{6.28}$$

In most of the cases, the density of states $g(\xi)$ is consider constant and calculated at the Fermi surface, and the integral in the RHS of the last equation is approximated to:

$$-g(0)\int_{-\infty}^{+\infty} d\xi\, \frac{\tanh\left(\beta\xi/2\right)}{\xi}\, \exp(-\alpha|\xi|), \tag{6.29}$$

where an exponential cut-off of the frequencies is inserted in order to assure converge. This passage is needed in order to simplify the calculations and to provide an analytic expression of χ_0, nevertheless it has also a physical meaning. Indeed, in order to have

a divergent χ_0, the condition in eq.(6.26) could be fulfilled not in the whole Brillouin zone, but in a finite domain around the Fermi surface. Therefore, in this case, the integral in eq.(6.30) would represent the summation over the subset of k-points where the nesting property is satisfied, and where the approximation on the density of states is now well understood. The integral in eq.(6.30) can be evaluated using the residue theorem and expressed as a summation over the Matsubara frequencies, i.e.:

$$\begin{aligned} -g(0)\int_{-\infty}^{+\infty} d\xi\, \frac{\tanh\left(\beta\xi/2\right)}{\xi}\, \exp(-\alpha|\xi|) \quad &= \\ -2\pi i\, g(0)\frac{2}{\beta}\sum_{i\omega_n}\frac{\exp(-\omega_n\,\alpha)}{i\omega_n} \quad &= \quad -4\pi\, g(0)\,\mathrm{atanh}\left(e^{-\pi\frac{\alpha}{\beta}}\right) \\ \sim -\ln(1/T)\,, \quad \text{when} \quad T\sim 0\,. \end{aligned} \tag{6.30}$$

One of the most representative example of nesting property of the Fermi surface is the case of the hyper-cubic lattice at half filling. This is the reason why for this kind of lattice at half filling the system has an antiferromagnetic order for arbitrary small values of the interaction.

The non interacting susceptibility has a similar behavior as a function of the chemical potential (or doping). Indeed, in the case of the hyper-cubic lattice, the nesting property is satisfied at half filling, where $\mu = 0$, i.e. $\xi = \epsilon$. In the case of $\mu \neq 0$ the Lindhard function at $T = 0$ reads:

$$-g(0)\int_{-\Lambda}^{+\Lambda} d\xi\, \frac{\theta(-\xi)-\theta(\xi+2\mu)}{2(\xi+\mu)} \sim -\ln\left(\frac{\Lambda}{\mu}\right), \tag{6.31}$$

where Λ is a finite cut-off and $\theta(x)$ is the Heaviside theta function.

6.2.2 Hartree-Fock calculations

The Hubbard model for three flavors interacting fermions reads:

$$H \;=\; -t\sum_{m=1}^{3}\sum_{<\mathbf{R}\mathbf{R}'>} c^{\dagger}_{\mathbf{R}m}c_{\mathbf{R}'m} + U\sum_{m<m'}\sum_{\mathbf{R}} n_{\mathbf{R}m}n_{\mathbf{R}m'}. \tag{6.32}$$

The hamiltonian above defined is $SU(3)$ symmetric, therefore commutes with the generators of the Lie $SU(3)$ algebra $S^m_{m'} = \sum_i c^{\dagger}_{\mathbf{R}m}c_{\mathbf{R}m'}$.

Under symmetry consideration can be derived a plausible effective mean field hamilto-

nian, using the Hartree-Fock theory, in order to study the magnetic solutions of the Hubbard Model. A magnetic field directed along the z-axis would break the symmetry, letting the hamiltonian in eq.(6.32) to commute not with all the $SU(3)$ generators, but only with the generators of the Cartan Subalgebra, given by the diagonal generators of $SU(3)$. For generic $SU(N)$ symmetry, the number of the generators of the Cartan generators are $N-1$. Therefore in the case of $SU(3)$ a two components magnetic field is expected.

According to these considerations, the effective hamiltonian should have the following form:

$$H_{eff} = -t \sum_{<\mathbf{R}\mathbf{R}'>} \psi^{\dagger}_{\mathbf{R}} \psi_{\mathbf{R}'} + U \sum_{\mathbf{R}} \psi^{\dagger}_{\mathbf{R}} \mathbb{T} \cdot \mathbf{\Delta}_{\mathbf{R}} \psi_{\mathbf{R}}, \tag{6.33}$$

where $\mathbb{T} = \left(\mathbb{T}^{(1)}, \mathbb{T}^{(2)}\right)$, that correspond to the Gell-Mann Matrices

$$\mathbb{T}^{(1)} = \begin{pmatrix} 1 & 0 & 0 \\ 0 & -1 & 0 \\ 0 & 0 & 0 \end{pmatrix} \qquad \mathbb{T}^{(2)} = \frac{1}{\sqrt{3}} \begin{pmatrix} 1 & 0 & 0 \\ 0 & 1 & 0 \\ 0 & 0 & -2 \end{pmatrix} \tag{6.34}$$

$\mathbf{\Delta}_{\mathbf{R}} = (\Delta_{\mathbf{R}1}, \Delta_{\mathbf{R}2})$, and $\psi_i = (c_{\mathbf{R}1}, c_{\mathbf{R}2}, c_{\mathbf{R}3})$ is the multi-flavor spinor at site i.
The effective hamiltonian in eq.(6.33) is a generic hamiltonian in the presence of a non-homogenous magnetic field along the z-axis in the case of $SU(3)$ fermions, and it is valid for any lattice topology. The particular case of a triangular lattice, with a non-homogenous magnetic field with a tripartite shape will be addressed, giving a generalization of antiferromagnetism in a tripartite lattice.

The effective hamiltonian

Now, the hamiltonian in eq.(6.32) can be written with an explicit spacial dependence of the order parameter:

$$\begin{aligned} H_{eff} &= -t \sum_{<\mathbf{R}\mathbf{R}'>} \psi^{\dagger}_{\mathbf{R}} \psi_{\mathbf{R}'} + U \sum_{\mathbf{R}} e^{i\mathbf{Q}\cdot\mathbf{R}} \psi^{\dagger}_{\mathbf{R}} \mathbb{T} \cdot \mathbf{\Lambda} \psi_{\mathbf{R}} \\ &+ U \sum_{\mathbf{R}} e^{-i\mathbf{Q}\cdot\mathbf{R}} \psi^{\dagger}_{\mathbf{R}} \mathbb{T} \cdot \mathbf{\Lambda}^{*} \psi_{\mathbf{R}}, \end{aligned} \tag{6.35}$$

where

$$\mathbf{\Lambda} = \frac{1}{2} \begin{pmatrix} \Delta_1 e^{-i\frac{\pi}{3}} + \Delta_2 e^{i\frac{\pi}{3}} \\ \\ \Delta_1 e^{i\frac{\pi}{6}} - \Delta_2 e^{-i\frac{\pi}{6}} \end{pmatrix} \tag{6.36}$$

represent a complex order parameter, that depends upon the two real parameters Δ_1, Δ_2 that must be determined self-consistently. The form of the order parameter $\mathbf{\Lambda}$ is justified in Appendix(D). After performing a Fourier transform of the fields the hamiltonian reads:

$$H_{\mathit{eff}} = \sum_{\mathbf{k}} \epsilon_{\mathbf{k}}\, \psi^{\dagger}_{\mathbf{k}} \psi_{\mathbf{k}} + U \sum_{\mathbf{k}} \left[\psi^{\dagger}_{\mathbf{k}}\, \mathbb{T} \cdot \mathbf{\Lambda}\, \psi_{\mathbf{k}+\mathbf{Q}} + \psi^{\dagger}_{\mathbf{k}}\, \mathbb{T} \cdot \mathbf{\Lambda}^{*}\, \psi_{\mathbf{k}-\mathbf{Q}} \right] . \tag{6.37}$$

In Fig.(6.8) it is shown how the Brillouin zone (BZ) can be partitioned into three domains BZ1 (magenta color), BZ2 (green color), BZ3 (brown color) such that:

$$\mathrm{BZ} = \bigcup_{i=1}^{3} \mathrm{BZ}i \quad \text{and} \quad \mathrm{BZ}i \cap \mathrm{BZ}j \equiv \emptyset,\ \forall\, i \neq j \tag{6.38}$$

and

$$BZi + \mathbf{Q} \equiv BZ(\,[i+1] \bmod 3\,). \tag{6.39}$$

This partition of the BZ allows the summation over the BZ to be splitted into three summations over the BZi and eventually to express all those sums as a function of a summation over BZ1 only.

Indeed:

$$\begin{aligned} &\sum_{BZ} \psi^{\dagger}_{\mathbf{k}}\, \mathbb{T} \cdot \mathbf{\Lambda}\, \psi_{\mathbf{k}+\mathbf{Q}} + \text{h.c.} = \sum_{i=1}^{3} \sum_{BZi} \psi^{\dagger}_{\mathbf{k}}\, \mathbb{T} \cdot \mathbf{\Lambda}\, \psi_{\mathbf{k}+\mathbf{Q}} + \text{h.c.} = \\ &\sum_{n=0}^{2} \sum_{BZ1} \psi^{\dagger}_{\mathbf{k}+n\mathbf{Q}}\, \mathbb{T} \cdot \mathbf{\Lambda}\, \psi_{\mathbf{k}+(n+1)\mathbf{Q}} + \text{h.c.} = \sum_{n} \sum_{BZ1} \phi^{\dagger\,(n)}_{\mathbf{k}}\, \mathbb{T} \cdot \mathbf{\Lambda}\, \phi^{(n+1)}_{\mathbf{k}} + \text{h.c.} \\ = \quad &\sum_{BZ1} \sum_{n=0}^{2} \sum_{\sigma} \lambda_{\sigma}\, \phi^{\dagger(n)}_{\mathbf{k}\sigma} \phi^{(n+1)}_{\mathbf{k}\sigma} + \lambda^{*}_{\sigma}\, \phi^{\dagger(n+1)}_{\mathbf{k}\sigma} \phi^{(n)}_{\mathbf{k}\sigma}, \end{aligned} \tag{6.40}$$

where $\lambda_{\sigma} \equiv \sum_i (\mathbb{T}_i)_{\sigma\sigma}\, \Lambda_i$ and $\phi_{\mathbf{k}} = (\phi^{(1)}_{\mathbf{k}}, \phi^{(2)}_{\mathbf{k}}, \phi^{(3)}_{\mathbf{k}})$ and $\phi^{(n)}_{\mathbf{k}} = \psi_{\mathbf{k}+n\mathbf{Q}}$, with $n = 0, 1, 2$.

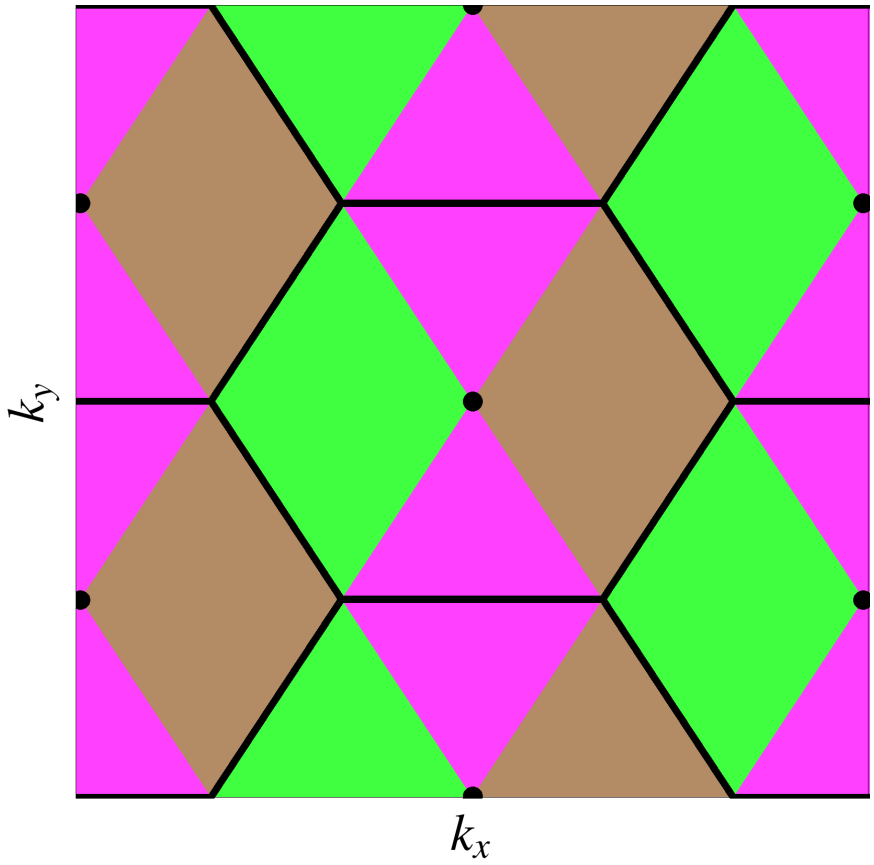

Figure 6.8: Partitioning of the Brillouin zone into the three subsets BZ_1 (brown color), BZ_2 (magenta color) and BZ_3 (green color). The Brillouin zone is given by the area of the hexagon drawn with thick lines. Since the length of the hexagon side is $4\pi/3$, it is easy to grasp that $BZ_1 \to BZ_2$ after a translation of $\mathbf{Q}$ and that $BZ_1 \to BZ_3$ after a translation of $2\mathbf{Q}$. Dots in the figure represent points of the reciprocal lattice.

Eqs.(6.38,6.39) guarantees that $\{\phi^{(i)}_{\mathbf{k}\sigma}, \phi^{(j)}_{\mathbf{k}'\sigma'}\} = \delta_{\sigma\sigma'}\,\delta_{ij}\,\delta_{\mathbf{k}\mathbf{k}'}$.

For simplicity the notation will be changed as $\phi^{(n)}_{\mathbf{k}\sigma} \to \phi_{\mathbf{k}\sigma n}$.

The hamiltonian is block diagonal in the spin sector, therefore it can be expressed as three 3×3 matrices whose indices correspond to the different color indices, i.e. $n = 1, 2, 3$.

After defining the color spinor as $\Phi_{\mathbf{k}\sigma} = (\phi_{\mathbf{k}\sigma 1}, \phi_{\mathbf{k}\sigma 2}, \phi_{\mathbf{k}\sigma 3})$, the full hamiltonian reads:

$$H_{eff} = \sum_{\mathbf{k}\in BZ1} \sum_{\sigma} \Phi^{\dagger}_{\mathbf{k}\sigma} \mathcal{H}_{\mathbf{k}\sigma} \Phi_{\mathbf{k}\sigma}, \tag{6.41}$$

where:

$$\mathcal{H}_{\mathbf{k}\sigma} = \begin{pmatrix} \epsilon(\mathbf{k}) & U\lambda_{\sigma} & U\lambda^{*}_{\sigma} \\ U\lambda^{*}_{\sigma} & -\frac{1}{2}\epsilon(\mathbf{k}) + g(\mathbf{k}) & U\lambda_{\sigma} \\ U\lambda_{\sigma} & U\lambda^{*}_{\sigma} & -\frac{1}{2}\epsilon(\mathbf{k}) - g(\mathbf{k}) \end{pmatrix}, \tag{6.42}$$

and where the relation $\epsilon(\mathbf{k}+\mathbf{Q}) = -\frac{1}{2}\epsilon(\mathbf{k}) + g(\mathbf{k})$, $\epsilon(\mathbf{k}+2\mathbf{Q}) = -\frac{1}{2}\epsilon(\mathbf{k}) - g(\mathbf{k})$ has been used, with:

$$g(\mathbf{k}) \equiv \sqrt{3}\left[\sin\left(\frac{k_x}{2} + \frac{\sqrt{3}}{2}k_y\right) + \sin\left(\frac{k_x}{2} - \frac{\sqrt{3}}{2}k_y\right) - \sin\left(k_x\right)\right]. \tag{6.43}$$

In its diagonal basis, the hamiltonian eventually reads:

$$H_{eff} = \sum_{\mathbf{k}\sigma n} \rho_{\mathbf{k}\sigma n}\, \hat{n}_{\mathbf{k}\sigma n}, \tag{6.44}$$

where $\rho_{\mathbf{k}\sigma n}$ are the eigenvalues of the matrix in eq.(6.42), $\hat{n}_{\mathbf{k}\sigma n} = \tilde{\phi}^{\dagger}_{\mathbf{k}\sigma n}\tilde{\phi}_{\mathbf{k}\sigma n}$, $\tilde{\phi}_{\mathbf{k}\sigma n} = \sum_m U_{nm}\phi_{\mathbf{k}\sigma m}$, where U is the eigenvectors matrix relative to $\mathcal{H}_{\mathbf{k}\sigma}$.

It is remarkable that, as in the case of the $SU(2)$ Hubbard model in the square lattice, the hamiltonian eigenvalues don't depend on the spin index. Therefore, the spectrum is three fold degenerate.

The self consistence equation for the magnetization

In this section, the self consistence equations for the order parameter $\mathbf{\Lambda}$ are derived. Comparing the hamiltonian in eq.(6.35) with the original Hubbard model of eq.(6.32), the order parameter must satisfies the following relations:

$$\begin{aligned}
\left[\Lambda_1 + \frac{\Lambda_2}{\sqrt{3}}\right] e^{i\mathbf{Q}\cdot\mathbf{R}} + \text{h.c.} &= \langle n_{\mathbf{R}2} + n_{\mathbf{R}3}\rangle - \frac{2}{3} \\
\left[\frac{\Lambda_2}{\sqrt{3}} - \Lambda_1\right] e^{i\mathbf{Q}\cdot\mathbf{R}} + \text{h.c.} &= \langle n_{\mathbf{R}1} + n_{\mathbf{R}3}\rangle - \frac{2}{3} \\
-\frac{2\Lambda_2}{\sqrt{3}} e^{i\mathbf{Q}\cdot\mathbf{R}} + \text{h.c.} &= \langle n_{\mathbf{R}1} + n_{\mathbf{R}2}\rangle - \frac{2}{3}\,,
\end{aligned} \tag{6.45}$$

therefore:

$$\begin{aligned}
-\frac{\langle n_{\mathbf{R}1} - n_{\mathbf{R}2}\rangle}{2} &= -\frac{1}{2}\left\langle \psi^\dagger_{\mathbf{R}}\, \mathbb{T}_1\, \psi_{\mathbf{R}}\right\rangle = \Lambda_1\, e^{i\mathbf{Q}\cdot\mathbf{R}} + \text{h.c.} \\
-\frac{\langle n_{\mathbf{R}1} + n_{\mathbf{R}2} - 2\, n_{\mathbf{R}3}\rangle}{2\sqrt{3}} &= -\frac{1}{2}\left\langle \psi^\dagger_{\mathbf{R}}\, \mathbb{T}_2\, \psi_{\mathbf{R}}\right\rangle = \Lambda_2\, e^{i\mathbf{Q}\cdot\mathbf{R}} + \text{h.c.}
\end{aligned} \tag{6.46}$$

In this way, after defining the 'staggered' magnetization components as:

$$\begin{aligned}
m_1 &\equiv -\frac{1}{2A}\sum_{\mathbf{R}} e^{i\mathbf{Q}\cdot\mathbf{R}} \left\langle \psi^\dagger_{\mathbf{R}}\, \mathbb{T}_1\, \psi_{\mathbf{R}}\right\rangle + \text{h.c.} \\
m_2 &\equiv -\frac{1}{2A}\sum_{\mathbf{R}} e^{i\mathbf{Q}\cdot\mathbf{R}} \left\langle \psi^\dagger_{\mathbf{R}}\, \mathbb{T}_2\, \psi_{\mathbf{R}}\right\rangle + \text{h.c.}
\end{aligned} \tag{6.47}$$

Using eq.(6.46), it is now possible to compute m_1 and m_2 as a function of $\mathbf{\Lambda}$.

Indeed:

$$\begin{aligned}
m_1 &= \frac{1}{A}\sum_{\mathbf{R}} e^{i\mathbf{Q}\cdot\mathbf{R}} \left(\Lambda_1^*\, e^{-i\mathbf{Q}\cdot\mathbf{R}} + \text{h.c.}\right) + \text{h.c.} = \Lambda_1^* + \text{h.c.} \\
m_2 &= \frac{1}{A}\sum_{\mathbf{R}} e^{i\mathbf{Q}\cdot\mathbf{R}} \left(\Lambda_2^*\, e^{-i\mathbf{Q}\cdot\mathbf{R}} + \text{h.c.}\right) + \text{h.c.} = \Lambda_2^* + \text{h.c.}
\end{aligned} \tag{6.48}$$

These relations have been carried out using the fact that the terms proportional to $\frac{1}{A}\sum_{\mathbf{R}} e^{i2\mathbf{Q}\cdot\mathbf{R}} \to 0$ when $A \to \infty$.

The self consistence condition reads:

$$\mathbf{m} = 2\text{Re}\left(\mathbf{\Lambda}\right). \tag{6.49}$$

Thus the physical meaning of $\mathbf{\Lambda}$ is now clear.

The condition in eq.(6.49) can be now explicited in the following way:

$$\begin{aligned} - & \frac{1}{2A}\sum_{\mathbf{R}} e^{i\mathbf{Q}\cdot\mathbf{R}}\psi^{\dagger}_{\mathbf{R}}\,\mathbb{T}_i\,\psi_{\mathbf{R}} + \text{h.c.} = -\frac{1}{2A}\sum_{\mathbf{R}\sigma}\tau^i_\sigma\, e^{i\mathbf{Q}\cdot\mathbf{R}}\,\psi^{\dagger}_{\mathbf{R}\sigma}\psi_{\mathbf{R}\sigma} + \text{h.c.} = \\ - & \frac{1}{2A}\sum_{\mathbf{k}\sigma}\tau^i_\sigma\,\psi^{\dagger}_{\mathbf{k}\sigma}\psi_{\mathbf{k}+\mathbf{Q}\sigma} + \text{h.c.} = -\frac{1}{2A}\sum_{BZ1}\sum_{\sigma n}\tau^i_\sigma\,\phi^{\dagger}_{\mathbf{k}\sigma n}\phi_{\mathbf{k}\sigma n+1} + \text{h.c.} = \\ - & \frac{1}{2A}\sum_{\mathbf{k}\sigma}\tau^i_\sigma\,\tilde{\Phi}^{\dagger}_{\mathbf{k}\sigma}\left(U_{\mathbf{k}\sigma}\mathcal{T}\,U^{\dagger}_{\mathbf{k}\sigma}\right)\tilde{\Phi}_{\mathbf{k}\sigma} \end{aligned} \tag{6.50}$$

where $U_{\mathbf{k}}$ is the matrix containing the eigenvectors of $\mathcal{H}_{\mathbf{k}\sigma}$, and $\tilde{\Phi}_{\mathbf{k}\alpha}$ is the quasi particle color spinor.

The average value of quantity in eq.(6.50) reads:

$$-\frac{1}{2A}\sum_{\mathbf{k}\sigma n}\tau^i_\sigma\,\left(U_{\mathbf{k}\sigma}\mathcal{T}\,U^{\dagger}_{\mathbf{k}\sigma}\right)_{nn} n_F(\rho_{\mathbf{k}\sigma n}) = 2\text{Re}(\Lambda_i) \tag{6.51}$$

Using the definition of $\mathbf{\Lambda}$ in eq.(D.11) this last equation can be written explicitly for the component of the field as:

$$\begin{aligned} \frac{1}{2A}\sum_{\mathbf{k}\sigma n}\tau^1_\sigma\,\left(U_{\mathbf{k}\sigma}\mathcal{T}\,U^{\dagger}_{\mathbf{k}\sigma}\right)_{nn} n_F(\rho_{\mathbf{k}\sigma n}) + \frac{\Delta_1+\Delta_2}{2} &= 0 \\ \frac{1}{2A}\sum_{\mathbf{k}\sigma n}\tau^2_\sigma\,\left(U_{\mathbf{k}\sigma}\mathcal{T}\,U^{\dagger}_{\mathbf{k}\sigma}\right)_{nn} n_F(\rho_{\mathbf{k}\sigma n}) + \sqrt{3}\,\frac{\Delta_1-\Delta_2}{2} &= 0 \end{aligned} \tag{6.52}$$

These equations together with:

$$1 = \frac{1}{A}\sum_{\mathbf{k}n\sigma} n_F(\rho_{\mathbf{k}\sigma n}), \tag{6.53}$$

that fixes the density to one fermion per site, correspond to the self consistence equations of the order parameter.

Numerical Results

Eqs.(6.52, 6.53) represent a set of three non-linear equations of three variables: Δ_1, Δ_2, that are the order parameter components and μ, the chemical potential needed to

fix the density.

The solutions of this system, that can be labeled as $X = (\bar{\Delta}_1, \bar{\Delta}_2, \bar{\mu})$, has been found numerically and they are of three kinds, where the following simple relations hold:

1. $\bar{\Delta}_1 = -\bar{\Delta}_2 \Longrightarrow n_1 = n_2$,
2. $\bar{\Delta}_1 = 2\bar{\Delta}_2 \Longrightarrow n_1 = n_3$,
3. $2\bar{\Delta}_1 = \bar{\Delta}_2 \Longrightarrow n_2 = n_3$,

where n_α are the occupation numbers evaluated in the sub-lattice A.

Hence, it is worth to note that the system spontaneously breaks the symmetry $SU(3) \to SU(2) \times U(1)$, therefore preserving a local $SU(2)$ symmetry, since the occupation numbers of two flavors are always degenerate.

This in accordance with the result shown in the introduction, in the case of the $SU(3)$-Heisenberg model, where the dispersion relation of the Flavor Waves of the flavor B and C are found to be degenerate in the sub-lattice A.

In Fig.(6.9) the solutions of the order parameter are shown as a function of the interaction strength. The thick lines refer to the solutions of eqs.(6.52, 6.53) that correspond to minima of the energy, while the dotted ones represent unstable solutions, i.e maxima of the energy. The dotted line interpolates between two spinodal points. The first one occurs at $U_{c1}/D \sim 0.87$ and it is the point such that for $U > U_{c1}$ magnetic solutions appear. The latter, occurs at $U_{c2}/D \sim 1.05$, that is such that for $U > U_{c2}$ the non-interacting gas begins to be unstable, that is in agreement with the value calculated via RPA in the previous section. The phase transition occurs at $U_c/D \sim 0.91$, that corresponds to the value of the interactions such that the free energies of the non-interacting gas and the AFM cross, as shown in Fig.(6.10). The order parameter jumps from a finite value to zero, signaling a first order phase transition.

The model with AGF

As discussed in the previous chapter, the introduction of the AGF with $\boldsymbol{\varphi} = 0$, is equivalent to introduce an hopping matrix between the fermion internal degrees of freedom (flavors).

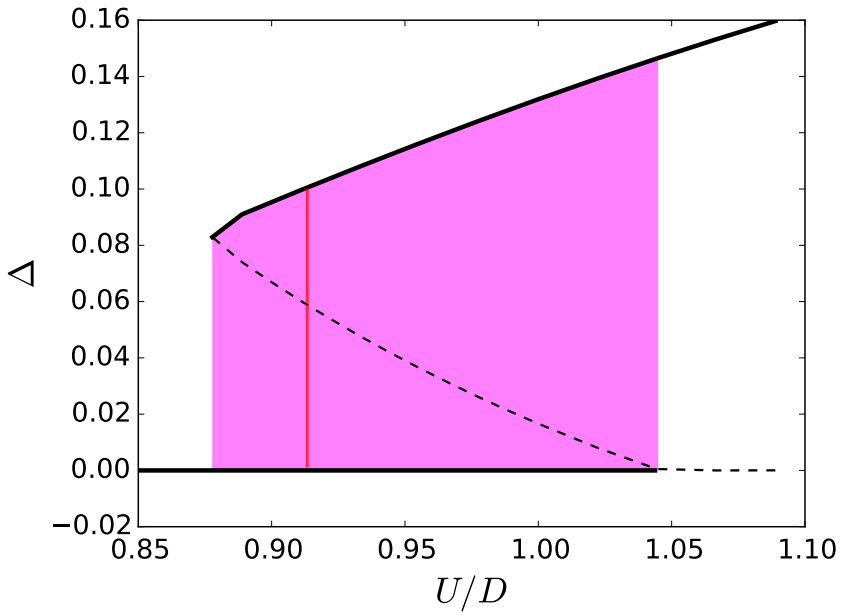

Figure 6.9: Solutions of the first kind ($\bar{\Delta}_1 \equiv \Delta = -\bar{\Delta}_2$) of the order parameter as a function of the interaction strength. The dotted line represent unstable solutions of the eqs.(6.52, 6.53), while the thick black lines refer to minima of the energy. The shaded area corresponds to the coexistence region between the normal phase and the AFM. The red vertical line indicates the critical value U_c such that for $U_{c1} < U < U_c$ the AFM is a metastable phase and the non-interacting gas is the actual ground state, while for $U_c < U < U_{c2}$ the actual ground state is the AFM and the normal phase corresponds to a relative minimum of the energy.

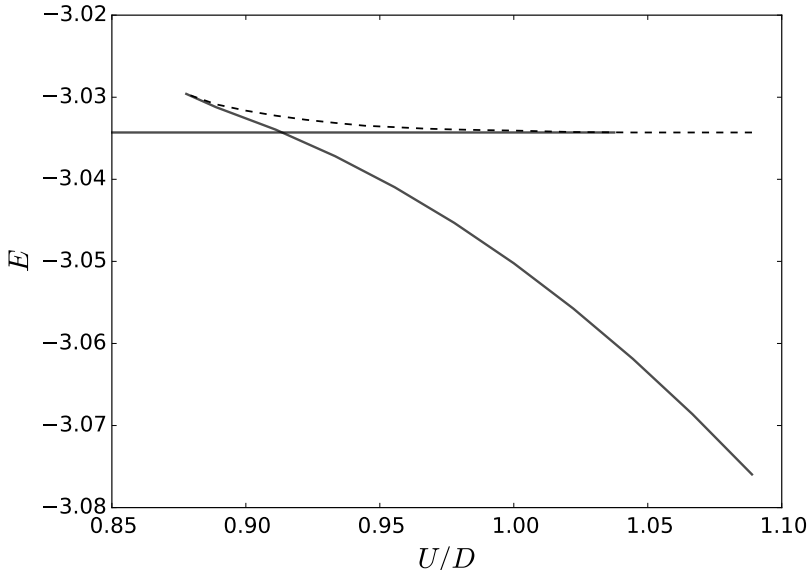

Figure 6.10: Cross of the free energies of the non-interacting gas and the AFM (thick lines). The dotted line corresponds to the energy relative to the unstable solutions shown in Fig.(6.9). This value corresponds to a maximum of the energy between the two minima when $U_{c1} < U < U_{c2}$.

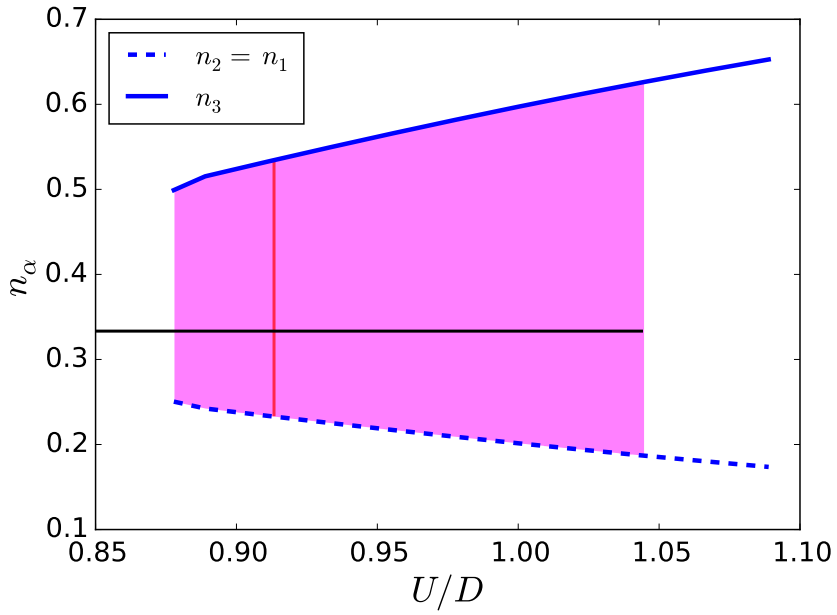

Figure 6.11: Occupation numbers as a function of the interactions.

Therefore, the onsite energy of fermions depends on the flavor index and it's given by the eigenvalues of the hopping matrix, that reads:

$$M = -\begin{pmatrix} 0 & t_1 & t_2 \\ t_1 & 0 & t_1 \\ t_2 & t_1 & 0 \end{pmatrix}, \tag{6.54}$$

In order to take into account of the ferromagnetic ordering in the HF scheme, two additional variational parameters are needed in the parametrization of the occupation numbers.

Therefore, eq.(D.2) has to be modified as following:

$$\begin{aligned} \langle n_{\mathbf{R}1}\rangle - \frac{1}{3} &= \delta n_1 - \Delta_{\mathbf{R}1} - \frac{1}{\sqrt{3}}\Delta_{\mathbf{R}2} \\ \langle n_{\mathbf{R}2}\rangle - \frac{1}{3} &= \delta n_2 + \Delta_{\mathbf{R}1} - \frac{1}{\sqrt{3}}\Delta_{\mathbf{R}2} \\ \langle n_{\mathbf{R}3}\rangle - \frac{1}{3} &= \delta n_3 + \frac{2}{\sqrt{3}}\Delta_{\mathbf{R}2}\,, \end{aligned} \tag{6.55}$$

where δn_α is the homogenous variation of the occupation number from the symmetric case where $\tau_1 = \tau_2 = 0$, that includes also the effect of the interactions. Fixing the density at $n = 1$, it's equivalent to impose a relation between theses variations. Hence, eq.(6.55) reads:

$$\begin{aligned} \langle n_{\mathbf{R}1}\rangle - \frac{1}{3} &= \delta n_1 - \Delta_{\mathbf{R}1} - \frac{1}{\sqrt{3}}\Delta_{\mathbf{R}2} \\ \langle n_{\mathbf{R}2}\rangle - \frac{1}{3} &= \delta n_2 + \Delta_{\mathbf{R}1} - \frac{1}{\sqrt{3}}\Delta_{\mathbf{R}2} \\ \langle n_{\mathbf{R}3}\rangle - \frac{1}{3} &= -(\delta n_1 + \delta n_2) + \frac{2}{\sqrt{3}}\Delta_{\mathbf{R}2}\,. \end{aligned} \tag{6.56}$$

The effective hamiltonian obtained using this parametrization is given by the following formula:

$$H_{\mathit{eff}} = \sum_{\mathbf{k}\sigma} \epsilon_{\mathbf{k}\sigma}\, c^\dagger_{\mathbf{k}\sigma} c_{\mathbf{k}\sigma} + U \sum_{\mathbf{k}} \left[\psi^\dagger_{\mathbf{k}}\, \mathbb{T}\cdot\mathbf{\Lambda}\, \psi_{\mathbf{k}+\mathbf{Q}} + \psi^\dagger_{\mathbf{k}}\, \mathbb{T}\cdot\mathbf{\Lambda}^*\, \psi_{\mathbf{k}-\mathbf{Q}}\right], \tag{6.57}$$

where:

$$\epsilon_{\mathbf{k}\sigma} = \epsilon_{\mathbf{k}} + \lambda_\sigma - U\delta n_\sigma$$

Eq.(6.57) differs from eq.(6.37) since the bands dependence on the flavor index. Following the same procedure used earlier for the symmetric case, the effective hamiltonian can be casted in a more compact form as in eq.(6.41) with a different color matrix that reads:

$$\tilde{\mathcal{H}}_{\mathbf{k}\sigma} = \mathcal{H}_{\mathbf{k}\sigma} + (\lambda_\sigma - U\delta n_\sigma)\mathbb{1}_{3\times 3} \tag{6.58}$$

Hence, the eigenvalues read:

$$\tilde{\rho}_{\mathbf{k}\sigma n} = \rho_{\mathbf{k}n} + \lambda_\sigma - U\delta n_\sigma \tag{6.59}$$

where $\rho_{\mathbf{k}n}$ are the eigenvalues of $\mathcal{H}_{\mathbf{k}\sigma}$ and obviously the eigenvectors are unchanged respect to the symmetric case.

The self-consistent equations for the staggered and the homogenous field are:

$$\begin{aligned}
\frac{1}{2\,A}\sum_{\mathbf{k}n}\left[n_F(\rho_{\mathbf{k}1n}) - n_F(\rho_{\mathbf{k}2n})\right] - \frac{\delta n_1 - \delta n_2}{2} &= 0 \\
\frac{1}{2\,A}\sum_{\mathbf{k}n}\left[n_F(\rho_{\mathbf{k}1n}) + n_F(\rho_{\mathbf{k}2n}) - 2\,n_F(\rho_{\mathbf{k}3n})\right] - (\delta n_1 + \delta n_2) &= 0 \\
\frac{1}{2A}\sum_{\mathbf{k}\sigma n}\tau^1_\sigma\left(U_{\mathbf{k}\sigma}\mathcal{T}\,U^\dagger_{\mathbf{k}\sigma}\right)_{nn} n_F(\rho_{\mathbf{k}\sigma n}) + \frac{\Delta_1 + \Delta_2}{2} &= 0 \\
\frac{1}{2A}\sum_{\mathbf{k}\sigma n}\tau^2_\sigma\left(U_{\mathbf{k}\sigma}\mathcal{T}\,U^\dagger_{\mathbf{k}\sigma}\right)_{nn} n_F(\rho_{\mathbf{k}\sigma n}) + \sqrt{3}\,\frac{\Delta_1 - \Delta_2}{2} &= 0 \\
\frac{1}{A}\sum_{\mathbf{k}n\sigma} n_F(\rho_{\mathbf{k}\sigma n}) - 1 &= 0\,,
\end{aligned} \tag{6.60}$$

where the tilde has been dropped in the notation of the eigenvalues defined in eq.(6.59).

The new set of self-consistent equations couples the staggered field $\Delta_{\mathbf{R}\alpha}$ and the homogenous magnetization δn_α.

6.2.3 A DMFT scheme in the case of a tripartite geometry

The DMFT equations presented in Chapts.(4,5) don't allow for solutions that display an antiferromagnetic long range order.

Therefore, this last section is devoted to the derivation of the DMFT equations that allow for tripartite antiferromagnetic solutions in addition to the paramagnetic and ferromagnetic solutions discussed in the previous chapters.

Self Consistence Equations in a tripartite geometry

A triangular lattice of side a can be viewed as a triangular lattice of side $\sqrt{3}a$ with three atoms per unit cell. In units of the original lattice side a, the vector of the basis are $\theta_1 = \frac{1}{2}(1, \sqrt{3})$ and $\theta_2 = (1, 0)$, while the primitive vectors of the new enlarged lattice are $\tau_{1/2} = \frac{1}{2}(3, \pm\sqrt{3})$.

In light of these considerations, the kinetic part of the hamiltonian in eq.(6.32) can be expressed as following:

$$\begin{aligned} H_{kin} &= -t \sum_{\langle \mathbf{R}\mathbf{R}' \rangle} \psi^\dagger_{\mathbf{R}} \psi_{\mathbf{R}'} \\ &= -\frac{t}{3} \sum_{\mathbf{r}\,\mu\,\nu} \psi^\dagger_{A\,\mathbf{r}} \left(\psi_{B\,\mathbf{r}+\mu} + \psi_{C\,\mathbf{r}+\nu} \right) + \psi^\dagger_{B\,\mathbf{r}+\theta_2} \psi_{C\,\mathbf{r}+\theta_2+\mu} + \text{h.c.}, \end{aligned} \tag{6.61}$$

where ψ is the three component spinor, A, B and C stands for the three fermion species in the unit cell, $\{\mu\} = \left\{(1,0);\, \frac{1}{2}(-1, \pm\sqrt{3})\right\}$, $\{\nu\} = \left\{(-1,0);\, \frac{1}{2}(1, \pm\sqrt{3})\right\}$, and $\mathbf{r}$ runs over the new enlarged triangular lattice.

The Fourier transform of the fields is defined as

$$\psi_{\alpha\,\mathbf{r}} = \frac{1}{\sqrt{N_\alpha}} \sum_{\mathbf{k} \in RBZ} e^{i\mathbf{k}\cdot\mathbf{r}}\, \psi_{\alpha\,\mathbf{k}}, \tag{6.62}$$

where N_α is the number of lattice sites of the species of fermions α.

Substituting eq.(6.62) in eq.(6.61) yields:

$$\begin{aligned} H_{kin} &= \sum_{\mathbf{k} \in RBZ} \gamma_{\mathbf{k}}\, \psi^\dagger_{A\mathbf{k}} \psi_{B\mathbf{k}} + \gamma^*_{\mathbf{k}} \psi^\dagger_{A\mathbf{k}} \psi_{C\mathbf{k}} + \gamma_{\mathbf{k}} \psi^\dagger_{B\mathbf{k}} \psi_{C\mathbf{k}} + \text{h.c.} \\ &= \sum_{\mathbf{k}\alpha\beta} \mathcal{H}_{\alpha\beta}(\mathbf{k})\, \psi^\dagger_{\alpha\,\mathbf{k}} \psi_{\beta\,\mathbf{k}}, \end{aligned} \tag{6.63}$$

where $\gamma_{\mathbf{k}} = -t\left[e^{ik_x} + 2e^{-ik_x/2}\cos\left(\frac{\sqrt{3}}{2}k_y\right)\right]$ and:

$$\mathcal{H}(\mathbf{k}) = \begin{pmatrix} 0 & \gamma_{\mathbf{k}} & \gamma_{\mathbf{k}}^* \\ \gamma_{\mathbf{k}}^* & 0 & \gamma_{\mathbf{k}} \\ \gamma_{\mathbf{k}} & \gamma_{\mathbf{k}}^* & 0 \end{pmatrix} . \tag{6.64}$$

Assuming a local form of the self energy, that is diagonal in the sub-lattices indices, the Green's function of the interacting system is obtained by inverting the following matrix:

$$G_m^{-1}(\mathbf{k}, i\omega_n) = \begin{pmatrix} \xi_{A\,m} & \gamma_{\mathbf{k}} & \gamma_{\mathbf{k}}^* \\ \gamma_{\mathbf{k}}^* & \xi_{B\,m} & \gamma_{\mathbf{k}} \\ \gamma_{\mathbf{k}} & \gamma_{\mathbf{k}}^* & \xi_{C\,m} \end{pmatrix} , \tag{6.65}$$

where m is the spin index and $\xi_{\alpha\,m}(i\omega_n) = i\omega_n + \mu_m - \Sigma_{\alpha\,m}(i\omega_n)$. Therefore, the green's function for the spin index m evaluated at site $\mathbf{r} = 0$, in the sub-lattice α is given by:

$$G_{\alpha m}(i\omega_m, \mathbf{r} = 0) = \sum_{\mathbf{k}\in RBZ} F_{\alpha m}(\mathbf{k}, i\omega_n), \tag{6.66}$$

where $F_{\alpha m}$ are the diagonal elements of $G_{\alpha\,m}(\mathbf{k}, i\omega_n)$, whose analytical form in addition to other details about the tripartite geometry are reported in the Appendix().

The cavity method can be now applied for every sub-lattice, and therefore the effective action for a given sub-lattice α reads:

$$\begin{aligned} S_{eff}^{(\alpha)}[\phi^*, \phi] &= -\int_0^\beta d\tau \int_0^\beta d\tau' \sum_m \phi_{\alpha,m}^*(\tau)\, \mathcal{G}_{W\,m}^{(\alpha)}(\tau - \tau')\, \phi_{\alpha\,m}(\tau') \\ &+ U\int_0^\beta d\tau \sum_{m<m'} \phi_{\alpha\,m}^*(\tau)\phi_{\alpha\,m'}^*(\tau)\phi_{\alpha\,m}(\tau)\phi_{\alpha\,m'}(\tau) - \int_0^\beta d\tau \sum_m \mu_m\, \phi_{\alpha\,m}^*(\tau)\phi_{\alpha\,m}(\tau), \end{aligned} \tag{6.67}$$

where ϕ and ϕ^* are now Grassmann variables, $\mathcal{G}_{W\,m}^{(\alpha)}$ is the Weiss field for the fermion species m. The thermal average of an operator acting in the sub-lattice α can be computed via the path integral

$$\langle O\rangle_\alpha = \frac{1}{Z_\alpha}\int \mathcal{D}[\phi, \phi^*]\, O[\phi, \phi^*]\, \exp\left(-S_{eff}^{(\alpha)}[\phi, \phi^*]\right) \tag{6.68}$$

Consequently, the local Green's function calculated as path integral reads

$$G_{\alpha m}(\tau - \tau') = -\left\langle \phi_{\alpha m}(\tau)\phi^*_{\alpha m}(\tau') \right\rangle_\alpha \tag{6.69}$$

Hence, using eq.(6.66), the self-consistence condition reads:

$$G_{\alpha m}(i\omega_n) = \sum_{\mathbf{k}\in RBZ} F_{m\alpha}(\mathbf{k}, i\omega_n), \tag{6.70}$$

where $G_{\alpha m}(i\omega_n)$ is the Matsubara Fourier transform of eq.(6.69).

Practical scheme using an ED-Solver

The action in eq.(6.67) corresponds to the following hamiltonian written in second quantization:

$$\begin{aligned} H_\alpha &= \sum_{l\,m} \epsilon^{(\alpha)}_{lm} d^\dagger_{lm} d_{lm} + \sum_{l\,m} V^{(\alpha)}_{lm} \left(d^\dagger_{l\,m} c_{\alpha\,m} + \text{h.c.} \right) \\ &+ U \sum_{m<m'} n_{\alpha m} n_{\alpha m'} - \sum_m \mu_m\, n_{\alpha\,m}, \end{aligned} \tag{6.71}$$

where $d_{l\,m}$, $V^{(\alpha)}_{lm}$ and $\epsilon^{(\alpha)}_{lm}$ are respectively the destruction operator, the hybridization amplitude, and the energy levels of the bath relative to the fermion species m in sub-lattice α.

In this representation, the non-interacting Green's function of the AIM in eq.(6.71) reads:

$$\mathcal{G}_{\alpha m}(i\omega_n; \{V^{(\alpha)}_{lm}, \epsilon^{(\alpha)}_{lm}\}) = i\omega_n + \mu_m - \sum_l \frac{|V^{(\alpha)}_{lm}|^2}{i\omega_n - \epsilon_{lm}}. \tag{6.72}$$

In principle the number of fermions in the bath is infinite, but for practical purpose as explained previously in Chapt.[4], this number is fixed to a finite value, namely N_S. With this approximation, the ground state of the AIM, and in case of needs also few excited states, can be evaluated numerically using Lanczos technique.

This, how explained in Sec.(), allows for the evaluation of several spectral properties among which the Green's function $G_{\alpha m}(i\omega_n)$ and consequently the Self Energy $\Sigma_{\alpha m}(i\omega_n)$, through the Dyson equation:

$$G^{-1}_{\alpha m}(i\omega_n) = \mathcal{G}^{-1}_{\alpha m}(i\omega_n) - \Sigma_{\alpha m}(i\omega_n). \tag{6.73}$$

Therefore, the DMFT-cycle reads as following:

- An initial guess of the Anderson parameters $V_{lm}^{(\alpha)}$, $\epsilon_{lm}^{(\alpha)}$ is chosen. This determines the non interacting local Green's function $\mathcal{G}_{\alpha m}(i\omega_n)$ through eq.(6.72) ;
- The AIM is solved separately for every sub-lattice, and the self-energy as well as the Green's function are evaluated ;
- Using eq.(6.66) yields a new Green's function, from which can be extrapolated a new non-interacting Green's function $\mathcal{G}_{\alpha m}^{NEW}(i\omega_n)$ using the Dyson equation ;
- A new set of Anderson parameters is obtained by minimizing a suitable norm between the old and the new non-interacting Green's functions $| \left(\mathcal{G}_{\alpha m}^{NEW}(i\omega_n)\right)^{-1} - \mathcal{G}_{\alpha m}^{-1}(i\omega_n; \{V_{lm}^{(\alpha)}, \epsilon_{lm}^{(\alpha)}\})|$.
- Then, a convergence test is performed. If it fails the cycle restarts. Conversely, in case of success, the cycle breaks and the final set of parameters $\{V_{lm}^{(\alpha)}, \epsilon_{lm}^{(\alpha)}\}$ defines the Weiss field $G_{W\,\alpha m} = \mathcal{G}_{\alpha m}^{-1}(i\omega_n; \{V_{lm}^{(\alpha)}, \epsilon_{lm}^{(\alpha)}\})$.

It is important to note that the solution $G_{W\,\alpha m}$ in the sub-lattice α strongly depends on the self-energy of the other sub-lattice hamiltonians, via the self-consistence equation. Therefore the sub-lattices, that are treated independently at the AIM level, are actually strongly coupled. The main approximation is made on the self-energy, that is assumed to be diagonal in the sub-lattice indices.

CHAPTER 7

CONCLUSIONS.

In this work the properties relative to multicomponent fermionic systems in optical lattices using Dynamical Mean-Field Theory at zero temperature have been studied. This work is inspired on one side by the realization of multicomponent fermi gases using cooled Ytterbium atoms, and on the other from advances in our understanding of multiorbital systems in solid state.

Both systems can give rise to a countless list of interesting phenomena which depend on several control parameters. This thesis mainly focuses on the possiblity of flavour-selective behavior in systems with 3 spin components.

First it is addressed the case of a completely $SU(3)$ symmetric system. First a complete phase diagram for the Mott transition is constructed in this situation. As expected, and previously found in some calculations, a Mott transition occurs for integer fillings, which imply either one fermion per site or two fermion per site. The half-filled condition which would correspond to 3/2 fermions per site, does not allow for Mott localization. Despite this important difference, the two Mott-Hubbard transitions are reminiscent of the popular Mott transition of a single-band Hubbard model showing a coexistence of metallic and insulating solutions.

Then, it was considered the case of artificial gauge fields (AGF) which are experimentally realized through Raman processes connecting the different nuclear spin levels.

In particular, it was addressed the case where the amplitude of these processes is a real number, which is formally equivalent to a local hybridization between the spin species or to a hopping in a synthetic dimension. Using this latter language, the results obtained can be classified in terms of "boundary conditions". In both cases it was convenient to work in the basis which diagonalizes the local Hamiltonian turning the AGF into energy splittings between the different levels.

In the case of a synthetic hopping with open boundary conditions, the local Hamiltonian has three different eigenvalues. If the chemical potential is increased the three levels fill at different rates. It has been shown that the system displays a flavor selective "metamagnetic" behavior at intermediate couplings. In particular, one flavor reaches complete saturation continuously as a function of the amplitude of the AGF, while two other species reach saturation through a first-order jump at a critical value of the AGF. In the same process the effective mass of the first species decreases as it approaches saturation, while the two other fermion experience a huge enhancement of the effective mass. This two distinct behaviors have been shown to occur in the single band Hubbard model in presence of a magnetic field, but always separately.

In the case of a synthetic hopping with PBC the spectrum of the local Hamiltonian has two generate states. The $SU(2)$ residual symmetry allows to reach a mixed state where one spin polarizes, while the two other species can combine in a paramagnetic Mott insulating state. Also in this case non-monotonic trends of the occupation numbers as a function of μ is observed for intermediate and small values of the AGF.

In both cases it has been observed, in the proximity of the values of the chemical potential when the majority species is polarized, a negative derivative of the population of some orbitals as a function of the chemical potential. This can be read as a sort of spin-selective negative compressibility, which has been discussed in relation with experiments on cold-atom systems.

Finally the magnetic state is studied. The formalism has been introduced to treat the $SU(3)$ case but the numerical study were limited to the doped $SU(2)$ case because this requires a smaller computational effort. Here it has been found that the compressibility actually diverges at finite temperatures when the antiferromagnet becomes unstable as a function of doping.

These results confirm the incredible richness of these multicomponent system which can both generalize properties of solid state system and give rise to novel physics. Even the simple $SU(3)$ system displays indeed a number of interesting phenomena

of different kinds. The new physics unveiled can be addressed experimentally with present experimental setups and can be enriched by including some of the aspects that have been neglected here.

APPENDIX A

ALKALINE-EARTH ATOMS MANY-BODY HAMILTONIAN

In this appendix the many-body hamiltonian in eq.(2.3) will be derived using simple considerations.

As mentioned in the first chapter, the interactions among atoms occur in different collision channels. Formally, if the coupling between different channels is neglected, this amounts to write the hamiltonian as summation of different operators acting on mutually orthogonal subspaces, each of them corresponding to a certain channel. Therefore:

$$\hat{H}_{int} = \sum_{c} \sum_{|\psi_c\rangle} U\big(\,|\psi_c\rangle\,\big)\,|\psi_c\rangle\,\langle\psi_c|\,, \tag{A.1}$$

where the subscript c runs over all possible channels, $\langle\psi_c|\psi_{c'}\rangle = 0$ if $c \neq c'$ and $U\big(\,|\psi_c\rangle\,\big)$ is the interaction strength that in principle depends on the generic many-body state $|\psi_c\rangle$ of the two particles colliding in the channel c.

Consider now the case of alkaline-earth atoms where the collision channel are labeled by the multi-orbital configurations ee, gg, eg^+ and eg^-, that correspond to states of two particles being in the same orbital (ee and gg), or states symmetric or anti-symmetric respect to orbital exchange of two particles in two different oribals (eg^+ and eg^-).

Therefore, in the case of alkali atoms the hamiltonian reads:

$$\begin{aligned}\hat{H}_{int} &= \sum_{\alpha=e,\,g} \hat{H}_{\alpha\alpha} + \hat{H}_{eg^+} + \hat{H}_{eg^-} \\ &= \sum_{\alpha} \sum_{|\alpha\alpha\rangle} U\big(\,|\alpha\alpha\rangle\,\big)\,|\alpha\alpha\rangle\,\langle\alpha\alpha| + \sum_{|eg^+\rangle} U\big(\,|eg^+\rangle\,\big)\,|eg^+\rangle\,\langle eg^+| \\ &+ \sum_{|eg^-\rangle} U\big(\,|eg^-\rangle\,\big)\,|eg^-\rangle\,\langle eg^-| \end{aligned} \tag{A.2}$$

In order to express the whole hamiltonian in second quantization, the fermi fields are defined as:

$$\begin{aligned}\big\{\Psi^\dagger_{\alpha m}(\mathbf{x}), \Psi_{\beta m'}(\mathbf{y})\big\} &= \delta(\mathbf{x}-\mathbf{y})\,\delta_{mm'}\,\delta_{\alpha\beta}\,, \\ \big\{\Psi_{\alpha m}(\mathbf{x}), \Psi_{\beta m'}(\mathbf{y})\big\} &= \big\{\Psi_{\alpha m}(\mathbf{x}), \Psi_{\beta m'}(\mathbf{y})\big\} = 0\,, \end{aligned} \tag{A.3}$$

where $\Psi^\dagger_{\alpha m}(\mathbf{x})$ is the Fermi field that creates a particle in $\mathbf{x}$ with orbital and spin quantum numbers α and m and $\{.\}$ is the anti-commutator.

The kets $|\alpha\alpha\rangle$ are symmetric under orbital exchange, therefore they can be anti-symmetric under spin or spatial exchange. Therefore, one should consider both the possibilities of a anti-symmetric and symmetric spatial wave function. In particular both the following possibilities are available:

$$\begin{aligned}|\alpha\alpha\rangle &= \frac{1}{2}\Big(\Psi^\dagger_{\alpha m}(\mathbf{x})\,\Psi^\dagger_{\alpha m'}(\mathbf{y}) - \Psi^\dagger_{\alpha m'}(\mathbf{x})\,\Psi^\dagger_{\alpha m}(\mathbf{y})\Big)\,, \\ |\alpha\alpha\rangle &= \Psi^\dagger_{\alpha m}(\mathbf{x})\,\Psi^\dagger_{\alpha m}(\mathbf{y}) \end{aligned} \tag{A.4}$$

Nevertheless interactions in cold atomic systems are usually considered as local, i.e. $U(|\alpha\beta\rangle) \equiv U^{\alpha\beta}_{mm'}(\mathbf{x}-\mathbf{y}) = U^{\alpha\beta}_{mm'}\,\delta(\mathbf{x}-\mathbf{y})$. This excludes the second relation in eq.(A.4) and the generic ket in the $\alpha\alpha$ channel can be expressed in the much simpler way as

$$|\alpha\alpha\rangle = \Psi^\dagger_{\alpha m}(\mathbf{x})\,\Psi^\dagger_{\alpha m'}(\mathbf{x})\,. \tag{A.5}$$

Therefore, the collisions in the $\alpha\alpha$ channel are governed by the many-body hamiltonian:

$$\hat{H}_{\alpha\alpha} = \int d\mathbf{x} \sum_{mm'} U^{\alpha\alpha}_{mm'}\,\Psi^\dagger_{\alpha m}(\mathbf{x})\Psi^\dagger_{\alpha m'}(\mathbf{x})\Psi_{\alpha m'}(\mathbf{x})\Psi_{\alpha m}(\mathbf{x})\,. \tag{A.6}$$

$U^{\alpha\alpha}_{mm'} = \frac{4\pi\hbar^2}{m} a^{\alpha\alpha}_{mm'}$, where $a^{\alpha\alpha}_{mm'} = a^{\alpha\alpha}$ is the s-wave scattering length relative to the channel $\alpha\alpha$ and it does not depend on the spin indices.

The generic ket relative to the $eg^{\pm}$ channel, in the case of local interactions are given by:

$$\left|eg^{\pm}\right\rangle = \frac{1}{2}\left(\Psi^{\dagger}_{gm}(\mathbf{x})\,\Psi^{\dagger}_{em'}(\mathbf{x}) \mp \Psi^{\dagger}_{gm'}(\mathbf{x})\,\Psi^{\dagger}_{em}(\mathbf{x})\right), \tag{A.7}$$

and the projector relative to this state reads

$$\left|eg^{\pm}\right\rangle\left\langle eg^{\pm}\right| = \frac{1}{2}\left(\Psi^{\dagger}_{gm}(\mathbf{x})\,\Psi^{\dagger}_{em'}(\mathbf{x})\Psi_{em'}(\mathbf{x})\Psi_{gm}(\mathbf{x}) \pm \Psi^{\dagger}_{gm}(\mathbf{x})\,\Psi^{\dagger}_{em'}(\mathbf{x})\Psi_{em}(\mathbf{x})\Psi_{gm'}(\mathbf{x})\right), \tag{A.8}$$

where the fact that m and m' are dummy indices was used. Finally, the interacting hamiltonians in the $eg^{\pm}$ channels read:

$$\hat{H}_{eg^{\pm}} = \frac{U^{eg^{\pm}}}{2}\int d\mathbf{x}\,\rho_g(\mathbf{x})\rho_e(\mathbf{x}) \mp \sum_{mm'}\Psi^{\dagger}_{gm}(\mathbf{x})\,\Psi_{gm'}(\mathbf{x})\,\Psi^{\dagger}_{em'}(\mathbf{x})\Psi_{em}(\mathbf{x}), \tag{A.9}$$

where $\rho_{\alpha}(\mathbf{x}) = \sum_m \Psi^{\dagger}_{\alpha m}(\mathbf{x})\Psi_{\alpha m}(\mathbf{x})$.

APPENDIX B

GAUSSIAN INTEGRALS

Within this appendix, quantities as partition functions, Green's functions and other physical observables are computed both for the non interacting and weakly interacting Fermi gases.

Basics of the path integral formulation of many-body systems are required for the comprehension of this chapter. In case of needs, the reader is invited to consult references [52][1], where a detailed derivation of the path integral formulation of many-body systems can be found.

B.1 Non interacting Fermi Gas

This section is dedicated to the computation of the partition function of the non-interacting fermi gas, whose hamiltonian is given by:

$$H = \sum_{\alpha} (\epsilon_\alpha - \mu) c_\alpha^\dagger c_\alpha \ . \tag{B.1}$$

The partition function of such a system can be expressed in terms of a functional integral:

$$\mathcal{Z} \;=\; \int \mathcal{D}[\phi,\phi^*] \exp\left\{ -\int_0^\beta \sum_\alpha \phi_\alpha^*(\tau)\left(\partial_\tau + \epsilon_\alpha - \mu\right)\phi_\alpha(\tau) \right\}, \tag{B.2}$$

where the integration is carried out over all possible anti-periodic coherent states trajectories, whose eigenvalues components are $\{\phi_\alpha\}$, that are grassmannian variables. The RHS of eq.(B.2) is a Gaussian integral and it can be computed straightforwardly using the determinant forumla:

$$\mathcal{Z} = \det\left(\partial_\tau + \xi_\alpha\right), \tag{B.3}$$

where $\xi_\alpha \equiv \epsilon_\alpha - \mu$. It is now required to calculate the determinant of a differential operator. It is possible to use the identity $\det A = \prod_{\lambda_A} \lambda_A$, where A is a generic operator and λ_A are its eigenvalues. Hence, once the eigenvalues of the operator in eq.(B.3) are known, the partition function can be evaluated.

The eigenvalues equation reads:

$$\begin{aligned} (\partial_\tau + \xi_\alpha)\psi(\tau) &= \lambda\,\psi(\tau)\ , \\ (-i\omega_n + \xi_\alpha)\psi(i\omega_n) &= \lambda_\alpha(i\omega_n)\psi(i\omega_n)\ , \\ \lambda_\alpha(i\omega_n) &= -i\omega_n + \xi_\alpha\ . \end{aligned} \tag{B.4}$$

Now, it is possible to calculate the gran potential defined as $\mathcal{Z} \equiv e^{-\beta\Omega}$.

Therefore, the gran potential is given by:

$$\Omega = -T\sum_{i\omega_n}\sum_\alpha \ln(-i\omega_n + \xi_\alpha)\ . \tag{B.5}$$

The summation over the Matsubara frequencies can be performed via the contour integral over the complex plane,

$$\frac{1}{2\pi i}\oint_C dz\, n_F(z)\ln(-z+\xi_\alpha) = -T\sum_{i\omega_n}\ln(-i\omega_n+\xi_\alpha), \tag{B.6}$$

where the integration contour $C = C_1 + C_2 + C_3 + C_4$ is described in Fig.[B.1].

The only finite contributions to the contour integral are given by the line integrations

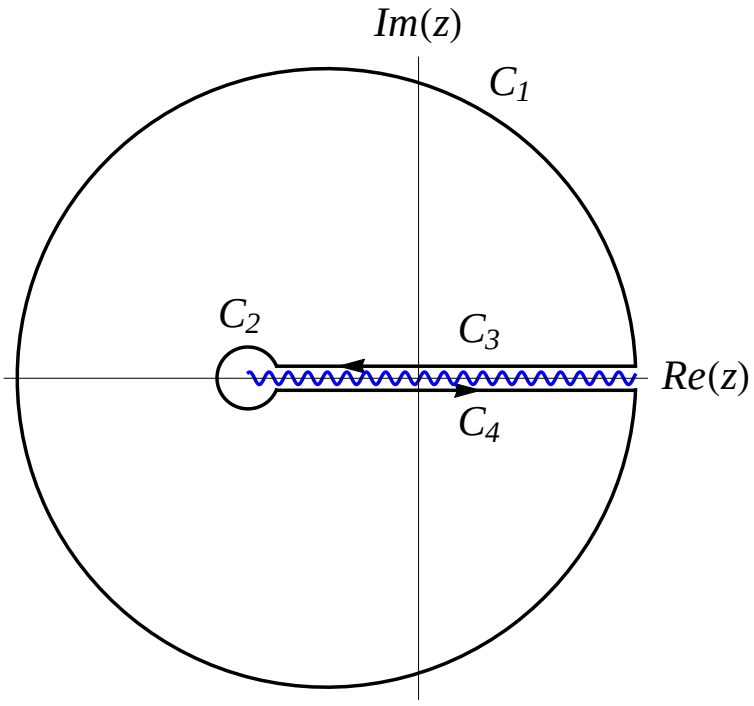

Figure B.1: Integration contour. The wavy line represents the branch cut of the logarithm.

over C_3 and C_4, that read:

$$-\frac{1}{2\pi i}\int_{\xi_\alpha}^{\infty} dx\,\left[\,\ln(-x+\xi_\alpha+i\epsilon)-\ln(-x+\xi_\alpha-i\epsilon)\,\right]n_F(x) = -\int_{\xi_\alpha}^{\infty} n_F(x)$$

$$T\int_{\xi_\alpha}^{\infty} dx\,\partial_x \ln[1+\exp(-\beta x)] = -T\,\ln\left[\,1+\exp(-\beta\xi_\alpha)\,\right]. \quad \text{(B.7)}$$

Hence, the final expression for the gran potential of a free fermion system reads:

$$\Omega = -T\sum_{\alpha}\ln\left[\,1+\exp(-\beta\xi_\alpha)\,\right]. \quad \text{(B.8)}$$

B.2 Effective action from the AIM

In DMFT the Anderson Impurity Model is often chosen as a representation of the effective local theory obtained through the cavity method. In fact, the effective action can be written starting from the AIM action and integrating out the bath degrees of freedom. In this appendix such a calculation will be carried out explicitly using the path integral formulation.

In particular, the AIM hamiltonian in second quantization reads:

$$H = \sum_{\ell m} \epsilon_{\ell m}\, d^\dagger_{\ell m} d_{\ell m} + \sum_{\ell m} V_{\ell m}\, c^\dagger_m d_{\ell m} + \text{h.c.} - \mu \sum_m \hat{n}_m + U \sum_{m<m'} \hat{n}_m \hat{n}_{m'}, \tag{B.9}$$

where $\hat{n}_m \equiv c^\dagger_m c_m$ is the number operator relative to the m-th component of the impurity and $d^\dagger_{\ell m}$ is the creation operator of a fermion in the bath relative to the m-component of the impurity, $V_{\ell m}$ is the amplitude of an hopping process from the impurity to the bath.

The partition function of the AIM can be written using the path integral formulation as:

$$Z = \int \prod_m \mathcal{D}\bar{c}_m\, \mathcal{D}c_m e^{-S_1[\bar{c},c]} \int \prod_{\ell\, m} \mathcal{D}\bar{\psi}_{\ell m}\, \mathcal{D}\psi_{\ell m} e^{-S_2[\bar{\psi},\bar{c},\psi,c]}, \tag{B.10}$$

where $S_1 = \int_0^\beta d\tau \sum_{m<m'} n_m(\tau) n'_m(\tau) - \mu \sum_m n_m(\tau)$

$$S_2 \;=\; \int_0^\beta d\tau \sum_{\ell m} \bar{\psi}_{\ell m}(\tau) \left(\partial_\tau + \epsilon_{\ell m}\right) \psi_{\ell m}(\tau) + \int_0^\beta \sum_{\ell m} \bar{\eta}_{\ell m}(\tau)\psi_{\ell m}(\tau) + \bar{\psi}_{\ell m}(\tau)\eta_{\ell m}(\tau), \tag{B.11}$$

where $c_{\ell m}$, $\bar{c}_{\ell m}$, $\psi_{\ell m}$, $\bar{\psi}_{\ell m}$ are grassmannian variables and $\eta_{\ell m} \equiv V^*_{\ell m} c_m$ is interpreted as the source relative to the field $\bar{\psi}_{\ell m}$.

The integral over the fields $\psi_{\ell m}$ and $\bar{\psi}_{\ell m}$, in eq.(B.10) can be computed straightforwardly since only quadratic terms appear in S_2. In fact, the following identity holds:

$$\int \prod_{\ell\, m} \mathcal{D}\bar{\psi}_{\ell m}\, \mathcal{D}\psi_{\ell m} e^{-S_2[\bar{\psi},\bar{c},\psi,c]} = Z_{bath} \exp\left[\int d\tau d\tau' \sum_{mm'\,\ell\ell'} \bar{\eta}_{\ell m}(\tau)\, h^{mm'}_{\ell\,\ell'}(\tau-\tau')\, \eta_{\ell m}(\tau')\right], \tag{B.12}$$

where Z_{bath} is the partition function of a non-interacting bath whose formal evaluation is given in eq.(), and $(\partial_\tau - \epsilon_{\ell m})\, h^{mm'}_{\ell\,\ell'}(\tau-\tau') = \delta_{mm'}\delta_{\ell\ell'}\delta(\tau-\tau')$, with $h^{mm'}_{\ell\ell'}(\tau-\tau') = \delta_{\ell\ell'}\delta_{mm'}h^m_\ell(\tau-\tau')$, therefore:

$$(\partial_\tau + \epsilon_m) h^m_\ell(\tau-\tau') = \delta(\tau-\tau'). \tag{B.13}$$

It is possible to write the integral in the exponential in eq.(B.12) expanding the fields

in Fourier series, i.e. $\eta_{\ell m}(\tau) = T\sum_{i\omega_n} e^{i\omega_n\tau}\eta_{\ell m}(i\omega_n)$:

$$
\begin{aligned}
& T^2 \sum_{i\omega_n\, i\nu_n} \int d\tau d\tau' \bar{\eta}_{\ell m}(i\omega_n) h_\ell^m(\tau-\tau')\eta_{\ell m}(i\nu_n) e^{-i\omega_n\tau} e^{i\nu_n\tau'} \\
= \; & T \sum_{i\nu_n\, i\omega_n} \bar{\eta}_{\ell m}(i\omega_n) \overbrace{\left(2T\int_0^{2\beta} dT\, e^{iT\frac{\omega_n-i\nu_n}{2}}\right)}^{\delta(\omega_n-\nu_n)} \overbrace{\left(\int_0^{\beta} dt e^{i\,t(\omega_n+\nu_n)/2} h_\ell^m(t)\right)}^{h_\ell^m(i\omega_n)} \eta_{\ell m}(i\nu_n),
\end{aligned}
\tag{B.14}
$$

where $T = \tau + \tau'$, $t = \tau - \tau'$, and $h_\ell^m(i\omega_n) = -\frac{1}{i\omega_n - \epsilon_{\ell m}}$ is the Fourier transform of the function $h_\ell^m(\tau-\tau')$ defined in eq.(B.13). Therefore, after the integration over the bath fermions the integral in eq.(B.12) reads:

$$
-Z_{bath}\, \exp\left[T\sum_{i\omega_n}\sum_m \bar{c}_m(i\omega_n)\,\Delta_m(i\omega_n)\,c_m(i\omega_n)\right], \tag{B.15}
$$

where

$$
\Delta_m(i\omega_n) = \sum_\ell \frac{|V_{\ell m}|^2}{i\omega_n - \epsilon_{\ell m}}, \tag{B.16}
$$

is the hybridization function of the AIM, that corresponds to an effective retarded potential felt by the m-th component of the impurity. Therefore the partition function of the AIM can be finally written as

$$
Z_{bath} \int \prod_m \mathcal{D}\bar{c}\,\mathcal{D}c \exp^{-S_{eff}[\bar{c},c]}, \tag{B.17}
$$

where:

$$
S_{eff}[\bar{c},c] = \int_0^\beta \int_0^\beta d\tau d\tau' \sum_m \bar{c}_m(\tau)\mathcal{G}_m^{-1}(\tau-\tau')\,c_m(\tau) + U\sum_{m<m'}\int_0^\beta n_m(\tau)n'_m(\tau'), \tag{B.18}
$$

where $\mathcal{G}_m^{-1}$ is the Weiss field whose Fourier transform reads:

$$
\mathcal{G}_m^{-1}(i\omega_n) = i\omega_n + \mu - \Delta_m(i\omega_n). \tag{B.19}
$$

APPENDIX C

SIMULATING ARTIFICIAL GAUGE FIELDS

This appendix is devoted to the derivation of the effective Zeeman field presented in eq.(2.10). For this scope, the general outlines of the 4-th chapter of the review by Goldman et al.[29] will be followed.

C.1 Light-Matter interaction

In general, the dominant light-matter coupling term is given by the electric dipole contribution [47], therefore the dipole hamiltonian reads:

$$H_{dip} = \hat{\mathbf{d}} \cdot \mathbf{E}(t) = \sum_i \hat{d}_i E_i \cos(\omega t - \phi_i), \tag{C.1}$$

where $\hat{\mathbf{d}} = -e \sum_\alpha \hat{\mathbf{r}}_\alpha$ is the electric dipole operator and $\hat{\mathbf{r}}_\alpha$ is the position of the α-th electron of the atom, E_i are the spatial components of the electromagnetic field. In practice, alkali and alkaline earth atoms are generally used in cold atoms experiments, where the lowest dipole transition occurs between the ground $(n)S$ electron orbital and the excited $(n)P$ orbital with excitation energy E_e. Therefore, it is enough to

consider the following atomic hamiltonian:

$$H_{at} = E_e\, P_e + \frac{A_{FS}}{\hbar^2}\hat{\mathbf{L}}\cdot\hat{\mathbf{S}}, \tag{C.2}$$

where $P_{g,e}$ are the projectors onto the ground and the excited states manifolds respectively, A_{FS} is the fine structure constant and $\hat{\mathbf{L}}$, $\hat{\mathbf{S}}$ are the total electronic orbital and spin angular momenta. Therefore, the orbital angular momentum eigenstates are $\{|l=0, m_L=0\rangle, |l=1, m_L=0, \pm 1\rangle\}$, with eigenvalues $\hbar m_L$ and $\hbar^2 l(l+1)$ for $\hat{\mathbf{L}}^2$ and $\hat{L}_z$ respectively. The excited state projector can be written explicitly as $P_e = \frac{\hat{\mathbf{L}}^2}{2\hbar^2}$, and consequently the ground state projector reads $P_g = 1 - P_e$.

The whole hamiltonian:

$$H = H_{at} + H_{dip} \tag{C.3}$$

is time dependent since its dipole contributions oscillates with frequency ω. To get rid of its time dependence, one can rotates the reference frame using the unitary transformation $U = \exp(-i\omega t P_e)$. This leads the whole hamiltonian to be mapped to another time dependent hamiltonian $H' = U^\dagger(t)\, H\, U(t) - i\hbar\, U^\dagger \partial_t U(t)$. At this point the rotating wave approximation (RWA) can be used, that consists in neglecting the oscillating terms with frequencies ω and 2ω and it is valid until $|E_e - \hbar\omega| \ll E_e$. This leads to the an effective time independent hamiltonian $H'_{RWA} = H'_{at} + H'_{dip}$, with:

$$\begin{aligned} H'_{dip} &= \frac{1}{2}\sum_i \widetilde{E}_i^* P_g d_i P_e + \text{h.c.} \\ H'_{at} &= \Delta_e P_e + \frac{A_{FS}}{2\hbar^2}\hat{\mathbf{L}}\cdot\hat{\mathbf{S}}, \end{aligned} \tag{C.4}$$

where $\widetilde{E}_i = E_i \exp(i\phi_i)$ and $\Delta_e = E_e - \hbar\omega$ is called detuning and it comes from the temporal dependence of the unitary transformation, i.e. $-i\hbar\, U^\dagger \partial_t U(t) = -\hbar\omega P_e$.

The light-matter interacting term H_{dip} can be treated via second order perturbation theory. For a generic hamiltonian $H = H_0 + \lambda V$, the energy deviation $\Delta E = E - E_0$ from the degenerate unperturbed eigenvalue E_0 can be expressed as:

$$\Delta E = \lambda PVP + \lambda^2 PVQ\,(E - QH_0Q)^{-1}\,QVP, \tag{C.5}$$

where P is the projector onto the degenerate subspace relative to the unperturbed eigenvalue E_0 and $Q = 1 - P$ is its orthogonal complement. Furthermore, the following

series expansion is valid:

$$(E - QHQ)^{-1} = \sum_{n=0}^{\infty} \lambda^n \left[(E - QH_0Q)^{-1} QVQ\right]^n (E - QH_0Q)^{-1}. \tag{C.6}$$

The energy deviation and the projection of the eigenket onto the degeneracy manifold can be expanded in series of λ as:

$$\begin{aligned} \Delta E &= \lambda\epsilon_1 + \lambda^2\epsilon_2 + \dots, \\ P\,|\psi\rangle &= |\phi_0\rangle + \lambda\,|\phi_1\rangle + \lambda^2\,|\phi_2\rangle + \dots. \end{aligned} \tag{C.7}$$

Therefore, expanding up to second order in λ the Schrödinger equation projected onto the degeneracy manifold, obtained by multiplying $P\,|\psi\rangle$ from the right to both sides of the relation in eq.(C.5), and equating terms of the same order in λ one obtains the following equations[1]:

$$\begin{aligned} PVP\,|\phi_0\rangle &= \epsilon_1\,|\phi_0\rangle \\ PVP\,|\phi_1\rangle + PVQ(E_0 - QH_0Q)^{-1}QVP\,|\phi_0\rangle &= \epsilon_2\,|\phi_0\rangle + \epsilon_1\,|\phi_1\rangle\,, \end{aligned} \tag{C.8}$$

In the case of light-matter interaction, the atom ground state does not posses a permanent electric dipole moment, i.e. $P_g\,\hat{\mathbf{d}}P_g = 0$. Therefore, the dipole interaction must be expanded at least at second order, and using eqs.(C.8, C.4) the effective hamiltonian of the system projected onto the ground state manifold can be written as:

$$H_{\mathit{eff}} = -P_g H'_{dip}\,(H'_{at})^{-1}\,H'_{dip}P_g. \tag{C.9}$$

In the simple case of $A_{FS} = 0$, the effective hamiltonian $H_{\mathit{eff}} = -\frac{\Delta_e^{-1}}{4}\sum_{ij}\widetilde{E}_i^* P_g \hat{d}_i\hat{d}_j\widetilde{E}_j$ and can be represented as

$$H_{\mathit{eff}} = -\frac{1}{4}\sum_{ij}\widetilde{E}_i^* D_{ij}\widetilde{E}_j^*, \tag{C.10}$$

where $\Delta_{ij} = \Delta_e^{-1}P_g\hat{d}_i\hat{d}_jP_g$ commutes with the orbital momentum, therefore it is a scalar operator, and its expression can be simplified as $D_{ij} = \left(\delta_{ij}\,P_g\,\hat{\mathbf{d}}\cdot\hat{\mathbf{d}}\,P_g\right)/3\Delta_e$.

[1]Note that in eq.(C.6), every single element of the series must be expanded in powers of λ as well, since E contains all the order of the expansion in eq.(C.7).

Hence, the effective atomic hamiltonian can be written as:

$$H_{\mathit{eff}} = u_s |\widetilde{\mathbf{E}}|^2 P_g, \tag{C.11}$$

where $u_s = -|\langle\|\mathbf{d}\|\rangle|^2/12(E_e - \hbar\omega)$, with $|\langle\|\mathbf{d}\|\rangle|^2 \equiv \sum_{m'=0,\pm1} |\langle l=0, m_L=0|\hat{\mathbf{d}}|l=1, m_L\rangle|^2$. Therefore, for $E_e > \hbar\omega$, when the detuning $\Delta_e \gg A_{FS}$, the dipole interaction induces an effective attractive field that depends on the laser intensity.

When A_{FS} is taken into account

$$u_s = -\frac{|\langle\|\mathbf{d}\|\rangle|^2}{36}\left(\frac{1}{E_{D2} - \hbar\omega} + \frac{1}{E_{D1} - \hbar\omega}\right), \tag{C.12}$$

where $E_{D1} = E_e - A_{FS}$, $E_{D2} = E_e + A_{FS}/2$, and the effective hamiltonian acquires another term that is proportional to the total angular momentum $\hat{\mathbf{J}} = \hat{\mathbf{L}} + \hat{\mathbf{S}}$. In other words, the fine structure term induces the effective magnetic field:

$$\mathbf{B}_{eff} = \frac{i u_v \left(\widetilde{\mathbf{E}}^* \times \widetilde{\mathbf{E}}\right)}{\mu_B\, g_J}, \tag{C.13}$$

where μ_B is the Bohr magneton, g_J is the electronic Landé factor and $u_v = 2u_s\Delta_{FS}/(\bar{E} - \hbar\omega)$, with $\bar{E} = (2E_{D1} + E_{D2})/3$.

In conclusion, the interaction between the atom with a laser field leads to the following effective hamiltonian:

$$H_{\mathit{eff}} = u_s\, \widetilde{\mathbf{E}}^* \cdot \widetilde{\mathbf{E}} + \frac{\mu_B\, g_J}{\hbar}\, \mathbf{B}_{eff} \cdot \hat{\mathbf{J}}. \tag{C.14}$$

C.2 The presence of an external magnetic field

In presence of an external magnetic field $\mathbf{B}$ the atomic hamiltonian reads:

$$H_{\mathbf{B}} = A_{hf}\hat{\mathbf{I}} \cdot \hat{\mathbf{J}} + \frac{\mu_B}{\hbar}\mathbf{B} \cdot \left(g_J\hat{\mathbf{J}} + g_I\hat{\mathbf{I}}\right), \tag{C.15}$$

where A_{hf} is the hyperfine structure constant and g_I is the nuclear Landé factor. In alkali atoms $|g_I/g_J| \simeq 5 \times 10^{-4}$, so the term proportional to g_I can be safely neglected in the atomic hamiltonian.

Since in a given alkali atom $E_e \gg A_{FS} \gg A_{hf}$, the combined effect of a static magnetic

field together with a laser field can be studied adding to the hamiltonian in eq.(C.14) (obtained in a perturbative manner) the contribution of the external magnetic field given in eq.(C.15).

Therefore, the full hamiltonian in presence of both a light and a magnetic field reads:

$$H_{\mathbf{B}\&\mathbf{E}} = A_{hf}\hat{\mathbf{I}}\cdot\hat{\mathbf{J}} + u_s\,\widetilde{\mathbf{E}}^*\cdot\widetilde{\mathbf{E}} + \frac{\mu_B\, g_J}{\hbar}\,(\mathbf{B}_{eff}+\mathbf{B})\cdot\hat{\mathbf{J}}\,. \tag{C.16}$$

Assuming that the Zeeman splitting are small compared with the hyperfine splitting, it is possible to proceed as for the anomalous Zeeman effect, by considering the term proportional to g_J as a perturbation. In this case, the left hand side of the first relation in eq.(C.8) is non trivial and reads

$$\frac{\mu_B\, g_J}{\hbar}\,\mathbf{B}_{tot}\cdot\sum_{m,m'}|j,i,f,m\rangle\,\langle j,i,f,m|\,\hat{\mathbf{J}}\,|j,i,f,m'\rangle\,\langle j,i,f,m'|\,, \tag{C.17}$$

where $\mathbf{B}_{tot} = \mathbf{B}_{eff}+\mathbf{B}$, $\{|j,i,f,m\rangle\}$ are simultaenous eigenkets of $\hat{\mathbf{J}}^2$, $\hat{\mathbf{I}}^2$, $\hat{\mathbf{F}}^2$ and $\hat{F}_z$ where $\hat{\mathbf{F}} = \hat{\mathbf{J}}+\hat{\mathbf{I}}$, and $\hbar m$, $\hbar^2 f(f+1)$ are the eigenvalues of $\hat{F}_z$, $\hat{\mathbf{F}}^2$ respectively. Note that the summation runs over the values of m only, since a generic degenerate hyperfine manifold is identified by the quantum number f.

The operator $\hat{\mathbf{J}}$ transforms as a vector under rotations[2], therefore the Wigner-Eckart theorem [10] implies that:

$$\langle j,i,f,m|\,\hat{\mathbf{J}}\,|j,i,f,m'\rangle = C\,\langle j,i,f,m|\,\hat{\mathbf{F}}\,|j,i,f,m'\rangle\,. \tag{C.18}$$

Using the relation $\langle j,i,f,m|\,\hat{\mathbf{J}}\cdot\hat{\mathbf{F}}\,|j,i,f,m'\rangle = Cf(f+1)\hbar^2$, eq.(C.17) transforms into:

$$\begin{aligned}
&\frac{\mu_B\, g_J}{\hbar}\,\mathbf{B}_{tot}\cdot\sum_{m,m'}|j,i,f,m\rangle\,\langle j,i,f,m|\,(\hat{\mathbf{J}}\cdot\hat{\mathbf{F}})\hat{\mathbf{F}}\,|j,i,f,m'\rangle\,\langle j,i,f,m'| \\
= \;&\frac{\mu_B\, g_F}{\hbar}\,\mathbf{B}_{tot}\cdot\sum_{m,m'}|j,i,f,m\rangle\,\langle j,i,f,m|\,\hat{\mathbf{F}}\,|j,i,f,m'\rangle\,\langle j,i,f,m'|
\end{aligned} \tag{C.19}$$

where $g_F = g_J\frac{f(f+1)-j(j+1)-i(i+1)}{2f(f+1)}$ and it has been used the relation $\hat{\mathbf{J}}\cdot\hat{\mathbf{F}} = (\hat{\mathbf{F}}^2-\hat{\mathbf{J}}^2-\hat{\mathbf{I}}^2)/2$.

Therefore, the effective hamiltonian acting on the hyperfine manifold with fixed

[2]Remember that in this case the generator of rotations in space is $\hat{\mathbf{F}}$.

quantum number f reads:

$$H_{eff} = u_s \, \widetilde{\mathbf{E}}^* \cdot \widetilde{\mathbf{E}} + \frac{\mu_B \, g_F}{\hbar} \, (\mathbf{B}_{eff} + \mathbf{B}) \cdot \hat{\mathbf{F}} \, . \tag{C.20}$$

C.3 Actual scheme used in AGF experiments

The effective hamiltonian in eq.(C.20) contains the operator $\hat{\mathbf{F}}$ whose components are $\hat{F}_z$, $\hat{F}_y = F_+ - iF_-$ and $\hat{F}_x = F_+ + iF_-$, where $F_\pm$ are the ladder operators, acting on the hyperfine manifold as $\hat{F}_\pm \, |f, m\rangle = \sqrt{f(f+1) - m(m \pm 1)} \, |f, m \pm 1\rangle$. Therefore, while $\hat{F}_z$ splits the hyperfine levels, $\hat{F}_\pm$ describes Raman transitions which change m by ± 1. Nevertheless, this scheme is not yet the one used in current experiments on AGF.

In a more realistic scenario, an ensemble of ultracold atoms is subjected to an external magnetic field $\mathbf{B} = B_0 \, \mathbf{e}_z$ and simultaneously is illuminated by several laser beams with two frequencies ω and $\omega + \delta\omega$, where $\delta\omega = g_F \, \mu_B \, B_0/\hbar + \delta$. Therefore, an effective magnetic field is induced by the electric field $\mathbf{E} = \mathbf{E}_- \exp(i\omega t) + \mathbf{E}_+ \exp[-i(\omega + \delta\omega)t]$ as stated in eq.(C.13). Hence, the hamiltonian in eq.(C.20) is now time-dependent and the RWA can be performed, as long as it is assumed that $|\delta/\delta\omega| \ll 1$. Therefore, sending $H_{eff} \to S^\dagger H_{eff} S - i\hbar S^\dagger \partial_t S$, where $S = \exp(-i\hat{F}_z \delta\omega t)$, the rotated hamiltonian after the RWA reads:

$$H_{eff} = u_s \left(\widetilde{\mathbf{E}}^*_{\omega_-} \cdot \widetilde{\mathbf{E}}_{\omega_-} + \widetilde{\mathbf{E}}^*_{\omega_+} \cdot \widetilde{\mathbf{E}}_{\omega_+} \right) + \mathbf{\Omega} \cdot \hat{\mathbf{F}}, \tag{C.21}$$

where $\Omega_z = \delta + \frac{\mathbf{B}_{eff\,0} \cdot \mathbf{e}_z}{\hbar}$, $\Omega_\pm = \frac{\mu_B \, g_F}{2\hbar} \, [\mathbf{B}_{eff\,\pm} \cdot (\mathbf{e}_x \pm \mathbf{e}_y)]$, with
$\mathbf{B}_{eff\,0} = \frac{iu_v}{\mu_B g_J} \left(\widetilde{\mathbf{E}}^*_{\omega_-} \times \widetilde{\mathbf{E}}_{\omega_-} + \widetilde{\mathbf{E}}^*_{\omega_+} \times \widetilde{\mathbf{E}}_{\omega_+} \right)$ and $\mathbf{B}_{eff\,\pm} = \frac{iu_v}{\mu_B g_J} \widetilde{\mathbf{E}}^*_{\omega_\mp} \times \widetilde{\mathbf{E}}_{\omega_\pm}$.

In the case of the two raman beams depicted in Fig.(2.7) the effective Zeeman field reads:

$$\mathbf{\Omega} = \delta \, \mathbf{e}_z + \Omega_R \, [\sin(2k_R x)\mathbf{e}_x - \cos(2k_R x)\mathbf{e}_y] \, , \tag{C.22}$$

where $\Omega_R = (g_F/g_J) u_v E^2/\hbar$ is the Rabi frequency of the Raman coupling.

APPENDIX D

THE ORDER PARAMETER OF THE TRIPARTITE AFM.

In order to be consistent with the model in eq.(6.32), the effective hamiltonian in eq.(6.33) must be obtained from the first one by the contractions of the interacting terms. This sets a first relation between the occupation numbers and the external effective field, that reads:

$$\begin{aligned}
\langle n_{\mathbf{R}3}\rangle + \langle n_{\mathbf{R}2}\rangle - \frac{2}{3} &= \Delta_{\mathbf{R}1} + \frac{1}{\sqrt{3}}\Delta_{\mathbf{R}2} \\
\langle n_{\mathbf{R}1}\rangle + \langle n_{\mathbf{R}3}\rangle - \frac{2}{3} &= -\Delta_{\mathbf{R}1} + \frac{1}{\sqrt{3}}\Delta_{\mathbf{R}2} \\
\langle n_{\mathbf{R}1}\rangle + \langle n_{\mathbf{R}2}\rangle - \frac{2}{3} &= -\frac{2}{\sqrt{3}}\Delta_{\mathbf{R}2}
\end{aligned} \tag{D.1}$$

that corresponds to

$$\begin{aligned}
\langle n_{\mathbf{R}1}\rangle - \frac{1}{3} &= -\Delta_{\mathbf{R}1} - \frac{1}{\sqrt{3}}\Delta_{\mathbf{R}2} \\
\langle n_{\mathbf{R}2}\rangle - \frac{1}{3} &= \Delta_{\mathbf{R}1} - \frac{1}{\sqrt{3}}\Delta_{\mathbf{R}2} \\
\langle n_{\mathbf{R}3}\rangle - \frac{1}{3} &= \frac{2}{\sqrt{3}}\Delta_{\mathbf{R}2}
\end{aligned} \tag{D.2}$$

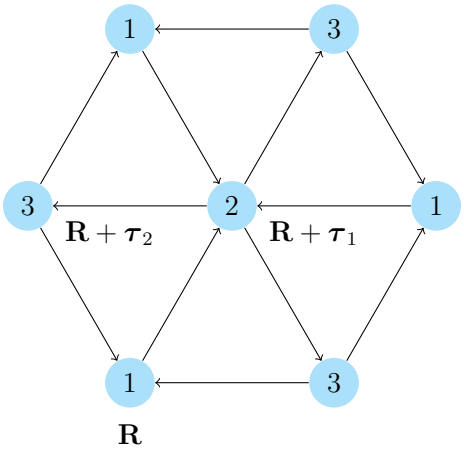

Figure D.1:

$\Delta_{\mathbf{R}_i}$ may be redefined using two linear transformation: the first one being: $\Delta_{\mathbf{R}2} \to \sqrt{3}\Delta_{\mathbf{R}2}$ and the second one reads: $(\Delta_{\mathbf{R}1} + \Delta_{\mathbf{R}2}) \to \Delta_{\mathbf{R}1}$, $(\Delta_{\mathbf{R}1} - \Delta_{\mathbf{R}2}) \to \Delta_{\mathbf{R}2}$. These transformations lead to a simplified linear system of equations:

$$\begin{aligned} \langle n_{\mathbf{R}1}\rangle - \frac{1}{3} &= -\Delta_{\mathbf{R}1} \\ \langle n_{\mathbf{R}2}\rangle - \frac{1}{3} &= \Delta_{\mathbf{R}2} \\ \langle n_{\mathbf{R}3}\rangle - \frac{1}{3} &= \Delta_{\mathbf{R}1} - \Delta_{\mathbf{R}2} \end{aligned} \tag{D.3}$$

Now, the explicit dependence of $\Delta_{\mathbf{R}}$ on the lattice site, will be carried out using the lattice geometry and imposing symmetries.

A generic lattice site can be expressed in terms of the generating vectors of the lattice, namely $\boldsymbol{\tau}_{1/2} = (\pm 1/2, \sqrt{3}/2)$, as $\mathbf{R}(m,n) = m\,\boldsymbol{\tau}_1 + n\,\boldsymbol{\tau}_2$, with $m, n \in \mathbb{Z}$. Therefore the system of eq.(D.3), it is expressed in terms of the integers m and n. In the case of a long range magnetic order of the form of Fig.(D.1), it is easy to see that a translation of $\boldsymbol{\tau}_1$ corresponds to a rotation of $2\pi/3$, while a translation of $\boldsymbol{\tau}_2$ to rotation of $-2\pi/3$. Thus $\boldsymbol{\Delta}_{\mathbf{R}}$ must be of the form such that, when it is translated of $\boldsymbol{\tau}_1$:

$$\langle n_{\mathbf{R}1}\rangle \to \langle n_{\mathbf{R}2}\rangle\,,$$

$$\langle n_{\mathbf{R}2}\rangle \to \langle n_{\mathbf{R}3}\rangle\,,$$

$$\langle n_{\mathbf{R}3}\rangle \to \langle n_{\mathbf{R}1}\rangle\,,$$

while when it is translated of $\boldsymbol{\tau}_2$ must give:

$$\langle n_{\mathbf{R}1}\rangle \to \langle n_{\mathbf{R}3}\rangle\,,$$

$$\langle n_{\mathbf{R}2}\rangle \to \langle n_{\mathbf{R}1}\rangle\,,$$

$$\langle n_{\mathbf{R}3}\rangle \to \langle n_{\mathbf{R}2}\rangle\,.$$

A possible parametrization of $\boldsymbol{\Delta}_{\mathbf{R}}$ is given by the following equations:

$$\begin{aligned}
\langle \delta n_1\rangle &= \Delta_1\, f(m-n-1) + \Delta_2\, f(m-n) \\
\langle \delta n_2\rangle &= \Delta_1\, f(m-n) + \Delta_2\, f(m-n+1) \\
\langle \delta n_3\rangle &= \Delta_1\, f(m-n+1) + \Delta_2\, f(m-n-1),
\end{aligned} \tag{D.4}$$

where $f(\ell) = \frac{2}{\sqrt{3}} \sin\left(\frac{2\pi\,\ell}{3}\right)$, where ℓ is an integer, therefore the final expression of the two component field is the following:

$$\begin{aligned}
\Delta_{\mathbf{R}1} &= -\Delta_1 f(m-n-1) - \Delta_2 f(m-n) \\
\Delta_{\mathbf{R}2} &= \Delta_1 f(m-n) + \Delta_2 f(m-n+1)
\end{aligned} \tag{D.5}$$

where Δ_1 and Δ_2 are the amplitudes of the field to be optimized in order to minimize the variational energy.

This results must be related to the previous definition of $\boldsymbol{\Delta}$ in the hamiltonian in eq.(6.33), therefore in order to obtain the original $\boldsymbol{\Delta}$ the results in eq.(D.5) are combined in the following way:

$$\begin{aligned}
\Delta_{\mathbf{R}1}^{\text{original}} &= \frac{\Delta_{\mathbf{R}1} + \Delta_{\mathbf{R}2}}{2} \\
&= \frac{1}{2}\left\{\Delta_1\left[f(m-n) - f(m-n-1)\right] + \Delta_2\left[f(m-n+1) - f(m-n)\right]\right\} \\
\Delta_{\mathbf{R}2}^{\text{original}} &= \frac{\sqrt{3}}{2}\left(\Delta_{\mathbf{R}1} - \Delta_{\mathbf{R}2}\right) \\
&= -\frac{\sqrt{3}}{2}\left\{\Delta_1\left[f(m-n) + f(m-n-1)\right] + \Delta_2\left[f(m-n+1) + f(m-n)\right]\right\}
\end{aligned} \tag{D.6}$$

Hereafter the apex *original* that has been used for clarity will be dropped.

The following formula:

$$A\sin(\alpha x)+B\sin[\alpha(x+y)]=B\cos(\alpha x)\sin(\alpha y)+[A+B\cos(\alpha y)]\sin(\alpha x)$$

implies that:

$$f(m-n)\mp f(m-n-1)=\pm g(m-n)+\left(1\pm\frac{1}{2}\right)f(m-n)$$

$$f(m-n)\pm f(m-n+1)=\pm g(m-n)+\left(1\mp\frac{1}{2}\right)f(m-n),$$

where $g(\ell)=\cos\left(\frac{2\pi\ell}{3}\right)$ and from which it can be recognized that $f(\ell)+f(\ell-1)+f(\ell+1)=0$. Using these formulae the expression of the order parameter reads:

$$\begin{aligned}\Delta_{\mathbf{R}1} &= \frac{\Delta_1}{2}\left[g(m-n)+\frac{3}{2}f(m-n)\right]+\frac{\Delta_2}{2}\left[g(m-n)-\frac{3}{2}f(m-n)\right]\\ \Delta_{\mathbf{R}2} &= -\frac{\sqrt{3}}{2}\left\{\Delta_1\left[-g(m-n)+\frac{1}{2}f(m-n)\right]+\Delta_2\left[g(m-n)+\frac{1}{2}f(m-n)\right]\right\}\end{aligned} \tag{D.7}$$

This last equation is almost fully simplified, as last step the following relation $A\cos(\alpha x)+B\sin(\alpha x)=\frac{1}{2}(A-iB)e^{i\alpha x}+\text{h.c.}$, and the following definition

$$\frac{2\pi(m-n)}{3}=\mathbf{Q}\cdot\mathbf{R},\ \text{ with }\mathbf{Q}=\left(\frac{4\pi}{3},0\right), \tag{D.8}$$

are plugged into eq.(D.7), leading to the final explicit form of the effective field:

$$\mathbf{\Delta_R}=e^{i\mathbf{Q}\cdot\mathbf{R}}\mathbf{\Lambda}+\text{h.c.}, \tag{D.9}$$

where $\mathbf{\Lambda}=(\Lambda_1,\Lambda_2)$

$$\begin{aligned}\Lambda_1 &= \frac{1}{4}\left[\Delta_1\left(1-i\sqrt{3}\right)+\Delta_2\left(1+i\sqrt{3}\right)\right]\\ \Lambda_2 &= \frac{\sqrt{3}}{4}\left[\Delta_1\left(1+i\frac{1}{\sqrt{3}}\right)-\Delta_2\left(1-i\frac{1}{\sqrt{3}}\right)\right]\end{aligned} \tag{D.10}$$

that can be rewritten in the more elegant polar form as

$$\mathbf{\Lambda} = \frac{1}{2} \begin{pmatrix} \Delta_1 e^{-i\frac{\pi}{3}} + \Delta_2 e^{i\frac{\pi}{3}} \\ \\ \Delta_1 e^{i\frac{\pi}{6}} - \Delta_2 e^{-i\frac{\pi}{6}} \end{pmatrix}. \tag{D.11}$$

BIBLIOGRAPHY

[1] A. Altland and B. D. Simons. *Condensed matter field theory*. Cambridge University Press, 2010.

[2] P. W. Anderson. Localized magnetic states in metals. *Phys. Rev.*, 124:41–53, Oct 1961.

[3] N. W. Ashcroft. Nd mermin solid state physics. *Saunders College, Philadelphia*, page 120, 1976.

[4] B. Bauer, P. Corboz, A. M. Läuchli, L. Messio, K. Penc, M. Troyer, and F. Mila. Three-sublattice order in the su (3) heisenberg model on the square and triangular lattice. *Physical Review B*, 85(12):125116, 2012.

[5] J. Bauer. Quasiparticle properties of strongly correlated electron systems with itinerant metamagnetic behavior. *The European Physical Journal B*, 68(2):201–208, 2009.

[6] J. Bauer and A. Hewson. Field-dependent quasiparticles in the infinite-dimensional hubbard model. *Physical Review B*, 76(3):035118, 2007.

[7] G. Baym and C. Pethick. *Landau Fermi-liquid theory: concepts and applications*. John Wiley & Sons, 2008.

[8] I. Bloch, J. Dalibard, and W. Zwerger. Many-body physics with ultracold gases. *Reviews of Modern Physics*, 80(3):885, 2008.

[9] M. M. Boyd, T. Zelevinsky, A. D. Ludlow, S. Blatt, T. Zanon-Willette, S. M. Foreman, and J. Ye. Nuclear spin effects in optical lattice clocks. *Phys. Rev. A*, 76:022510, Aug 2007.

[10] B. H. Bransden and C. J. Joachain. *Physics of atoms and molecules*. Pearson Education India, 2003.

[11] H. Bruus and K. Flensberg. *Many-body quantum theory in condensed matter physics: an introduction*. Oxford University Press, 2004.

[12] A. Camjayi, R. Chitra, and M. Rozenberg. Electronic state of a doped mott-hubbard insulator at finite temperatures studied using the dynamical mean-field theory. *Physical Review B*, 73(4):041103, 2006.

[13] M. Capone, M. Fabrizio, C. Castellani, and E. Tosatti. Strongly correlated superconductivity. *Science*, 296(5577):2364–2366, 2002.

[14] M. Capone, M. Fabrizio, C. Castellani, and E. Tosatti. *Colloquium* : Modeling the unconventional superconducting properties of expanded A_3c_{60} fullerides. *Rev. Mod. Phys.*, 81:943–958, Jun 2009.

[15] G. Cappellini, M. Mancini, G. Pagano, P. Lombardi, L. Livi, M. Siciliani de Cumis, P. Cancio, M. Pizzocaro, D. Calonico, F. Levi, C. Sias, J. Catani, M. Inguscio, and L. Fallani. Direct observation of coherent interorbital spin-exchange dynamics. *Phys. Rev. Lett.*, 113:120402, Sep 2014.

[16] M. Cazalilla, A. Ho, and M. Ueda. Ultracold gases of ytterbium: Ferromagnetism and mott states in an su (6) fermi system. *New Journal of Physics*, 11(10):103033, 2009.

[17] A. Celi, P. Massignan, J. Ruseckas, N. Goldman, I. Spielman, G. Juzeliūnas, and M. Lewenstein. Synthetic gauge fields in synthetic dimensions. *Physical review letters*, 112(4):043001, 2014.

[18] C. Chin, R. Grimm, P. Julienne, and E. Tiesinga. Feshbach resonances in ultracold gases. *Reviews of Modern Physics*, 82(2):1225, 2010.

[19] A. Chubukov and P. J. Hirschfeld. Iron-based superconductors, seven years later. *Physics Today*, 68:46, 2015.

[20] J. Dalibard, F. Gerbier, G. Juzeliūnas, and P. Öhberg. Colloquium: Artificial gauge potentials for neutral atoms. *Reviews of Modern Physics*, 83(4):1523, 2011.

[21] L. de' Medici, G. Giovannetti, and M. Capone. Selective mott physics as a key to iron superconductors. *Phys. Rev. Lett.*, 112:177001, Apr 2014.

[22] L. de' Medici, S. R. Hassan, M. Capone, and X. Dai. Orbital-selective mott transition out of band degeneracy lifting. *Phys. Rev. Lett.*, 102:126401, Mar 2009.

[23] L. de'Medici, A. Georges, and S. Biermann. Orbital-selective mott transition in multiband systems: Slave-spin representation and dynamical mean-field theory. *Phys. Rev. B*, 72:205124, Nov 2005.

[24] T. Esslinger. Fermi-hubbard physics with atoms in an optical lattice. *arXiv preprint arXiv:1007.0012*, 2010.

[25] R. P. Feynman. Simulating physics with computers. *International journal of theoretical physics*, 21(6):467–488, 1982.

[26] S. Florens, A. Georges, G. Kotliar, and O. Parcollet. Mott transition at large orbital degeneracy: Dynamical mean-field theory. *Physical Review B*, 66(20):205102, 2002.

[27] A. Georges, L. de' Medici, and J. Mravlje. Strong correlations from hund coupling. *Annual Review of Condensed Matter Physics*, 4(1):137–178, 2013.

[28] A. Georges, G. Kotliar, W. Krauth, and M. J. Rozenberg. Dynamical mean-field theory of strongly correlated fermion systems and the limit of infinite dimensions. *Reviews of Modern Physics*, 68(1):13, 1996.

[29] N. Goldman, I. Spielman, et al. Light-induced gauge fields for ultracold atoms. *Reports on Progress in Physics*, 77(12):126401, 2014.

[30] E. Gorelik and N. Blümer. Mott transitions in ternary flavor mixtures of ultracold fermions on optical lattices. *Physical Review A*, 80(5):051602, 2009.

[31] A. Gorshkov, M. Hermele, V. Gurarie, C. Xu, P. Julienne, J. Ye, P. Zoller, E. Demler, M. Lukin, and A. Rey. Two-orbital su (n) magnetism with ultracold alkaline-earth atoms. *Nature Physics*, 6(4):289–295, 2010.

[32] M. Greiner, O. Mandel, T. Esslinger, T. W. Hänsch, and I. Bloch. Quantum phase transition from a superfluid to a mott insulator in a gas of ultracold atoms. *nature*, 415(6867):39–44, 2002.

[33] P. Hansmann, R. Arita, A. Toschi, S. Sakai, G. Sangiovanni, and K. Held. Dichotomy between large local and small ordered magnetic moments in iron-based superconductors. *Phys. Rev. Lett.*, 104:197002, May 2010.

[34] K. Haule and G. Kotliar. Coherence–incoherence crossover in the normal state of iron oxypnictides and importance of hund's rule coupling. *New journal of physics*, 11(2):025021, 2009.

[35] K. Held, M. Ulmke, N. Blümer, and D. Vollhardt. Correlated-electron theory of strongly anisotropic metamagnets. *Physical Review B*, 56(22):14469, 1997.

[36] M. Höfer, L. Riegger, F. Scazza, C. Hofrichter, D. R. Fernandes, M. M. Parish, J. Levinsen, I. Bloch, and S. Fölling. Observation of an orbital interaction-induced feshbach resonance in ^{173}Yb. *Phys. Rev. Lett.*, 115:265302, Dec 2015.

[37] L. Huang, Z. Meng, P. Wang, P. Peng, S.-L. Zhang, L. Chen, D. Li, Q. Zhou, and J. Zhang. Experimental realization of two-dimensional synthetic spin-orbit coupling in ultracold fermi gases. *Nature Physics*, 12(6):540–544, 2016.

[38] M. Imada, A. Fujimori, and Y. Tokura. Metal-insulator transitions. *Reviews of Modern Physics*, 70(4):1039, 1998.

[39] S. Inouye, M. Andrews, J. Stenger, H.-J. Miesner, D. Stamper-Kurn, and W. Ketterle. Observation of feshbach resonances in a bose–einstein condensate. *Nature*, 392(6672):151–154, 1998.

[40] D. Jaksch, C. Bruder, J. I. Cirac, C. W. Gardiner, and P. Zoller. Cold bosonic atoms in optical lattices. *Phys. Rev. Lett.*, 81:3108–3111, Oct 1998.

[41] A. Koga, N. Kawakami, T. M. Rice, and M. Sigrist. Orbital-selective mott transitions in the degenerate hubbard model. *Phys. Rev. Lett.*, 92:216402, May 2004.

[42] G. Kotliar, S. Y. Savrasov, G. Pálsson, and G. Biroli. Cellular dynamical mean field approach to strongly correlated systems. *Physical review letters*, 87(18):186401, 2001.

[43] L. Laloux, A. Georges, and W. Krauth. Effect of a magnetic field on mott-hubbard systems. *Physical Review B*, 50(5):3092, 1994.

[44] L. D. Landau. A possible explanation of the field dependence of the susceptibility at low temperatures. *Phys. Z. Sowjet*, 4:675, 1933.

[45] E. H. Lieb and F. Y. Wu. Absence of mott transition in an exact solution of the short-range, one-band model in one dimension. *Physical Review Letters*, 20(25):1445, 1968.

[46] P. Limelette, A. Georges, D. Jérome, P. Wzietek, P. Metcalf, and J. Honig. Universality and critical behavior at the mott transition. *Science*, 302(5642):89–92, 2003.

[47] R. Loudon. *The quantum theory of light*. OUP Oxford, 2000.

[48] J. M. Luttinger and J. C. Ward. Ground-state energy of a many-fermion system. ii. *Physical Review*, 118(5):1417, 1960.

[49] T. Maier, M. Jarrell, T. Pruschke, and M. H. Hettler. Quantum cluster theories. *Reviews of Modern Physics*, 77(3):1027, 2005.

[50] M. Mancini, G. Pagano, G. Cappellini, L. Livi, M. Rider, J. Catani, C. Sias, P. Zoller, M. Inguscio, M. Dalmonte, et al. Observation of chiral edge states with neutral fermions in synthetic hall ribbons. *Science*, 349(6255):1510–1513, 2015.

[51] G. Moeller, Q. Si, G. Kotliar, M. Rozenberg, and D. S. Fisher. Critical behavior near the mott transition in the hubbard model. *Physical review letters*, 74(11):2082, 1995.

[52] J. W. Negele and H. Orland. *Quantum many-particle systems*, volume 200. Addison-Wesley New York, 1988.

[53] Y. Ōno, M. Potthoff, and R. Bulla. Mott transitions in correlated electron systems with orbital degrees of freedom. *Physical Review B*, 67(3):035119, 2003.

[54] G. Pagano, M. Mancini, G. Cappellini, L. Livi, C. Sias, J. Catani, M. Inguscio, and L. Fallani. Strongly interacting gas of two-electron fermions at an orbital feshbach resonance. *Phys. Rev. Lett.*, 115:265301, Dec 2015.

[55] G. Pagano, M. Mancini, G. Cappellini, P. Lombardi, F. Schäfer, H. Hu, X.-J. Liu, J. Catani, C. Sias, M. Inguscio, et al. A one-dimensional liquid of fermions with tunable spin. *Nature Physics*, 10(3):198–201, 2014.

[56] N. Papanicolaou. Pseudospin approach for planar ferromagnets. *Nuclear Physics B*, 240(3):281–311, 1984.

[57] N. Papanicolaou. Unusual phases in quantum spin-1 systems. *Nuclear Physics B*, 305(3):367–395, 1988.

[58] D. Parihari, N. Vidhyadhiraja, and A. Taraphder. Field-dependent dynamics in the metallic regime of the half-filled hubbard model. *Journal of Physics: Condensed Matter*, 23(5):055602, 2011.

[59] C. J. Pethick and H. Smith. *Bose-Einstein condensation in dilute gases*. Cambridge university press, 2002.

[60] D. Pines and P. Nozières. *The theory of quantum liquids*. Addison-Wesley, 1990.

[61] J. J. Sakurai and J. Napolitano. *Modern quantum mechanics*. Addison-Wesley, 2011.

[62] F. Scazza, C. Hofrichter, M. Höfer, P. De Groot, I. Bloch, and S. Fölling. Observation of two-orbital spin-exchange interactions with ultracold su (n)-symmetric fermions. *Nature Physics*, 10(10):779–784, 2014.

[63] B. Song, C. He, S. Zhang, Y. Zou, E. Haciyev, W. Huang, X.-J. Liu, and G.-B. Jo. Spin-orbit coupled two-electron fermi gases of ytterbium atoms. *arXiv preprint arXiv:1608.00478*, 2016.

[64] L. Tagliacozzo, A. Celi, P. Orland, M. Mitchell, and M. Lewenstein. Simulation of non-abelian gauge theories with optical lattices. *Nature communications*, 4, 2013.

[65] T. A. Tóth, A. M. Läuchli, F. Mila, and K. Penc. Three-sublattice ordering of the su (3) heisenberg model of three-flavor fermions on the square and cubic lattices. *Physical review letters*, 105(26):265301, 2010.

[66] F. Werner, O. Parcollet, A. Georges, and S. R. Hassan. Interaction-induced adiabatic cooling and antiferromagnetism of cold fermions in optical lattices. *Phys. Rev. Lett.*, 95:056401, Jul 2005.

[67] P. Werner and A. J. Millis. High-spin to low-spin and orbital polarization transitions in multiorbital mott systems. *Physical review letters*, 99(12):126405, 2007.

[68] Z. P. Yin, K. Haule, and G. Kotliar. Kinetic frustration and the nature of the magnetic and paramagnetic states in iron pnictides and iron chalcogenides. *Nat Mater*, 10(12):932–935, 12 2011.

[69] R. Zhang, Y. Cheng, H. Zhai, and P. Zhang. Orbital feshbach resonance in alkali-earth atoms. *Phys. Rev. Lett.*, 115:135301, Sep 2015.

[70] X. Zhang, M. Bishof, S. Bromley, C. Kraus, M. Safronova, P. Zoller, A. Rey, and J. Ye. Spectroscopic observation of su (n)-symmetric interactions in sr orbital magnetism. *science*, 345(6203):1467–1473, 2014.

[71] X. Zhang, M. Rozenberg, and G. Kotliar. Mott transition in the d=° hubbard model at zero temperature. *Physical review letters*, 70(11):1666, 1993.